GLUCAGON-LIKE PEPTIDE-1 RECEPTOR AGONIST, DULAGLUTIDE, AMELIORATES KIDNEY FUNCTION IN DIET-INDUCED OBESE MICE BY REGULATING LIPIDS AND METABOLITES.

YEUNG HO YIN MARTIN

PhD

The Hong Kong Polytechnic University

2022

The Hong Kong Polytechnic University

Department of Health Technology and Informatics

GLUCAGON-LIKE PEPTIDE-1 RECEPTOR AGONIST, DULAGLUTIDE, AMELIORATES KIDNEY FUNCTION IN DIET-INDUCED OBESE MICE BY REGULATING LIPIDS AND METABOLITES.

YEUNG HO YIN MARTIN

A Thesis Submitted in Partial Fulfilment of the

Requirements for the degree of Doctor of Philosophy

August 2021

CERTIFICATE OF ORIGINALITY

I hereby declare that this thesis is my own work and that, to the best of my knowledge and belief, it reproduces no material previously published or written, nor material that has been accepted for the award of any other degree or diploma, except where due acknowledgement has been made in the text.

_____(Signed)

YEUNG, HO YIN MARTIN (Name of student)

Acknowledgement

First and foremost, thank you God for granting this opportunity for me to pursue further studies. Thank you for blessing me in completing this degree and for taking care of me and my family throughout this process. Thank you for equipping me with knowledge and for providing me with the peers and support when I need it most. You have taught me to be humble, to trust in you and be patient, for you will always be there and to provide. This journey has not been easy, but only through rejoicing in our suffering will we grow strong and continue to be hopeful.

"Not only that, but we rejoice in our sufferings, knowing that suffering produces endurance, and endurance produces character, and character produces hope,"

(Romans 5:3-4, English Standard Version).

I would like to express my sincere gratitude to my chief supervisor Dr. WONG, Chi-ming and co-supervisor Dr. YOO, Jung Sun for providing the support and guidance required for me to achieve this award. Your comments and insightful thoughts have broadened my perspective and will allow me to develop myself further, in the future, to new heights.

Furthermore, I would like to show my greatest appreciation to Dr. ZOU, Xiang, Dr. CHENG, Kenneth King-yip, Dr. WONG, Cesar Sze Chuen and Dr. TSE, Franki Kai-Hei for their time to provide invaluable comments and feedback on my research work and progress. I am thankful to be given the opportunity to be trained by you all and for also giving me the opportunity to participate in practical sessions as a teaching assistant.

In addition, I would like to thank Dr. SO, Pui-kin, Dr and Dr. LI, Rachel Wai-sum from the department of the University Research Facilities in Life Sciences for their

professional service and advice on the use of major high-tech equipment including mass spectrometers to digital metabolic cage for animal studies.

I would also like to extend my appreciation and thanks to Prof. XU, Aimin from The University of Hong Kong for his feedback, guidance and support throughout my studies.

I must also take this opportunity to thank Prof. CHAN, Chi Ming and Prof. Lin, Betty from The Hong Kong University of Science and Technology for their continuous encouragement. You have demonstrated clearly, through your love and action, the qualities to become a successful and well-respected academic advisor and role model.

I would like to extend my appreciation and acknowledgement to my fellow friends and colleagues including Mr. WONG, Alex Ngai Nick and Mr. CHAN, Brandon Dow. I am very grateful for your patience and I very much appreciate the conversations and discussions we have had.

I would like to sincerely thank my mentor and Senior Medical Technologist, Mr. YAU, Alan Man Cheung for his kindness and patience in giving me the opportunity and to train me to become a professional Medical Laboratory Technologist. Your selfless encouragement to me to pursue further studies will never be forgotten. You have always been self-sacrificing through your work and have lived up to the standard of being a true allied health professional by putting patients first. Thank you, Alan.

I would like thank my parents and my brother for their continuous support throughout my life. Your continuous patience, support and encouragement is vital for me to get through this process.

My deepest gratitude goes to my wife, Dr. CHAN, Angela Zaneta, for having to go through the whole PhD process with me. You have been very understanding of my

situation and have shown ultimate patience to me. I will forever be in debt to you for unfailing love and kindness.

Abstract

Obesity is associated with metabolic syndromes, which lead to dyslipidaemia, hyperglycaemia, and ectopic lipid accumulation. Metabolic syndromes increase the risk of type-2 diabetes mellitus (T2DM) and contributes to the development of diabetic kidney disease (DKD). Dulaglutide is a glucagon-like peptide-1 receptor (GLP-1R) agonist drug used for glycaemic control in diabetic patients. Multiple assessments of weekly administration of dulaglutide in diabetes (AWARD) randomized clinical trials have shown beneficial effects in kidney function, including a reduction of composite renal outcomes; however, the pharmacological mechanism is still not clear. In this study, a high-fat diet-induced obese mouse model with kidney dysfunction was established. These mice were subsequently treated with dulaglutide for 4 weeks, then measurements were made to assess its renoprotective effects. An untargeted lipidomics analysis using ultra-performance liquid chromatography-quadrupole time-of-flight mass spectrometry was developed and performed to obtain lipidome profiles of the kidneys after dulaglutide treatment. Dulaglutide-treated mice showed improvement in metabolic disorders, including improved glucose tolerance and reduction in body weight. In the kidney of the treated mice, there is a reduction in albuminuria. Further morphological examinations showed that the increased capsular space, thickening of the basement membrane and increased ectopic lipid accumulation were ameliorated after the treatment. A multivariate analysis on the kidney lipidome was performed and 65 differential compounds of interest, which are involved in glycerophospholipid metabolism, sphingolipid metabolism and ether lipid metabolism, were identified after the treatment. Ultra-high-performance liquid chromatography-quadrupole time-of-flight mass spectrometry (UHPLC/ESI-QTOF-MS) and matrix-assisted laser desorption/ionization time-of-flight/time-of-flight mass spectrometry imaging

(MALDI-MSI) results showed in the kidney cortex region an overall increase in cardiolipin (CL), which is a part of glycerophospholipid metabolism. CL is involved in the structural integrity of mitochondria complexes and essential for normal electron transport function to generate energy for cellular function. Our results have demonstrated that dulaglutide may play a role in renoprotective effects in high-fat diet-induced obese mice with kidney dysfunction. The current study has shed light for understanding the mechanism of glucagon-like peptide-1 (GLP-1) receptor (GLP-1R) agonists on DKD via an unbiased untargeted lipidomics approach.

Table of content

Contents

List of figures

List of tables

List of abbreviations

Full name	Abbreviation
^{1}H Nuclear magnetic resonance-based analyser	^{1}H-NMR
2,5-Dihydroxybenzoic acid	DHB
3,3'-diaminobenzidine	DAB
Acetyl-coa carboxylase	ACC
Acyl-coa:lysocardiolipin acyltransferase 1	ALCAT1
Adenosine triphosphate	ATP
Adipose triglyceride lipase	ATGL
Angiotensin II receptor blocker	ARB
Angiotensin-converting-enzyme	ACE
Animal Subjects Ethics Sub-committee	ASESC
Area under the curve receiver operating characteristic	AUC-ROC
Assessment of Weekly Administration of LY2189265 (Dulaglutide) in Diabetes 7	AWARD-7
Body mass index	BMI
Canagliflozin and Renal Events in Diabetes with Established Nephropathy Clinical Evaluation	CREDENCE
Cardiolipin	CL
Cardiolipin synthase	CLS
Cardiovascular diseases	CVD
Chronic kidney disease	CKD
Cluster of differentiation 36	CD36
Complimentary DNA	cDNA
Cytidine diphosphate diacylglycerol synthetase 1	CDS1

Cytochrome b	CYTB
Cytochrome oxidase III	CoxIII
Diabetic kidney disease	DKD
Dipeptidyl peptidase-4	DPP-4
Electrospray ionization	ESI
Empagliflozin Cardiovascular Outcome Event Trial in Type 2 Diabetes Mellitus Patients-Removing Excess Glucose	EMPA-REG OUTCOME
End-stage renal disease	ESRD
Enhanced chemiluminescence	ECL
Enzyme-linked immunosorbent assay	ELISA
Fatty acid synthase	FAS
Foetal bovine serum	FBS
Food and Drug Administration	FDA
Formalin-fixed paraffin embedded block	FFPE
Free fatty acid	FFA
Genomic DNA	gDNA
Glomerular filtration rate	GFR
Glucagon-like peptide-1	GLP-1
Glucagon-like peptide-1 receptor	GLP-1R
Gluconeogenic phosphoenolpyruvate carboxykinase	PEPCK
Glyceraldehyde 3-phosphate dehydrogenase	GAPDH
Haematoxylin and Eosin	H&E
High-fat diet (group)	HFD
High-fat diet with dulaglutide treatment	H+Dula

Hormone-sensitive lipase	HSL
Human metabolome Database	HMDB
Hypoxia inducible factor-1 α	HIF-1α
Immunohistochemical	IHC
Indium tin oxide	ITO
Intraperitoneally injected glucose tolerance test	IPGTT
Kyoto Encyclopedia of Genes and Genomes	KEGG
LIPID MAPS structure database	LMSD
Liquid chromatography mass spectrometry	LC-MS
Liquid-liquid extraction	LLE
Liraglutide Effect and Action in Diabetes: Evaluation of Cardiovascular Outcome Results	LEADER
Low-density lipoprotein	LDL
Mass spectrometry	MS
Matrix-assisted laser desorption/ionization time-of-flight/time-of-flight mass spectrometry imaging	MALDI-MSI
Messenger RNA	mRNA
Mitochondrial DNA	MtDNA
Mitochondrial manganese superoxide dismutase	Mn-SOD
Mitochondrial transcription factor A	TFAM
Monounsaturated fatty acid	MUFA
Multiple assessments of weekly administration of dulaglutide in diabetes	AWARD
NADH-ubiquinone oxidoreductase chain 5 protein	ND5
Nicotinamide adenine dinucleotide phosphate oxidase	NOX

Nitric oxide synthase	NOS
Nuclear respiratory factor 1	NRF1
Oil red o	ORO
Orthogonal partial least-squares-discriminant analysis	OPLS-DA
P-adenosine 5`-monophosphate	AMP
P-adenosine 5`-monophosphate activated protein kinase	AMPK
Partial least squares-discriminant analysis	PLS-DA
Periodic acid-Schiff methenamine	PASM
Phosphate-buffered saline	PBS
Phosphatidic acid	PA
Phosphatidylcholine	PC
Phosphatidylethanolamine	PE
Phosphatidylglycerol	PG
Phosphatidylglycerol phosphate synthase	PGPS
Phosphatidylinositol	PI
Phosphatidylserine	PS
Polyunsaturated fatty acid	PUFA
Polyvinylidene difluoride	PVDF
Principal components analysis	PCA
Proliferator-activated receptor gamma coactivator 1-alpha	PGC-1α
Proximal tubule cell	PTC
Quadrupole-time of flight mass analyser	QTOF/MS
Quality control	QC
Quantitative reverse transcription polymerase chain reaction	RT-qPCR

Reactive oxygen species	ROS
Receiver operating characteristic	ROC
Renin-angiotensin-system	RAS
Researching Cardiovascular Events with a Weekly Incretin in Diabetes	REWIND
Respiratory exchange ratio	RER
Saturated fatty acids	SFA
Sodium glucose cotransporters	SGLT
Sodium-glucose cotransporter 2	SGLT2
Standard chow control	STC
Standard error of the mean	SEM
Sterol-regulatory element binding proteins	SREBP
Superoxide dismutase	SOD
Tafazzin	TAZ
The irbesartan diabetic nephropathy trial	IDNT
The National Institute of Health	NIH
The Reduction of Endpoints in NIDDM with the Angiotensin II Antagonist Losartan	RENAAL
Trifluoroacetic acid	TFA
Triglyceride	TG
Tris-buffered saline with Tween20	TBS-T
Tumour necrosis factor alpha	TNF-α
Type-2 diabetes mellitus	T2DM
Ultra-high-performance liquid chromatography	UHPLC

Ultra-high-performance liquid chromatography-quadrupole time-of-flight mass spectrometry	UHPLC/ESI-QTOF-MS
Urinary albumin and creatinine ratio	UACR
Variable importance plot	VIP
World health organization	WHO

1. Introduction to diabetic kidney disease and current treatment strategies

1.1. Epidemiology of obesity, diabetes and diabetic kidney disease

Obesity is a chronic disease and by definition, it is the condition of excessive accumulation of fat in adipose tissues, which leads to impaired health (Ofei, 2005). Obesity is commonly determined in clinical setting by using the body mass index (BMI). The index is calculated by dividing the weight in kilograms by the height in meters of the patient. The subsequent value in kg/m^2 approximates the total adipose percentage in the body. According to the World Health Organization (WHO), a healthy individual should have a BMI index between 18.5 to 24.9kg/m^2, whilst individuals with index between 25.0 to 29.9 kg/m^2 are considered overweight and others with 30 kg/m^2or above are considered obese. As BMI is a convenient and simple method to determine the ratio between weight and height, it almost certainly has its limitations. A few examples of this is that this method of screening for obesity does not identify area of excessive fat, hence it is possible that a patient with a normal BMI but may have an excessive body fat near the abdominal area, which increases their risk of obesity related diseases (Sweeting, 2007). There are many risk factors that can lead to obesity, an individual person's diet and physical activity are the most fundamental and obvious cause of obesity. The amount of calories intake is higher than the total utilization of calories per day will lead to the excess build-up of energy in the form of lipids in the adipose tissue (Buscemi *et al.*, 2017). Socioeconomics is another major factor that contribute to the increasing number of obese amongst a population. Previous data indicates a positive relationship between prevalence of obesity with high income (Kim and Von Dem Knesebeck, 2018). However, in areas in which there are low-income families, obesity is also prevalent due to the reduced choice of food available. Low cost fast food is popular to low-income family, which are mainly

processed meat, which contain high calorie and high sodium; this regrettably, increases their chances of having metabolic syndrome leading to obesity (Burgoine *et al.*, 2018).

In obese patients, it is observed that the majority of them have a combination of metabolic syndrome such as, hyperglycaemia, dyslipidaemia, impaired insulin signalling and ectopic lipid accumulation (Smith, 2015). It is becoming more common due to the increasing prevalence of obesity. These comorbidities increase the risk factors to a range of diseases like T2DM, cardiovascular diseases (CVD) and chronic kidney diseases (CKD) (Gai *et al.*, 2019). T2DM resulting from both obesity and metabolic syndrome are highly associated with mortality with CVD and there is new evidence that showed they are independent risk factors that contribute to CKD (Maric and Hall, 2011, Lakka *et al.*, 2002). Previously, the role of T2DM and metabolic syndrome causing CKD were questioned and were believed to be associated with hypertension. However, evidence have shown from a study that a minimum of 30% of cases of new CKD cases led to end-stage renal disease (ESRD) as a result of metabolic syndrome (Kincaid-Smith, 2004). Further research and studies affirmed with this direction by assessing obesity and its direct relationship with worsening of pre-existing renal disease in patients (Bonnet *et al.*, 2001, Mcpherson *et al.*, 2019). Moreover, kidney function from live donors were assessed for their glomerular filtration rate (GFR) between obese and non-obese donors before transplantation. After transplantation, it is observed that recipients of kidney from obese donors showed a lower GFR as compared to non-obese donors further suggesting that obesity can contribute independently to kidney function (Espinoza *et al.*, 2006).

1.1. Kidney structure, function and relation to diabetic kidney disease

The pair of kidneys are positioned at the posterior of the lower back and is an organ responsible for the filtration of body waste in the form of urine. Healthy kidneys are

capable of filtering approximately 200 litres of blood per day, among this 1% of the filtrate are removed as waste with the rest recovered back within the circulation. This is an energy demanding process, which utilizes approximately 25 % of the overall oxygen consumption in the body for aerobic respiration. Structurally, the kidney is surrounded and protected by renal fascia, perirenal fat and renal capsule. These structures support and allow correct positioning of the kidney in the body. Internally, it is comprised of three distinct regions, which are the outer cortex, medulla and renal pelvis. Filtration and waste removal are performed in the cortex region of the kidney, specifically in nephrons. They consist of several key structures and cell types, which includes renal corpuscle, renal tubules and a vast network of capillaries. The capillaries when bundled closely together is called glomerulus, the site where blood is filtered to remove by-products from the circulation. This action is performed by the glomerular endothelial cells and podocytes, acting as sieves, to filter water and metabolites in blood plasma. High molecular weight proteins and anionic macromolecules including albumin are not filtered and are retained in blood making urine protein-free (Scott and Quaggin, 2015). Proximal tubules are long tubular structure directly connected to the glomerulus which allows water and other important metabolites and ions such as glucose, sodium and potassium to be reabsorbed to ensure extracellular body fluid levels and to maintain correct balance of salts and minerals (Agnoli and Garutti, 1976). They cover approximately 90 % of the surface of the outer cortex and the lumen of proximal tubule cell (PTC) has surface brush borders that increases its surface area dramatically for efficient reabsorption (Kruger *et al.*, 2019). The active reabsorption process is energy demanding and hence they consist of large numbers of mitochondria for energy production. However, with the prevalence T2DM caused by obesity and metabolic syndrome, it is important to have good glucose control to prevent

hyperglycaemia-associated microvascular complications leading to neuropathy, retinopathy and nephropathy (Altaf and Tahrani, 2015).

Diabetic nephropathy or DKD is defined as CKD caused by diabetes. It is common amongst the obese and is a result of vascular damage found in the glomeruli leading to mesangial expansion and reduced thickening of the glomerular basement membrane (Fioretto and Mauer, 2007). The main function of the glomerular basement membrane is to act as a non-cellular filtration barrier, however when the structure is disrupted, it can reduce glomerular filtration capacity by leakage of albumin into the urine leading to proteinuria (Figure 1). DKD is defined when there is a reduced glomerular filtration rate to less than 60 mL/min per 1.73 m^2 (Lee *et al.*, 2007). Alternative kidney damage indicators, such as proteinuria, are also used despite the underlying root cause. A population health survey conducted between 2014/15 by the Department of Health in Hong Kong revealed 0.6% of the surveyed population self-reported to have chronic kidney disease. Statistics from the Global Burden of Disease Study 2017 have shown a 33.7% increase in the number of deaths worldwide caused by CKD between 2007 and 2017. The key drivers of DKD is linked to the rising prevalence of obesity, T2DM and hypertension. As mentioned previously, obesity is a risk factor for CKD onset leading to DKD as most obese patients have a wide range of metabolic syndromes (Farah *et al.*, 2016).

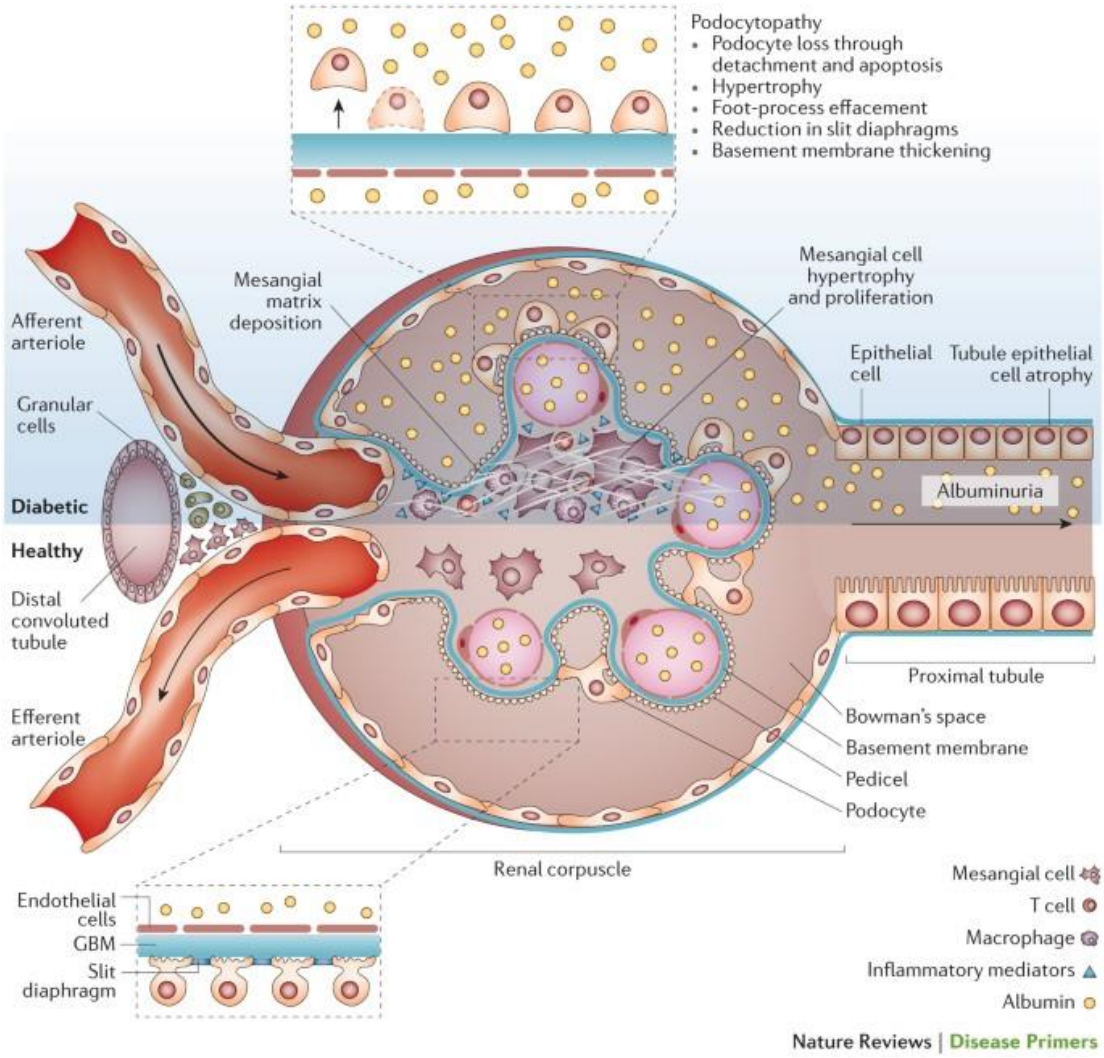

Figure 1. A summary of the morphological and functional changes of diabetic kidney disease within the glomeruli.

(Thomas *et al.*, 2015)

1.2. Mechanisms of diabetic kidney disease progression

1.2.1. Inflammation

In the obese and diabetic, pro-inflammatory cytokines such as Tumour Necrosis Factor Alpha (TNF-α) levels are moderately elevated leading to a state of chronic low-grade inflammation (Cranford *et al.*, 2016). It contributes to the progression of insulin resistance leading to DKD development (Xu *et al.*, 2003). Pro-inflammatory cytokines are regulators of the innate immune response yet they can similarly contribute to damage by initializing a large inflammatory response within the local microenvironment of the renal parenchyma by the recruitment and infiltration of inflammatory cells, particularly activated T cells and macrophages, into the glomerulus and renal parenchyma leading to PTC damage and fibrosis (Wolf *et al.*, 1991). Macrophages are responsible for the destruction of harmful organisms. After phagocytosis, they can present antigens to T cells for activation of an inflammatory response by secreting cytokines. Research have shown that inflammation with increased macrophage infiltration correlate with albuminuria and with the worsening of GFR (Reidy *et al.*, 2014).

1.2.2. Reactive oxygen species

There are multiple pathways for the generation of reactive oxygen species (ROS) in the kidney. The most common pathways are xanthine oxidase, cytochrome P450, uncoupled nitric oxide synthase (NOS) and nicotinamide adenine dinucleotide phosphate oxidase (NOX). There is a high expression of xanthine oxidase present in the kidney and it is responsible for production of ROS during the process of catalysing the oxidation of hypoxanthine to uric acid via xanthine (Kooij, 1994). Under conditions including inflammation and hypoxia and may increase the expression of xanthine oxidase further, therefore increasing the rate of ROS production (Berry and

Hare, 2004). It is reported that xanthine oxidase derived ROS can further lead to inflammation by regulating endothelial function by increasing the permeability of vessel linings and causing vasoconstriction thus, leading to hypertension which is strongly associated with atherosclerosis and cardiovascular diseases. (Briffa *et al.*, 2015). Cytochrome P450 pathway plays an indirect role in ROS generation by regulating NOXes. A study has shown that the activation of cytochrome P450, specifically, of the 4A family showed an led to an increase in NOXes regulation leading to increased ROS productions. Furthermore, the inhibition of cytochrome P450 reduced oxidative stress and have improved renal function by reduction in albuminuria in a type 1 diabetes mellites mouse model (Eid *et al.*, 2009). Nitric oxide plays an important role in the vasculature system. It is known to have positive effects such as increasing vasodilation in vessels, inhibits platelets aggregation, prevents the attachment of neutrophils to the endothelial lining of vessel structures and regulates the endothelial barrier function and modulate cell apoptosis (Moncada and Higgs, 2006). It is produced by nitric oxide synthase via the conversion of arginine to citrulline (Forstermann and Sessa, 2012). Despite its many beneficial properties, the enzyme nitric oxide synthase, under oxidative stress can further contribute to ROS production by NOS uncoupling. This process further depletes the amount of nitric oxide present but further produces superoxide anions which will worsen the endothelial cell function by vascular restriction leading to ischemia in the kidney (Goligorsky *et al.*, 2002).

As mentioned, inflammation is also generated by macrophages after they are stimulated and can further worsen kidney function by oxidation of DNA, proteins and lipids resulting in cellular damage. Furthermore, ROS in the form of hydrogen peroxide, hydroxyl radicals and superoxide anion are generated in excess with

hyperglycaemia and are also harmful to other organs. A major source of endogenous ROS is from oxidative phosphorylation in the mitochondria. Superoxide anions are produced when there is a reduced efficiency of electron transfer from nutrients to oxygen and are regulated by ROS scavenging enzymes. Superoxide dismutase (SOD) is a group of enzymes which includes Cu/Zn SOD and mitochondrial manganese SOD (Mn-SOD) that facilitates the neutralization of ROS by dismutation processing of superoxide anions to a more stable form either as water or hydrogen peroxide. Further degradation of hydrogen peroxide is required and are performed by other enzymes such as glutathione peroxidase. Oxidative stress occurs when there are excessive amounts of ROS present in the system because of imbalance of production and breakdown of ROS. As previously mentioned, the kidney is a very energy-demanding organ to perform active reabsorption and filtration. ATP is required for the active reabsorption process by the PTCs and are produced via oxidative phosphorylation. Dysfunctional mitochondria will produce less ATP and allow leakage of electrons to increase endogenous ROS levels further. Studies have shown that damage to mitochondria by high oxidative stress can lead to apoptosis of PTCs resulting in DKD. Therefore, the quality of mitochondria is an important factor that may determine kidney function.

1.2.3. Hypoxia

Another possible factor that lead to the onset and progression of DKD is hypoxia (Takiyama and Haneda, 2014). It has been reported that the kidney under hyperglycaemic conditions will result in reduced oxygenation in the renal parenchyma with increase in oxygen consumption, causing hypoxia (Lin *et al.*, 2018). Hypoxia in the kidney results in tubulointerstitial fibrosis and reduced kidney function. Due to this, hypoxia has been suggested as a possible final common pathway that contributes

further to the development of DKD leading to ESRD (Nangaku, 2004). It has been reported that hypoxia is an event that occurs in the early development of DKD and is assessed by the increase in hypoxia inducible factor-1 α (HIF-1α) in diabetic mouse kidney using mouse model. (Palm *et al.*, 2004, Rosenberger *et al.*, 2008). Under normal physiological conditions, sufficient oxygenation is achieved by determining the blood flow rate with total tissue oxygen consumption, unfortunately, it is very difficult to calculate this in the kidney as the main kidney function is to receive blood from the circulation for filtration. High circulating blood glucose is the culprit for inducing glomerular hyperfiltration as more glucose is required to be reabsorbed by PTCs through the sodium glucose cotransporters (SGLTs) which increases the sodium/potassium-ATPase activity thus increasing oxygen consumption (Jerums *et al.*, 2010). This vicious cycle will continue, leading to further increase in the demand for oxygen, leading to ischemia in the kidney contributing to the progression of DKD and ESRD (Gullans *et al.*, 1984).

1.2.4. Dyslipidaemia - Excessive ectopic lipid accumulation

The abnormal intake of lipids and lipid metabolism leads to dyslipidaemia. It is a major constituent on metabolic syndrome which represents an increased in triglyceride and reduced low-density lipoprotein cholesterol (Kolovou *et al.*, 2005). The alterations in lipid content in DKD patients are beyond the measured clinical parameters, only through detail chemical analysis of lipid sub-fractions can reveal specific lipid class changes including glycerides and phospholipids (Bobulescu *et al.*, 2014). Obese patients have the tendency to consume diet with high fat content. The extra intake of fatty acids from the diet will trigger the body to store the excessive lipid in white adipose tissue; however, the additional circulating lipids are stored in non-adipose tissues such as liver and kidney (Huang *et al.*, 2013). In the kidney, excessive lipids,

mainly triglycerides, are stored predominantly in the PTCs (Bobulescu *et al.*, 2014). Triglycerides itself is not toxic but is an active source of fatty acids, hence, the over accumulation of triglycerides leads to the build-up of potential lipotoxic fatty acids such as fatty acyl-CoA, diacylglycerols and ceramides. These compounds can subsequently trigger mechanisms related to the generation of reactive oxygen species, pro-inflammatory saturated fatty acids, and endoplasmic reticulum stress (Solinas *et al.*, 2015).

1.2.4.1. CD36

It has been proposed in the 1980s that dyslipidaemia promotes and contributes to kidney dysfunction leading to renal nephropathy (Moorhead *et al.*, 1982). It is believed that the altered lipids in the kidney causes inflammation, oxidative stress and endothelial distress. This hypothesis was put to test by many and research using both animal and human samples have shown lipids play a direct role in renal dysfunctional (Kennedy *et al.*, 2013). Specifically, PTCs prefer the use of fatty acids as their primary energy source and that any disruptions in fatty acid oxidation will lead to disrupted lipid metabolism and balance. The kidney takes up fatty acid including long chain fatty acids from the circulation and enters the PTCs via a multifunctional transmembrane glycoprotein called cluster of differentiation 36 (CD36), which also mediates the uptake of oxidized low-density lipoprotein (LDL) (Jay *et al.*, 2015). It is also responsible for the uptake of fatty acid into the kidney and is proven to play an important role in DKD development and progression. CD36 is found highly expressed in patients and animals with kidney damage and is believed that inflammation is associated with CD36 expression (Kennedy *et al.*, 2013). It is also known that renal CD36 expression is upregulated in patients with DKD (Herman-Edelstein *et al.*, 2014). Furthermore, it is reported that under hyperglycaemic conditions, the expression of

CD36 is increased in PTCs and can lead to tubular epithelial apoptosis (Susztak *et al.*, 2005). As mentioned, the disruption of fatty acid oxidation will cause altered lipid metabolism in the kidney leading to renal dysfunction and progress to renal nephropathy. Research have shown that fatty acid oxidation genes are downregulated in the kidney in both animal and humans (Kang *et al.*, 2015). Comparison between human renal biopsies of diabetics and non-diabetics show ectopic lipid accumulation in the tubulointerstitium with increased CD36 expression in the diabetic group (Herman-Edelstein *et al.*, 2014).

1.2.4.2. De novo lipogenesis and lipolysis

Lipid homeostasis is clearly disrupted in patients with metabolic syndromes. Normally, the body responds to abnormally triglyceride store by lipolysis via hydrolysis. The hydrolysis of triglycerides produces free fatty acids (FFA), which can result in different forms. It is possible through hydrolysis of lipids to form polyunsaturated fatty acids (PUFA), saturated fatty acids (SFA) and monounsaturated fatty acids (MUFA). In general, fatty acids regulate cellular metabolism by acting as agonistic ligands on a variety of nuclear receptors. When bounded, it activates these factors to promotor regions of specific gene to alter their transcription. SFA are associated with adverse effects on metabolism via sterol-regulatory element binding proteins (SREBP) (Jackson *et al.*, 2006). On the other hand, PUFAs is associated with beneficial effects such as the inhibition of fatty acid oxidation and act as feedback inhibitors lowering the production of all new fatty acids.

Adipose triglyceride lipase (ATGL) and hormone-sensitive lipase (HSL) are two common lipases involved in the hydrolysis of triglycerides to diglycerides and monoglycerides. ATGL and HSL expression are decreased in the obese insulin

resistant state (Jocken *et al.*, 2007). This partly explains the triglyceride accumulation in adipose tissues and other organs, which leads to lipotoxicity.

In high fat diet fed mice, it is known that p-adenosine 5`-monophosphate (AMP)-activated protein kinase (AMPK) is inhibited which leads to the upregulation of acetyl-CoA carboxylase (ACC) 1 at Ser^{79} and ACC2 at Ser^{212}. This results in the increase of fatty acid synthase (FAS) leading to the increase of intracellular FFA acting as a substrate for lipogenesis to acyl-CoA and to triglycerides. SREBP is another group of protein that are involved in de novo lipogenesis. SREBP1 and SREBP2 are variants of SREBP and are involved in different aspects of lipogenesis. SREBP1 main involves in fatty acid and triglyceride synthesis and SREBP2 is involved in cholesterol synthesis and uptake (Horton *et al.*, 2002). Both of these proteins are normally suppressed by the presence of phosphorylated AMPK, however, obesity induced suppression of phosphorylated AMPK leads to the increase in SREBP levels resulting to the increased de novo lipogenesis of triglycerides and cholesterol.

1.2.5. Cardiolipin and mitochondrial dysfunction

The kidney is a highly metabolic organ and requires high amounts of adenosine triphosphate (ATP) for its proper function (Pagliarini *et al.*, 2008). Mitochondria is an important organelle found in cells and is involved ATP production, which is used for vital physiological functions and for cell survival. Moreover, the mitochondria is known to be involved in cell survival and apoptosis hence, their quantity and quality are vital to circumvent cell apoptosis, especially in the kidney (Li and Dewson, 2015). The quality of mitochondria is regulated by ROS, fission and fusion and mitophagy. In the case of DKD, the damaged kidney further worsens and it is known that the mitochondria found in PTCs have a reduced mitochondrial membrane potential. Other renal diseases such as Fanconi syndrome and glomerulosclerosis share similar features

and is associated with mitochondrial dysfunction (Forbes and Thorburn, 2018). Mitochondrial dysfunction, in DKD, is caused by impaired respiratory chain function, loss of structural integrity and cristae structures which will further lead to mitochondrial proton leak which can combine with oxygen to form superoxide (Coughlan *et al.*, 2009). However, there is conflicting findings that reveal superoxide production is reduced in DKD mouse model (Dugan *et al.*, 2013). As DKD is a continuous process, the increase in superoxide formation may form only the initial stage of DK. As DKD progresses, it may lead to the reduction of mitochondrial biosynthesis and quantity, which may be a compensatory effect, leading to a reduction in superoxide formation. This reduction of total mitochondria may also reduce the overall energy production.

Under normal physiological conditions, there is a balance of fatty acid peroxidation which forms part of the oxidative signalling process (Kang *et al.*, 2015). However, in DKD, there is a high ROS content and along with a deregulation of lipid peroxidation, which leads to an excessive build-up of lipid peroxidation products (Niki *et al.*, 2005). Cardiolipin is an important lipid which is associated with the proper functioning of the mitochondria. Cardiolipin is a tetra-acyl anionic glycerol and thus contain four acyl chains attached to two phosphates. It has a unique structure where all four acyl chains are grouped on one side making the overall structure asymmetric (Lecocq and Ballou, 1964). It is this special property that gives mitochondria their curvature and cristae structures. Cardiolipin also maintains the membrane potential between the outer and inner mitochondrial membrane. Any alterations in the properties of cardiolipin found in the mitochondria will have large effects to its structure and stability (Saric *et al.*, 2015). Cardiolipin peroxidation is known to contribute to renal adiposity and its depletion contributes to mitochondrial dysfunction in the kidney (Szeto, 2014a). A

recent study have shown that there is a decrease in cardiolipin signal in the kidney of a non-alcoholic steatohepatitis mouse model which suggests the depletion of cardiolipin may play a role in the progression of DKD (Hayasaka *et al.*, 2016). Overall, the mitochondria play a critical role in supplying enough energy for the normal function of the kidney, however in DKD, there is a reduction in cardiolipin which is associated with mitochondrial dysfunction hence, further investigation should focus on the understanding the role and treatment strategies to prevent, prolong or treat DKD before progression to ESRD.

1.3. Current treatments of diabetic kidney disease

It has been nearly three decades since the first introduction of renin-angiotensin-system (RAS) inhibitors for the treatment of hypertension and it has been used as the main therapeutic method in DKD management (Bomback and Toto, 2009). It is often also accompanied by multidisciplinary treatment for glycaemic control, lipid control and other life style changes. Metformin is an affordable and effective glycaemic control drug and exerts its effect mainly by decreasing gluconeogenesis in the liver via the activation of AMPK and increasing insulin sensitivity by an increase in the recruitment of GLUT4 glucose transporters for insulin-dependent glucose uptake (Musi *et al.*, 2002, Yang and Holman, 2006). Comparing it with other T2DM control drugs such as sulfonylureas and insulin, it shows greater effect in the prevention of end-point diabetes-related outcomes. Studies have also shown that metformin also has additional beneficial effects on DKD by reducing inflammation and ROS, leading to renal tubular fibrosis (Kawanami *et al.*, 2016, Kawanami *et al.*, 2017, Opazo-Rios *et al.*, 2020). Metformin has a half-life of approximately five hours and that it is excreted, as is, via the kidney in the urine. Therefore, DKD patients, with a reduced eGFR < 30 ml/min per 1.73 m^2 have an increased risk of adverse side effects such as

hypoglycaemia and lactic acidosis, from the reduction of gluconeogenesis and metformin use should be stopped.

1.3.1. Renin-angiotensin-system inhibitors

As mentioned, RAS inhibitors are the most common and traditional drugs prescribed to DKD patients. RAS inhibitors include two class of drugs namely angiotensin-converting-enzyme (ACE) inhibitor and angiotensin II receptor blocker (ARB). The main purpose of prescribing these drugs are to reduce the production of angiotensin II and the activation of angiotensin II receptors, which aims to prevent vasoconstriction which contributes to cardiovascular diseases and hypertrophy. In DKD, RAS inhibitors have shown to reduce disease progression by lowering of blood pressure. As a result, will reduce the glomerular pressure leading to reduced hyperfiltration (Lewis *et al.*, 1993). This was proven through a series of RCTs which includes The Collaborative Study Group which uses Captopril as the ACE inhibitor (Lewis *et al.*, 1993), The Reduction of Endpoints in NIDDM with the Angiotensin II Antagonist Losartan (RENAAL) which uses Losartan as the ARB inhibitor (Brenner *et al.*, 2001) and The Irbesartan Diabetic Nephropathy Trial (IDNT) which uses Irbesartan as the ARB inhibitor. The measured outcomes from RCTs showed a reduction in the rate of progression to DKD, independent of the effects of blood pressure lowering, by lowering the risk of increasing serum creatinine and associated risks to ESRD, transplant and death (Ravid *et al.*, 1993). Although the use of RAS inhibitors is common, it was believed that the combination therapy of both ACE inhibitor and ARB inhibitor may show greater renoprotective effects. Interestingly, studies have shown that a combination therapeutic strategy further increased the risk of acute kidney injury, hyperkalaemia and reduction in eGFR rate. Although the combination therapy reduced proteinuria, there is still an overall worsening to renal function and outcomes leading

to the early termination of some RCTs (Fried *et al.*, 2013, Mann *et al.*, 2008). Overall, RAS inhibitors are effective in reducing the rate of decline of renal function in DKD but unable to prevent the eventual progression to ESRD. The major side effects of patients taking RAS inhibitors are hypotension, hyperkalaemia and reduction of renal function (Yacoub and Campbell, 2015).

1.3.2. Sodium-glucose cotransporter 2 inhibitors

Sodium-glucose cotransporter 2 (SGLT2) inhibitors is another class of drugs recommended for patients with T2DM and CKD. SGLT2 inhibitors can reduce blood glucose levels by inhibiting the reabsorption of glucose by the renal tubules via SGLT2, leading to glycosuria. Renal output will also increase due to altered osmotic gradient caused by glycosuria (Ansary *et al.*, 2019). SGLT2 inhibitors have shown to reduce the risk of negative cardiovascular and renal outcomes through RCTs. In Empagliflozin Cardiovascular Outcome Event Trial in Type 2 Diabetes Mellitus Patients-Removing Excess Glucose (EMPA-REG OUTCOME) and other similar RCTs measured cardiovascular outcome as their primary aim whilst kidney outcomes secondary. For the kidney, key outcomes including the increase in albuminuria, serum creatinine and a deterioration of the eGFR $\leq$ 45 ml/min per 1.73 m^2, kidney transplant or renal death was considered. Patients taking the SGLT2 inhibitor showed a lower worsening in kidney outcomes versus the control group (Zinman *et al.*, 2016). Another important RCT called Canagliflozin and Renal Events in Diabetes with Established Nephropathy Clinical Evaluation (CREDENCE) was designed specifically for measuring primary kidney outcomes to assess the ability of SGLT2 inhibitor, canagliflozin, on renal outcomes of patients with T2DM. Overall, patients in canagliflozin group showed 30% lower risk of worsening in kidney outcomes including the increase in serum creatinine, progression to ESRD or death. Secondary

measurements for kidney outcomes such as the need for kidney dialysis and transplant were reduced significantly (Perkovic *et al.*, 2019). SGLT2 inhibitors show kidney function benefits by the inhibition of SGLT2 at the PTCs and it is observed that there is a reduction in glomerular hyperfiltration which reflects by a reduction in albuminuria and improved eGFR (Mori *et al.*, 2009). As glucose is prohibited from being reabsorbed by the PTCs, sodium is also allowed to pass from the PTCs, increasing natriuresis, to the mascula densa cells of the distal tubule cells to improve tubuloglomerular feedback (Kato and Natarajan, 2019). Despite the benefits, the exact mechanism of the renoprotective effects is not well understood, however, there are still risks involving the use of SGLT2 inhibitors. The most common side effect is genital mycotic infections and a possible chance of ketoacidosis. Current practice would limit the use of this class of drug to patients with eGFR $\geq$ 30 ml/min per 1.73 m^2 as there is a lack of evidence from RCT conducted on patients with low eGFR < 30 ml/min per 1.73 m^2.

1.3.3. Glucagon-like peptide-1 receptor agonists

Glucagon-like peptide-1 (GLP-1) is an incretin that was found after the sequencing of proglucagon molecule in 1985 (Schmidt *et al.*, 1985). GLP-1 is formed from 92-128 amino acid of proglucagon and exerts insulintropic properties only in its active form of 7-37. GLP-1 is secreted in the intestine after oral ingestion of glucose and exert the secretion of insulin from ß-cells in a glucose-dependent manner (Doyle and Egan, 2007). Endogenous GLP-1 is readily degraded endogenously by dipeptidyl peptidase-4 (DPP-4) and only has an estimated half-life of 1.5 – 2 min. This limits the ability for GLP-1 as a potential long-term incretin for glycaemic control in T2DM patients. However, long-acting GLP-1 receptor (GLP-1R) agonists were created to mimic the structure of GLP-1 and are enhanced to prevent the endogenous degradation by DPP-

4. This has led to a new class of glycaemic control drugs. It has been noted that GLP-1Rs not only improve blood glucose control, but also show potential renoprotective benefits in the prevention of albuminuria and maintaining eGFR in diabetic patients as GLP-1Rs are found in organs including the kidney and the heart (Tanaka *et al.*, 2014). Several RCTs were performed on the use of different variants of GLP-1RA drugs and assessed their effect on kidney outcomes. In the Liraglutide Effect and Action in Diabetes: Evaluation of Cardiovascular Outcome Results (LEADER) trial, liraglutide is the GLP-1R agonist, kidney outcomes were compared between the liraglutide and placebo group. There is a significant 22% overall reduction in the worsening of kidney outcome and mainly contributed by the prevention of new albuminuria cases (Mann *et al.*, 2017). Furthermore, in the Researching Cardiovascular Events with a Weekly Incretin in Diabetes (REWIND) trial, patients with T2DM and cardiovascular risk factors were recruited for either weekly subcutaneous administration of dulaglutide or placebo for two years and their renal component of the composite microvascular outcome was investigated, as part the secondary outcome. Overall, there is a clear reduction of new severe albuminuria, sustained decline in eGFR of 30% and requirement for renal transplant in the dulaglutide-treated group. Long-term use of dulaglutide show beneficial effects for renal function mainly by reduction in albuminuria progression with minimal adverse side effects (Gerstein *et al.*, 2019). Another trial called the Assessment of Weekly Administration of LY2189265 (Dulaglutide) in Diabetes 7 (AWARD-7) compared between the use of dulaglutide over insulin glargine in patients with CKD. The eGFR and albumin-creatinine ratio were measured as the secondary outcomes showed a significantly less decline in eGFR. Renal benefits were observed also in patients with severe albuminuria however, gastrointestinal side effects were seen. In this study, dulaglutide have shown good

overall performance and safety in glycaemic control and renal composite outcomes in severe cases of CKD and has received approval from the Food and Drug Administration (FDA) for dulaglutide to be used in diabetic patients with eGFR ≥ 15 ml/min per 1.73 m^2 (Tuttle *et al.*, 2018).

2. UHPLC/ESI-QTOF-MS based metabolomics

2.1. Introduction to metabolomics

Since the success of the Human Genome Project, researchers around the world have used the database as a tool to understand and discover genes responsible for genetic diseases (Collins and Fink, 1995). However, not all diseases are caused by genetics and are a result of a combination of factors. In the biological system, genes are made of DNA and is hereditary. It is the starting point for protein production and consists of two major steps, transcription and translation. Transcription is a process where a DNA information is replicated to a messenger RNA (mRNA) which contains the 'message' or recipe for subsequent translation of the code for protein synthesis. The interactions between genetics, transcriptomes and proteins form only part of the story for disease phenotype and pathogenesis **(**Figure 2**)**. The discovery of new treatments, early diagnosis and monitoring are restricted by the limited data obtained from these correlations thus, it is important to overcome these hurdles by developing new research techniques. Around two decades ago, The National Institute of Health (NIH) has committed to a roadmap to address the urgent need for the discovery and understanding of complex biological pathogenesis pathways using metabolomics (Zerhouni, 2003). Metabolomics, as defined by Fiehn, is "a comprehensive and quantitative analysis of all metabolites" that can reveal the metabolome of samples within a study to help researchers understand in more detail the exact biological interactions between groups (Fiehn, 2001). The metabolome consists of a highly diverse group of compounds including amino acids, sugars, organic acids, nucleotides and lipids. They all have a wide range of chemical properties and their concentration can vary within the biological system. Metabolites are responsible for the metabolic reactions that occurs for the normal functioning of cells and organs and is disrupted in the diseased thus,

metabolites represent the most downstream candidates caused by gene expressions and plays a huge role in the determinants of the final biological status and phenotype (Færgestad *et al.*, 2009). Metabolomics can be performed on a variety of sample types including tissue, serum, urine and cells (Turi *et al.*, 2018). By performing metabolomics studies, one can compare and identify important changes between different states during or after disease pathogenesis in tissue or cells. The changes in metabolites can be used to trace upstream candidates to elucidate potential molecular pathway alterations or be used as potential biomarkers for early disease diagnostic indicators or recovery (Gieger *et al.*, 2008).

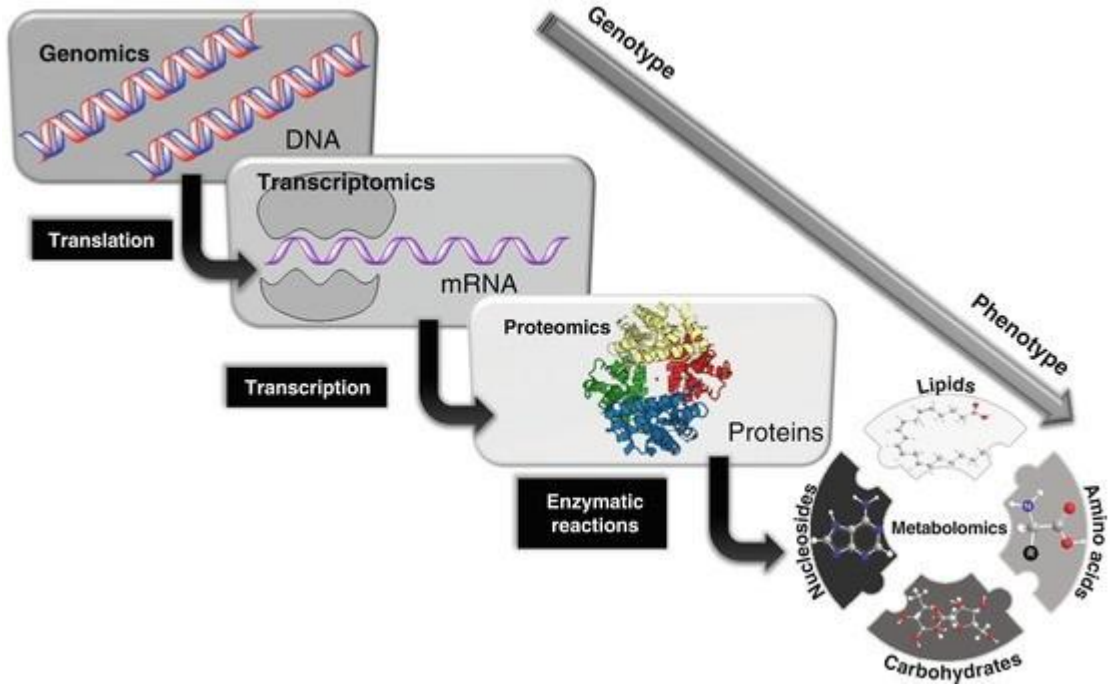

Figure 2. A schematic diagram representing the interrelationship between the different omics techniques and their applications in biological studies.

(Klassen *et al.*, 2017)

2.2. Untargeted metabolomics

Generally, metabolomics studies are separated into two different strategies, either targeted or untargeted metabolomics. In brief, the major difference between these two methods is the study objective. Targeted study is a type of hypothesis-testing, which assesses known metabolite targets of interest, that may be related to their chemical structures or that of a specific metabolic pathway, are quantified. However, this method is limited by the amount of currently known metabolites and the availability of stable internal standards used for calibration and absolute quantifications (Ioannidis and Khoury, 2011). Untargeted metabolomics study is a form of hypothesis-generating experiment that is an unbiased analysis of samples for the determination of changes in compound abundances under different physiological conditions (Fiehn, 2002). This method is unbiased as no metabolites were first selected for sample analysis however, the use of different analytical systems and conditions may enhance the collection of metabolite data thus, by having a prior understanding of possible changes in selected metabolites or metabolite groups, the metabolite extraction and running conditions of the analytical tools can be optimized. Similar to targeted metabolomics, the identification of compounds is limited to the availability of known chemical standards and that the process of untargeted metabolomics requires significantly more time for the samples to be processed. However, the benefits of untargeted metabolomics study can reveal differential compounds between groups and these candidates may potentially be used as novel biomarkers. Other limitations of using untargeted metabolomics approach is ensuring the stability of the analytical tool such as liquid chromatography coupled with a mass spectrometry (LC-MS), the difficulties in data processing and analysis and the identification of compounds. Depending on the method of sample preparations, the detection of interesting compounds may also be

affected by the highly abundant metabolites within the sample, leading to a relative weakening in signal detection (Roberts *et al.,* 2012). Untargeted metabolomics has been applied to areas such as ethnopharmacology for evaluating the therapeutic response and discovery of biomarkers after treatment (Xiao *et al.,* 2018).

2.3. General workflow

Metabolomics study nowadays is mass spectrometry (MS)-based, we will briefly introduce the workflow based on this platform. The workflow for conducting either targeted or untargeted metabolomics study is very similar. The fundamental steps include sample collection, preparation, sample analysis by firstly metabolite separation followed by detection by a mass spectrometry, data import and processing and finally data analysis.

To begin, sample collection is an important aspect of metabolomic studies. The samples used is mostly hypothesis driven. The number of samples is also an important factor, especially when conducting experiments with animal or human samples as there is a wide range of variation in their background. This may include their gender, age, diet and even genetics. Therefore, it is important to conduct statistical analysis prior the metabolomics experiment to ensure sample number is of satisfactory. Once the samples are collected, they are required to be prepared in a manner that is capable of being analysed by a MS. To preserve the integrity of the samples from degradation due to enzymes present in the sample and oxidation, quenching is performed to inhibit these processes and this can be done by using cold solvents or by freezing in liquid nitrogen. Once quenched, the samples are further stored in -80 °C before sample preparations. When handling with tissue samples such as the kidney and liver, additional step of tissue homogenization is required. There are a few ways to homogenize the tissue and includes freeze-drying the then crushed into a powder or

using a bead homogenizer prefilled with extraction solvents. Nevertheless, any form of additional sample preparation will eventually contribute to loss of metabolites and may reduce signal detection afterwards. It is important to minimize the necessity for additional sample preparation when planning any metabolomics study.

Both solid and aqueous based samples require metabolite extraction before analysis. The most commonly used extraction method is the liquid-liquid extraction (LLE). As mentioned previously, this step can be integrated in sample collection for tissues. Organic solvents such as methanol, ethanol or acetonitrile are used for the separation of hydrophilic metabolites whilst chloroform is used to extract lipophilic metabolites. A classic method for sample preparation is the "Bligh and Dyer" method which uses a mixture of chloroform/methanol/water. This will result in a phase separation which allows the collection of polar metabolites from the top phase whilst lipids will be separated in the bottom phase. Furthermore, depending on your experimental design and objectives, not all samples require sample extraction. Urine can be diluted and directly injected into the analytical tool for metabolomic studies (Khamis *et al.*, 2017). By doing so, there is theoretical no metabolite loss via sample preparations and extractions. Depending on the sample type, most biological samples are high in salt contents and may cause ion suppression and adduct formation, leading to high contamination in the analytical equipment. Hence, by using types of chromatography for compound separation can remove the excessive background and also reduce the contamination in sample analysis, to produce high quality, comparable and repeatable results.

To reduce the previously mentioned effects, biological samples can be analysed by firstly separation by chromatography coupled to an MS. Liquid chromatography is one of the common methods for metabolite separation and with technology advancement,

ultra-high-performance liquid chromatography (UHPLC) is now available. A commonly used column for reverse-phased chromatographic separation of metabolites is the C18 column. The high quantity of carbons attached to the silica created a bigger surface area and higher resistance for the metabolites to travel past. This allows a slower elution of compounds but with higher separation ability. The output of the chromatographic separation will be directly injected into an MS for sample analysis.

A mass spectrometry is an analytical tool that can separate and measure the abundance of mass-to-charge ratios (m/z) by coupling with a detector (Chernushevich *et al.*, 2001). The quadrupole-time of flight mass analyser (QTOF/MS) is a powerful and robust instrument that is capable of obtaining highly accurate mass measurements with good resolution for compound identification and for subsequent compound structural identifications. Structural identification is performed by utilizing the first quadrupole as a mass scanner and can selectively 'pick' precursor ions of interest for tandem MS/MS. As this system has a high mass accuracy reading with low mass error between 2- 5 ppm, the use of UHPLC/ESI-QTOF-MS as a platform for untargeted metabolomics has thus gained in popularity (Kofeler and Gross, 2005).

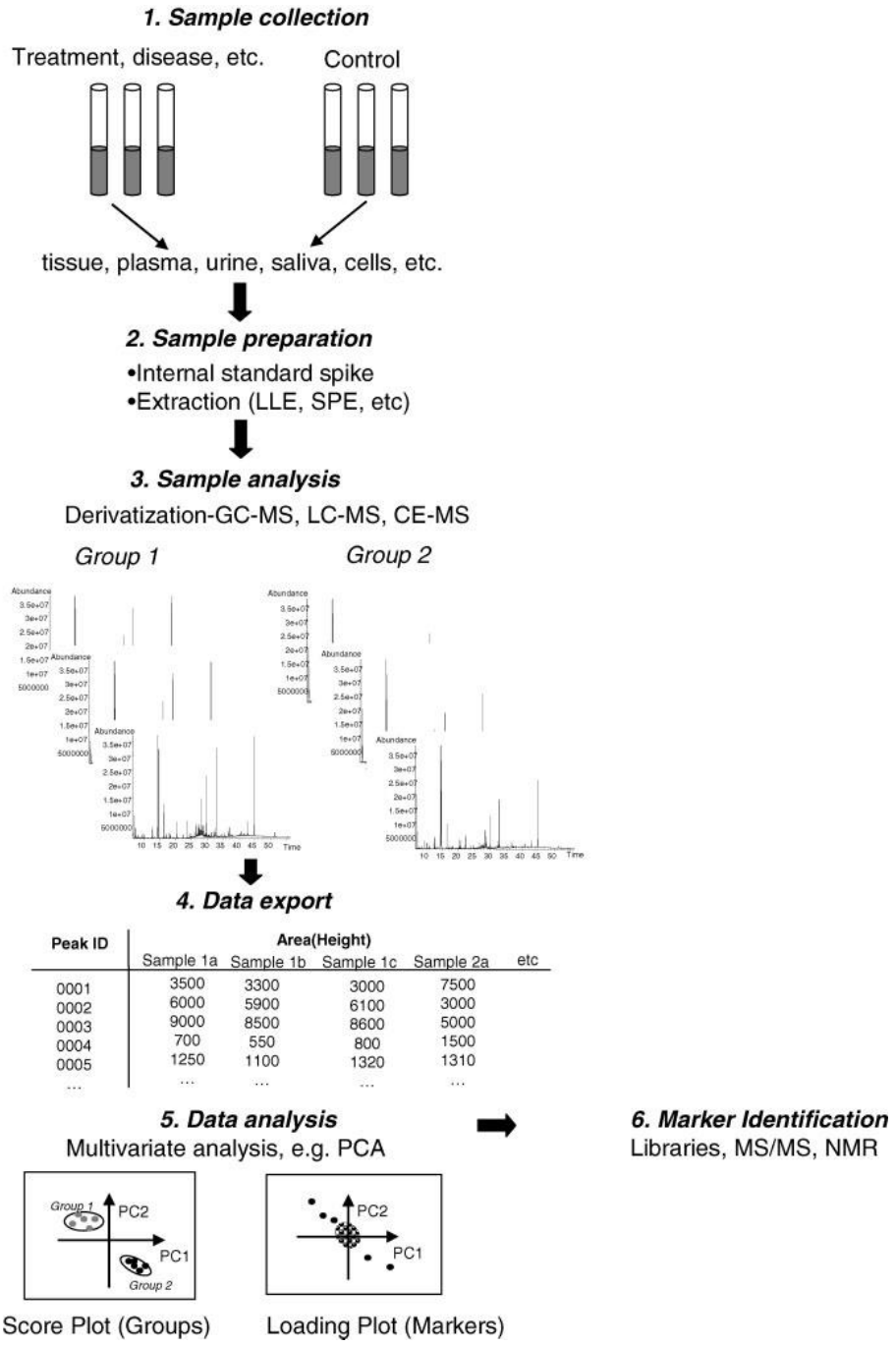

Figure 3. Schematic of the general metabolomics workflow

(Dettmer *et al.*, 2007)

2.4. Analysis and interpretation

Once the metabolite data is collected from the mass spectrometry, the raw data is required to be pre-processed by analysis software such as Progenesis QI. Afterwards, univariate and multivariate analysis will be performed to highlight and identify possible relationships and targets of interests within samples. By performing statistical analysis, the objective is to allow the categorization of your samples into different groups, based on their metabolic profile differences or similarities. Mass spectrometry data collected contains specific information about each compound and is represented by their m/z and their signal intensity. This data is normalized by analysis software using total ion count method which in short is performed by dividing the spectrum of each metabolite by the total ion count in a sample before analysis (Veselkov *et al.*, 2018).

The common statistical analysis in use for metabolomics analysis are Principal Components Analysis (PCA), orthogonal partial least-squares-discriminant analysis (OPLS-DA) and partial least squares-discriminant analysis (PLS-DA). In brief, PCA is an unsupervised method for dimension reduction of a dataset whilst retaining the variability within the dataset. Furthermore, this method of analysis provides a general overview of class separation and for the identification of potential outliers. This can be caused by the sample preparations process, contamination of samples or a result of an unstable data acquisition. OPLS-DA is a supervised model approach that allows the maximum separations of data between two groups. The continuous data, representing the signal intensity of specific m/z are divided into two classes. This allows a clear separation between the control and intervention groups in an experiment. Importantly, this allows the identification of new variables or compounds of interest (Jolliffe and Cadima, 2016). PLS-DA is also a supervised model approach for discrimination of

more than two classes (Barker and Rayens, 2003). Samples are represented in a scores plot which can be interpreted by observing the distance of each sample from the origin. The loading plot allows the identification of potential compounds that are highly correlated to a specific class.

2.5. Data interpretation

Once potential compounds are identified from the statistical analysis, they are required to be 'matched' or identified based on their mass spectrum and fragmentation patterns. This information will be uploaded to online biochemical databases such as the Human metabolome Database (HMDB) or LIPID MAPS structure database (LMSD) for comparison of known metabolites with the experimental data. In untargeted metabolomics, there will be multiple potential metabolites that contributes to disease pathogenesis or recovery; in order to analyse these metabolites in relevant manner, metabolic pathway and enrichment analysis could be performed. This process allows the metabolites previously identified to be matched or be represented in their related pathways. By doing so can enhance the interpretability of the metabolite results and allow a better insight into the underlying pathways involved in the process of pathogenesis or recovery. This method of analysis can act as a platform for novel biomarker discovery or used to reveal possible pathways altered or involved in disease progression or prevention. A few common online software used for this type of analysis includes MetaboAnalyst, Kyoto Encyclopedia of Genes and Genomes (KEGG) Pathway and Ingenuity Pathway Analysis (Chong *et al.*, 2019, Kanehisa *et al.*, 2017, Kramer *et al.*, 2014).

3. Objectives of this study

DKD is caused by diabetes and is an epidemic. The slow degradation of the kidney function, due to pathomorphological changes caused by vascular damage in the glomerulus can lead to basement membrane and mesangial cell expansion (Fioretto *et al.*, 2007), will eventually lead to end-stage renal disease.

Currently, it is known that there are multiple factors that may contribute to the progression and worsening of DKD, examples include but not limited to, inflammation, ROS, hypoxia and dyslipidaemia. Obesity is known to be associated with chronic inflammation which causes the release of pro-inflammatory cytokines. This can lead to the infiltration of macrophages and can cause renal interstitial fibrosis leading to PTC damage (Wolf *et al.*, 1991). Dyslipidaemia is also a symptom in diabetic patients, as obesity worsen, insulin resistance increases resulting in the development of high triglycerides present with excessive ectopic lipid accumulation in the kidney (Trouwborst *et al.*, 2018).

Previous studies have shown that GLP-1R mRNA and protein expression are also present in rat and human renal proximal tubules (Crajoinas *et al.*, 2011, Schlatter *et al.*, 2007) and that treatment with GLP-1R agonist may play a role in renoprotection (Mann *et al.*, 2017, Gerstein *et al.*, 2019, Tuttle *et al.*, 2018). Its activation on GLP-1R may be responsible for the improvement of kidney function by inhibition of inflammation and ROS production (Kawanami and Takashi, 2020), however, the direct mechanism of how GLP-1R agonist may exert its renoprotection requires further investigation.

The objective of this study is to develop a simple and robust untargeted metabolomics analysis platform with the use of ultra-high-performance liquid chromatography for metabolite separation and detection by quadrupole time-of-flight mass spectrometry.

The developed platform will be used to study the altered metabolites in diabetic kidney disease.

A DKD mouse model will be established and the mice with DKD will be treated with a GLP-1R agonist, dulaglutide, for 4 weeks for the study of renoprotective effects. Kidney function and mice body composition will be measured before and after treatment whilst metabolic and behaviour screening will also be performed to study these changes. Afterwards, the mice will be sacrificed and the kidneys used to identify important metabolite changes involved in renoprotection. To further clarify the deposition of metabolite changes, MALDI-MSI technique will be developed to spatially visualize and quantification of metabolite changes in the kidney in a label-free manner.

4. Material and methods

4.1. Animal model

C57BL/6 male mice of 8 weeks old were purchased from the Centralized Animal Facility of The Hong Kong Polytechnic University (Hong Kong SAR, China). Throughout the experiment, all mice were housed in a temperature (25 ± 2 °C) and humidity (60 ± 5% RH) controlled environment with 12-hour light and dark cycle. Mice were given *ab libitum* access to water and diet.

Mice after acclimation for 7 days in their housed environment, they were divided randomly, using a random number generator into three sub-groups: standard chow control (STC), high-fat diet (HFD) and high-fat diet with dulaglutide treatment (H+Dula). STC group will act as the standard lean control group, HFD as the induced diabetic nephropathy group and H+Dula as the diabetic nephropathy group with dulaglutide treatment to observe for improved renal outcome. Standard chow consists of 13.2 % fat, 24.7 % protein and 62.1 % carbohydrates (PicoLab Rodent Diet 20 #5053, St. Louis, USA). High-fat diet was purchased from Research diets Inc., New Brunswick, USA and the diet consists of 60 % fat, 20 % protein and 20% carbohydrates. STC mice were fed with standard chow, the other groups were fed with high-fat diet for 12 weeks. After 12 weeks, the treatment group was intraperitoneally administrated with dulaglutide in the morning at a dose of 0.6 mg/kg body weight at the end of each week, once every 7 days and lasted for 4 weeks. STC and HFD group mice were administered with sterile saline instead as control for treatment intervention.

The body weights of each mouse were measured at the start of the week, weekly. Fasting and fed glucose were measured after 12 weeks of standard chow or high-fat diet feeding. After 4 weeks of dulaglutide treatment, fasting and fed glucose were also measured. 24-hour urine volume was measured and collected before and after

dulaglutide treatment. Mice were transferred to individual cages with *ab libitum* access to water and diet. The mice were left to acclimatize for 24 hours prior to urine volume measurement and collection. The urine collected were centrifuged at 2.0 ×g for 10 min at 4 °C, aliquoted and stored at -80 °C before analysis. Metabolic and behavioural screening was performed before and after dulaglutide treatment. The mice were individually housed with *ab libitum* access to water and diet. The mice were left to acclimatize for 24 hours prior to metabolic and behaviour screening. The parameters are digitally recorded for subsequent analysis. Intraperitoneal glucose tolerance test (IPGTT) was performed before and after dulaglutide treatment. Mice were fasted overnight for 16 hours with *ab libitum* access to water only. Basal tail vein fasting blood glucose was obtained and measured before intraperitoneal injection of D-glucose solution at a dose of 1.5 g/kg/mouse. After treatment for 4 weeks, the mice were fasted overnight for 16 hours overnight and then sacrificed with overdose of anaesthetics. Cardiac puncture was performed for the removal of blood followed by collection of metabolic organs including the kidneys were weighted, harvested and separated for snap-freezing in liquid nitrogen or formalin-fixed for subsequent analyses.

The experimental design and protocol were submitted to the Animal Subjects Ethics Sub-committee (ASESC) of The Hong Kong Polytechnic University and was approved with ASESC number 18-19/23-HTI-R-GRF. Animal license was also obtained from the Department of health of The Government of the Hong Kong Special Administrative Region under the Animals (Control of Experiments) Ordinance (Cap. 340) with license number: Rev (20-225) in DH/HT&A/8/2/4 Pt.3. All animal procedures were handled in accordance to the Guide for the care and use of laboratory animals based on the Declaration of Helsinki.

4.2. Glucose measurements

Fed glucose was measured in the morning, early in the week. For fasting glucose, mice were fasted overnight for 16 hours and tail-vein blood glucose was measured using the Accu-Chek® glucometer (Roche Diagnostics, Indiana, USA).

4.3. Glucose tolerance test

To conduct intraperitoneal glucose tolerance test (IPGTT), the animals were fasted overnight for 16 hours and baseline plasma glucose was measured using an Accu-Chek® glucometer (Roche Diagnostics, Indiana, USA). Immediately, the mice were given D-glucose solution at a dose of 1.5 g/kg/mouse. Blood glucose was measured from tail-vein at 0, 15, 30, 60, 90, 120 and 180 min post-intraperitoneal injection.

4.4. Urinary albumin and creatinine test

To quantify urinary albumin and creatinine, the collected urine was thawed on ice at 4 °C and vortexed. Urinary albumin and creatinine enzyme-linked immunosorbent assay (ELISA) kit was purchased and performed in accordance to manufacturer protocol.

For urinary albumin, briefly, 50 μL of diluted urine (1:6000) was added to 96-well plate and incubated with albumin antibody cocktail. The samples were incubated up to 1 hour at room temperature on an orbital shaker set at 400 rpm. After washing, the sample mixture was incubated with a development solution for 10 min in the dark at room temperature on an orbital shaker set at 400 rpm for 10 min. A stop solution was applied and the final solution was shaken on an orbital shaker. To determine the concentration, optical density was measured at 450 nm using a microplate spectrophotometer system (Benchmark Plus, BIO-RAD, California, USA).

For urinary creatinine, 200 μL of diluted urine (1:20) was added to 96-well plate and incubated with creatinine reaction reagent. The sample mixture was incubated on an orbital shaker set at 400 rpm at room temperature. To determine the concentration of urinary creatinine, optical density was measured at 490 nm using a microplate spectrophotometer system (Benchmark Plus, BIO-RAD, California, USA).

4.5. Metabolic and behavioural screening

To measure the metabolic and behaviour of mice, mice were individually housed in metabolic cages with free access to water and diet. Briefly, mice were left to acclimatize for 24 h before data collection. The metabolic cages are placed in a temperature-regulated environmental control cabinet set at 23 °C with 12-hour light and dark cycle (Promethion BX1, Sable Systems International, Las Vegas, USA). Parameters measured are total volume intake of oxygen, output of carbon dioxide, body weight and cumulative food intake, water intake, energy expenditure and movement in 24 h. The respiratory exchange ratio (RER) was also calculated.

4.6. Body composition analysis via ^{1}H Nuclear magnetic resonance

Mice body composition was measured before and after treatment. In brief, each mouse is individually transferred into a compressed chamber to prevent movement. The chamber is placed into an ^{1}H Nuclear magnetic resonance-based analyser (^{1}H-NMR) (MiniSpec LF90, Bruker, Germany). Fat, lean and fluid mass and percentage mass over body weight are measured. Lean fat ratio is further calculated.

4.7. Histological analysis of kidney tissue

4.7.1. Tissue fixation and slide preparation

After the mice are sacrificed, metabolic organs were collected. For the kidney, it was bisected and inserted into a histology cassette for fixation in 10% neutral buffered

formalin for 24 hours. Afterwards, the tissues are dehydrated in increasing grades of ethanol, cleared and infiltrated with paraffin wax in a tissue processor (Excelsior AS, Thermo Scientific, USA). The infiltrated tissue is paraffin-embedded onto the base of the histology cassette as formalin-fixed paraffin embedded blocks (FFPE) and were left to cool on ice. In order to produce thin tissue sections, microtomy was performed using a Leica RM2235 manual rotary microtome (Leica Biosystems, Wetzlar, Germany). Briefly, the FFPS blocks were trimmed until the largest surface area is exposed, and the tissues were sectioned at 4 μm in thickness. The sections were gently placed on a water bath filled with distilled water and set at 42 °C to float and to be "fished" up onto a glass slide. The prepared slides were left to dry in a temperature-regulated oven set at 37 °C overnight before staining.

4.7.2. Slide deparaffinization and rehydration

Briefly, the prepared slides are heated on a heat plate for 10 min and deparaffinized in two tanks of xylene for 3 x 5 min each. The tissues are rehydrated in ethanol for 3 x 5 min starting from 100%, 100%, 95% and 70% followed by immersion in running tap water for 10 min.

4.7.3. Haematoxylin and eosin stain

Haematoxylin and eosin (H&E) staining was performed for the study of morphological changes. Haematoxylin stains cell nuclei purple and eosin stain the cytoplasm pink. The hydrated tissue is stained in Harris's haematoxylin solution for 10 min, rinsed in running tap water to remove excessive solution for 10 sec, differentiated in 1% acid alcohol solution for 5 sec and bluing of nuclei was performed in Scott's tap water for 10 sec before rinsed in running tap water. Tissue is counterstained in eosin for 3 min and rinsed briefly in running tap water to remove excess staining.

4.7.4. Periodic acid-Schiff methenamine stain

Periodic acid-Schiff methenamine (PASM) staining was performed for the detection of dialdehydes. It is useful for the visualization of the renal glomerular basement membrane. Briefly, the hydrated tissue is rinsed in distilled water for 1 min and subsequently treated in 1% period acid for 10 min for oxidation. Slides are rinsed in distilled water and were immersed in freshly filtered silver methenamine solution and incubated in a pre-heated water bath set at 60 °C for 35 min. The slides are rinsed in distilled water and toned in 0.1% gold chloride solution until tissue become pale grey. After rinsing in distilled water, 1% sodium thiosulphate was applied to stop further silver staining and to remove background staining. Slides are rinsed in running tap water for 1 min prior to Harris's haematoxylin staining for 15 min, differentiated and blued as previously described and eosin was stained for 3 min. Excessive eosin stain was removed by briefly rinsing in running tap water.

4.7.5. Dehydration, clearing and mounting

Stained sections on slides are dehydrated, cleared and mounted onto a glass coverslip for the protection of the tissue and preservation of the stain. Briefly, stained slides are dehydrated by immersion in increasing concentration of ethanol starting from 70%, 95%, 100% and 100% for 3 x 5 min. The ethanol is cleared in two tanks of xylene for 3 x 5 min and the slides are coverslipped in a xylene-based mounting medium and left to dry overnight before microscopic examination and analysis.

4.7.6. Fresh tissue and slide preparation

After the mice are sacrificed, metabolic organs were collected. For the kidney, it was bisected and transferred to an Eppendorf for snap freezing in liquid nitrogen for 5 min before stored in -80 °C. In order to obtain a thin section of fresh tissue, cyrosectioning was performed using a cryostat (Cyrostar NX70, Thermo Scientific, USA). Tissue was

trimmed and sectioned at 8 μm in thickness with chamber and blade temperature set at -15 °C and -10 °C respectively. The sections were thaw-mounted onto glass slides for subsequent staining.

4.7.7. Oil red o staining

Oil red o (ORO) staining was performed for the visualization of neutral lipids in tissues. Freshly sectioned tissue on glass slides were rinsed in distilled water before briefly fixed in 4% neutral buffered formalin for 5 min. The slides are gently rinsed in running tap water for 5 min and are immersed in freshly prepared oil red o reagent (Biognost, Croatia) for 10 min. Afterwards, excessive oil red o reagent was rinsed off in running tap water and counter stained with Mayer's haematoxylin with Lillie's modification for 1 min. Slides were rinsed gently under tap water for 5 min. The slides are mounted on to a glass slide using an aqueous mounting medium for subsequent microscopic analysis.

4.7.8. Immunohistochemical staining

Immunohistochemical (IHC) staining was performed to semi-quantify and visualize spatially specific protein expression of interest on tissue sections. Briefly, the hydrated tissue is subjected to heat-induced epitope retrieval using sodium citrate antigen retrieval buffer, pH 6.0, in a microwave set at medium power for 20 min. The tissue in solution was left to cool to room temperature and was rinsed under running tap water for 5 min. 3% hydrogen peroxide, acting as a peroxidase inhibitor, was applied on top of the tissue section in a staining box for 5 min at room temperature. The slides were washed for 3 x 5 min in phosphate-buffered saline (PBS) in a coplin jar. To minimize nonspecific staining with antibodies, 10% foetal bovine serum (FBS) was applied on the tissue section for 30 min in room temperature and enclosed in a moist staining box. The slides were washed for 3 x 5 min in phosphate-buffered saline (PBS) in a coplin

jar. The antibody specific to your protein of interest is added on to the tissue section evenly and incubated in an enclosed staining box for 30 min and placed in a water bath set at 37 °C. Afterwards, the antibody solution is gently poured away and washed in PBS for 3 x 5 min in a coplin jar. In order to visualize the antibody binding, a second antibody conjugated with horseradish peroxidase was applied onto the tissue section in a staining box for 30 min at room temperature. Tissue section was washed in PBS for 3 x 5 min to reduce background noise and non-specific staining. A substrate-chromogen, 3,3'-Diaminobenzidine (DAB), was incubated on the tissue section in an enclosed staining box for 15 min at room temperature. To stop the reaction, the slides are immersed in running tap water for 2 min. Counterstaining with Mayer haematoxylin for 30 sec and blued in Scott's tap water for 10 sec was performed to lightly visualize the nuclei of cells to allow differentiation of cell types or region within the tissue section for subsequent analysis. Slides are rehydrated, cleared and mounted as previously mentioned.

The antibodies and the parameters used in this study are as follows:

Table 1 List of antibodies used for immunohistochemical staining

Primary antibody	**Species**	**Dilution**	**Type**	**Supplier**	**Catalog number**
Glp-1r	Rabbit	1:200	Monoclonal	Abclonal	A8547
Kim-1	Rabbit	1:200	Monoclonal	Abclonal	A2831
Secondary antibody		**Dilution**	**Type**	**Supplier**	**Catalog number**
Anti-rabbit IgG		1:1000	HRP-linked	Agilent Dako	K400311-2

4.7.9. Whole slide imaging and image analysis

Stained tissue sections were subjected to whole slide imaging using a slide scanner (Aperio CS2, Leica Biosystems, Germany). Slides were scanned by an optical lens at 20- and 40-times magnification. Background removal was performed to ensure a white background for subsequent image analysis.

Image analysis was performed to semi-quantify the staining intensity after ORO and IHC staining. Software ImageJ was used for image analysis. For the quantification of red coloured ORO staining of lipids, colour thresholding was performed and extracted from selected regions of interest. The coloured stain is thresholded and converted black and the number of black pixels is quantified. The total stained pixel is normalized by total number of nuclei in each region of interest and is counted by the circularity feature extraction of the nuclei. For IHC staining, the intensity of DAB of converted into optical density (OD) prior to analysis. Firstly, the images are deconvoluted by the H DAB vector setting and brown-coloured DAB staining are separated. Region of interest are selected and the staining intensity is measured. Subsequently, the optical density is calculated using the formula (where the maximum intensity is 255 for 8-bit images):

$$OD = \log\left(\frac{maximum\ intensity}{mean\ intensity}\right)$$

For calculating the area in whole slide images, ImageScope software was used and the region of interest is selected and analysed (Leica Biosystems, Germany). For each group, 10 images from each mouse are captured randomly for analysis.

4.8. Ultra-performance liquid chromatography-quadrupole time of flight-mass spectrometry (UPLC-QTOF/MS)

4.8.1. Sample preparation

Snap frozen tissue were retrieved from -80 °C storage and transferred to a cytostat set at -20 °C and acclimated for 1 hour. Each kidney is attached onto a sample holder with minimal optimal cutting compound (OCT) and 15 serial cyto-homogenized kidney cross sections were cyrotomed and transferred to an eppendorf for lipid and metabolite extraction. Briefly, 200 μL of ice-cold methanol was added, vortexed for 30 s and sonicated for 10 min in a sonicator with ice. 200 μL of ice-cold chloroform was added and vortexed for 30 s. 100 μL of distilled water was added and vortexed for 30 s. The Mixture was kept on ice for 10 min before centrifugation at 1000 rpm for 5 min at 4 °C. This will result in a three-phased system, separating the metabolite on the top, protein in the middle and lipid at the bottom. The top aqueous phase and bottom organic phase were collected and transferred to a new eppendorf tube and dried using a DryVac for 3 h and stored at -80 °C. Before ultra-performance liquid chromatography-quadrupole time of flight-mass spectrometry (UPLC-QTOF/MS) analysis, metabolite and lipids were reconstituted in 110 μL methanol and 50% methanol and 50% chloroform respectively.

4.8.2. Quality control sample preparation

10 μL of each sample was aliquoted and pooled as a quality control (QC) sample. Prior to UHPLC/ESI-QTOF-MS analysis, the QC sample is injected into the system to equilibrate the column for 5 times and to ensure the stability of the UHPLC/ESI-QTOF-MS. For analysis, every 6 study samples, a QC sample was injected to continually monitor the instrument to identify systemic errors which may invalidate the data collected.

4.8.3. UHPLC-ESI-QTOF/MS condition for untargeted lipidomic analysis

Lipid samples were analysed in both positive and negative mode by UHPLC/ESI-QTOF-MS. 1 µL and 5 µL of sample was injected into an Agilent 1290 UHPLC system respectively. The sample separation was performed on a Waters ACQUITY UHPLC BEH C18 column (2.1 x 100 mm, 1.7 μm attached to a Waters ACQUITY BEH C18 VANGUARD (2.1 x 5 mm, 1.7 μm) pre-column filter. The mobile phases include a mobile phase A consisted of 60% acetonitrile and 40% water, 5 mM ammonium formate and 0.1% formic acid (v/v) and a mobile phase B which consisted of 90% isopropyl alcohol, 10% acetonitrile, 5 mM ammonium formate and 0.1% formic acid (v/v). The elution gradient was set as follows:

Table 2. The conditions and elution gradient set for C18 column.

Time (min)	Mobile phase A (%)	Mobile phase B (%)	Flow rate (mL/min)	Maximum pressure (Bar)
0	60	40	0.300	1000
2	60	40	0.300	1000
2.5	42	58	0.300	1000
18	1	99	0.300	1000
20	1	99	0.300	1000
21.10	60	40	0.300	1000
24.0	60	40	0.300	1000

The column was equilibrated for 3 min after each sample. The column chamber was set to 40 °C and the sample chamber was set to 4 °C.

4.8.4. Mass spectrometry condition

Mass spectrometry was performed on an Agilent 6540 UHD Quadrupole Time-of-Flight Accurate-Mass Mass spectrometer (Agilent, USA) in both positive and negative mode by electrospray ionization (ESI) method. The acquisition range was set to 100 – 3000 *m/z* with MS/MS isolation width set as "Narrow". The source parameters were set as follows: gas temperature, 300 °C, gas flow, 8 (L/min), nebulizer, 40 (psig), sheath gas temperature, 320 °C and sheath gas flow, 11. For scan source parameters in positive and negative mode: VCap, 4000 and 2800, nozzle voltage, 1500 V and 0 V, fragmentor, 140. A locked mass for high mass accuracy for both positive and negative ESI mode. In positive mode, mass [M+H]+: 102.1283 ,121.0509, 391.289 and 922.0098) were used and in negative mode, mass [M-H]−: 112.985587, 966.000725 and 1033.988109 were measured throughout the data acquisition. Mass fragmentation analysis was performed on targets of interest.

4.8.5. Data processing and multivariate analysis

Raw data files from UHPLC/ESI-QTOF-MS are imported into Progenesis QI 2.4 (Nonlinear Dynamics, United Kingdom). After data import, the runs are aligned and normalized according to the total ion count (TIC) of each sample. Data was further filtered out with coefficient of variation bigger than 30%. The dataset was than exported to EZInfo 2.0 (Umetrics, Sweden) for further multivariate analysis.

Scores plot of PCA, PLS-DA and OPLS-DA were plotted to gather insights into the separation between experimental groups. Variable importance plot (VIP) was also plotted to identify targets with the most significant contribution to group separation. Targets from OPLS-DA with VIP ≥ 1.0 were considered as potential compounds of interest. These compounds were identified using databases HMDB and LMSD based on retention time, mass-to-charge (*m/z*) ratio, mass accuracy and fragmentation pattern.

4.8.6. Pathway and enrichment analysis

Identified lipids and metabolites were further processed by MetaboAnalyst 5.0 (https://www.metaboanalyst.ca) to integrate and visualize the data in a biologically relevant manner based on the KEGG database. Compound enrichment analysis was also performed to identify over-represented compounds that may be involved in the biological or pathological process development. All compounds were converted to HMDB identifier number prior to MetaboAnalyst 5.0 analysis.

4.8.7. Area under the curve receiver operating characteristic (AUC-ROC)

In order to measure the differential ability of identified compounds between groups, the receiver operating characteristic curve (ROC) was plotted and the area under the curve (AUC-ROC) was calculated. The AUC-ROC value is used as a representation of the ability a compound to separate between two groups or classes. Briefly, the identified compounds were converted to HMDB identifier numbers and the normalized peak intensity of each compound from different mouse were formatted on to a table and saved in comma-separated values format. The AUC-ROC value was calculated by MetaboAnalyst 5.0.

4.9. Matrix-assisted laser desorption/ionization-mass spectrometry imaging

4.9.1. Tissue and slide preparation

Fresh kidney cross sections were sectioned using a cryostat as previously described. The sections were thaw-mounted onto indium tin oxide (ITO) coated glass slides. The slides were put under vacuum and dried in a desiccator for 30 min before stored in -80 °C and used within 7 days. Prior to use, the slides were equilibrated in room temperature for 30 min under vacuum in a desiccator.

4.9.2. MALDI-MSI analysis

In order for the compounds on the tissue to be ionized, a matrix was applied with an automatic sprayer (HTX TM-Sprayer, HTX Technologies, USA) filled with matrix solution. A 2,5-Dihydroxybenzoic acid (DAB) matrix solution (1.5 mg/ mL) in 70% ACN with 0.1% trifluoroacetic acid (TFA) was prepared freshly. The automatic sprayer was set to spray the matrix on to the ITO slide with the following settings:

Table 3. The parameters for matrix preparation using the HTX TM-Sprayer.

Parameter	**Time / concentration**
Nozzle height (mm)	40
Nitrogen gas pressure (psi)	10
Nozzle temperature (°C)	70
Solvent flow rate (ml/min)	0.125
Z-arm velocity (mm/min)	1200
Number of passes	14
Moving pattern	CC
Track spacing (mm)	3
Drying time (s)	0

Imaging was performed on a Bruker ultrafleXtreme matrix-assisted laser desorption/ionization (MALDI)-Time-of-flight mass spectrometry (MALDI-TOF/MS) (Bruker, Germany) and is equipped with a smartbeam laser with up to 1000 Hz laser repetition rate. Mass calibration was performed with peptide standards (Bruker, Germany) to achieve less than 5 ppm mass accuracy. The dynamic mass spectra range

to be gathered was set between 400 – 1500 *m/z* in both positive and negative mode. Mass spectra data was collected from 100 um spatial resolution using 500 accumulation shots per pixel at 75% laser power with detector gain set at 1998 – 2162 V. The remaining laser parameters are as set as follows: global attenuator offset, 28%, attenuator offset, 40% and attenuator range, 20%.

The ITO slide was imaged using a low-resolution slide scanner to obtain an overview kidney sections on the slide. The image was transferred into FlexImaging 4.1 (Bruker, Germany) for regions of interest selection before imaging.

4.9.3. Data analysis

The raw data collected were processed and calibrated using FlexAnalysis 3.4 (Bruker, Germany) using the batch processing mode for external mass calibration. The calibrated spectra were processed with FlexImaging 4.1 and the data was exported to SCiLS Lab 2020b Pro (Bruker, Germany) for visualization and statistical analysis. The data were normalized by root mean square method.

4.10. SDS-polyacrylamide Gel Electrophoresis and Western Blot Analysis

Tissue extracted were homogenized using a tissue homogenizer (Bertin Instruments, France) in RIPA with enzyme inhibitors. The homogenate was centrifuged at 13000 RPM for 15 minutes at 4°C and the supernatant was collected. Protein concentration was calculated using the Pierce BCA protein assay kit (Thermo Fisher Scientific, USA) as per manufacture procedure.

The protein concentration of the lysate was quantified using the Pierce BCA Protein Assay Kit (23225, Thermo Scientific, USA) for equal loading of protein samples during gel electrophoresis. The samples were first diluted in sodium dodecyl sulfate

loading buffer (0.0012% bromophenol blue, 0.5 M dithiothreitol, 30% glycerol, 10% SDS, 0.28 M tris-hydrochloide pH 6.8) and boiled at 99 °C for 5 min. The samples were resolved by a 10% SDS-polyacrylamide gel and were transferred onto polyvinylidene difluoride (PVDF) membrane. The membrane was then blocked in 10% non-fat dried milk at room temperature for 1 h. Primary antibody were diluted accordingly and the PVDF membrane was incubated at 4 °C, overnight with gentle agitation. On the next day, the membrane was washed with TBS-T for 3 x 10 min. Thereafter the membrane was incubated with horseradish peroxidase-linked horse secondary antibody diluted in 10% non-fat dried milk at room temperature for 1 h. The antigen-antibody complex was detected by enhanced chemiluminescence (ECL) (Abcam, United Kingdom) with exposure to X-ray film (Fujifilm, Japan).

Table 4. List of antibodies and dilution used for protein analysis.

Primary antibody	**Species**	**Dilution**	**Type**	**Supplier**	**Catalog number**
Glp-1r	Rabbit	1:200	Monoclonal	Abclonal	A8547
Gapdh	Rabbit	1:200	Monoclonal	Proteintech	60004-1-Ig
Secondary antibody		**Dilution**	**Type**	**Supplier**	**Catalog number**
Anti-rabbit IgG		1:1000	HRP-linked	Proteintech	SA00001-2

4.11. Quantitative reverse transcription polymerase chain reaction (RT-qPCR)

In order to quantify the gene expression in tissue, tissue was homogenized in RNAiso (Takara, China) using a tissue homogenizer as previously described. Total RNA was

extracted as according to manufacturer's protocol. RNA concentration and quality were measured using a spectrophotometer (Nanodrop 2000, Thermo Scientific, USA). The quality of RNA was assessed by the absorbance ratio of 260 and 280 with value of 2.0 ± 0.1 considered as high purity. The resulting product was normalized to 1000 ng/μL for complimentary DNA (cDNA) synthesis by using the PrimeScript first strand cDNA Synthesis Kit (Takara, China).

The resulting product was then used to before quantitative PCR using SYBR green kit (Takara, China) along with the primers (Genewiz, China). The quantitative PCR was performed on a LightCycler 96 (Roche, Switzerland), with 40 cycles. Quantitation and normalization of the mRNAs was performed using the $2^{-\Delta\Delta Ct}$ method using glyceraldehyde 3-phosphate dehydrogenase (GAPDH) as a housekeeping gene.

The primers and their design are as follows:

Table 5. List of primers used for real-time quantitative PCR analysis.

	Primer sequence (5' to 3')	
Target gene	**Forward**	**Reverse**
Cds1	TGTTCCCATATCAAGCGTCA	GGCTCACACTCTGTCACGAA
Pgps	CGACCTCAAGGTCTCCATTC	GTTTGCACCACTCAGGATGA
Cls	ATCAGCTTTGGGAAGTGCTC	ACCTTGCTGATGAATGTTGGT
Taz	CTGGGGGATCCTAAAACTCC	AGCGCAGGAACTCAGAACTC
Alcat1	CCATGAACCACTACAGCTTC	GCATCGAGGTTCTTCCCTT

CoxII (mtDNA)	TTTTCAGGCTTCACCCTAGATGA	GAAGAATGTTATGTTTACTCCTACGAATATG
B-globin (gDNA)	GAAGCGATTCTAGGGAGCAG	GGAGCAGCGATTCTGAGTAGA
Nrf1	GCACCTTTGGAGAATGTGGT	GGGTCATTTTGTCCACAGAGA
Tfam	CCTTCGATTTTCCACAGAACA	GCTCACAGCTTCTTTGTATGCTT
Pgc-1α	AAACTTGCTAGCGGTCCTCA	TGGCTGGTGCCAGTAAGAG
Pepck	AGTGCCCATCCCCAAAACT	CACCACATAGGGCGAGTCTG
mtnd5	ACCAGCATTCCAGTCCTCAC	ATGGGTGTAATGCGGTGAAT
Cytb	CCCTAGCAATCGTTCACCTC	TCTGGGTCTCCTAGTATGTCTGG
CoxIII	CGTGAAGGAACCTACCAAGG	ATTCCTGTTGGAGGTCAGCA
Gapdh	AGGTCGGTGTGAACGGATTTG	TGTAGACCATGTAGTTGAGGTCA

Primers were validated using the Primer-BLAST tool from the U.S National Library of Medicine.

4.12. Statistical analysis

Statistical analysis was performed routinely using Graphpad Prism 8 (GraphPad Software, San Diego, CA), with $P < 0.05$ considered as significant. All values were expressed as mean ± standard error of the mean (SEM). For comparisons amongst groups, One-way ANOVA was performed with Tukey post-hoc test with HFD group

set as the reference group to compare multiple groups. Each experiment was repeated at least three times.

5. Results

5.1. Dulaglutide reduce body weight after dulaglutide treatment

Mice at the age of 8 weeks were randomly allocated into 3 groups for either HFD, H+Dula or STC to serve as a lean control. After 12 weeks of feeding, HFD and H+Dula group mice showed a substantial increase in body weight as compared with STC. Subsequently, H+Dula group was intraperitoneally given 4 weeks of dulaglutide treatment whilst both HFD and STC group were given phosphate-buffered saline instead as a vehicle control. As a result, the body weight of H+Dula mice were significantly lower than that of HFD group mice. STC mice showed consistent body weight throughout the duration of the experiment (Figure 4).

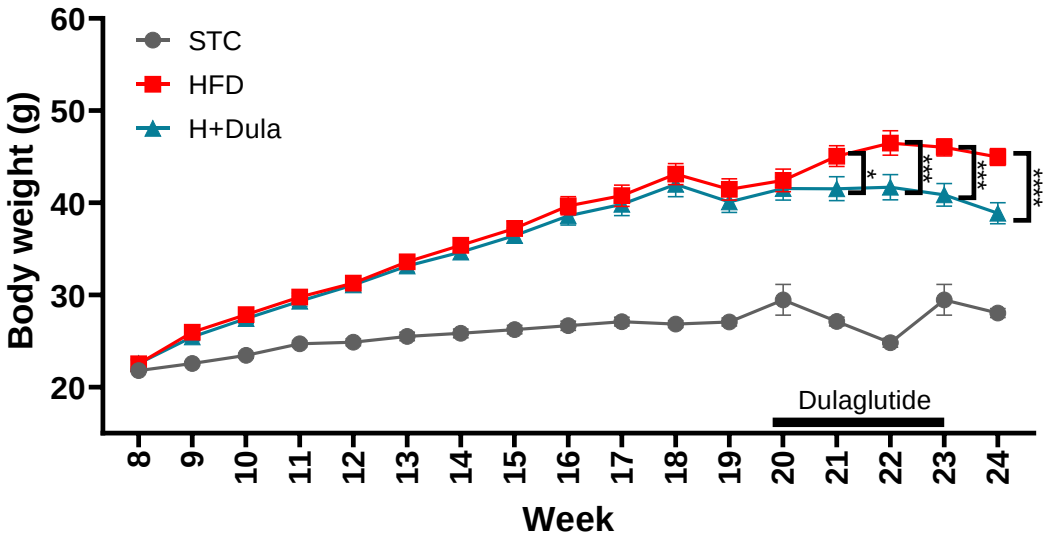

Figure 4. Body weight was reduced in high-fat diet with dulaglutide treated mice after 4-weeks of treatment.

Comparison of body weight changes between STC, HFD and H+Dula group. Mice of 8-weeks old were fed high-fat diet for 12 weeks and H+Dula were further treated with dulaglutide. Data represents means ± SEM, n = 6 – 9 mice per group. * $P < 0.05$, *** $P < 0.001$ and **** $P < 0.0001$.

5.2. Dulaglutide treatment improves fasting and fed glucose

Blood glucose as an indicator of diet-induced obesity with decrease in insulin sensitivity was monitored in both 16-hour fast and fed state before dulaglutide treatment and prior to animal sacrifice. Before treatment with dulaglutide, both HFD and H+Dula group showed increased basal glucose levels, denoting that the glucose tolerance of mice after high-fat diet for 12 weeks showed reduced glucose tolerance as compared to STC lean control. There is also no significant difference in the blood glucose level between the HFD and H+Dula in both fasting (Figure 5A) and fed (Figure 5B) state before treatment. After treatment, HFD group continued to showed a significantly higher fed and fast blood glucose concentration as compared to STC but was significantly reduced in the H+Dula group as compared with the HFD group (Figure 6A and B).

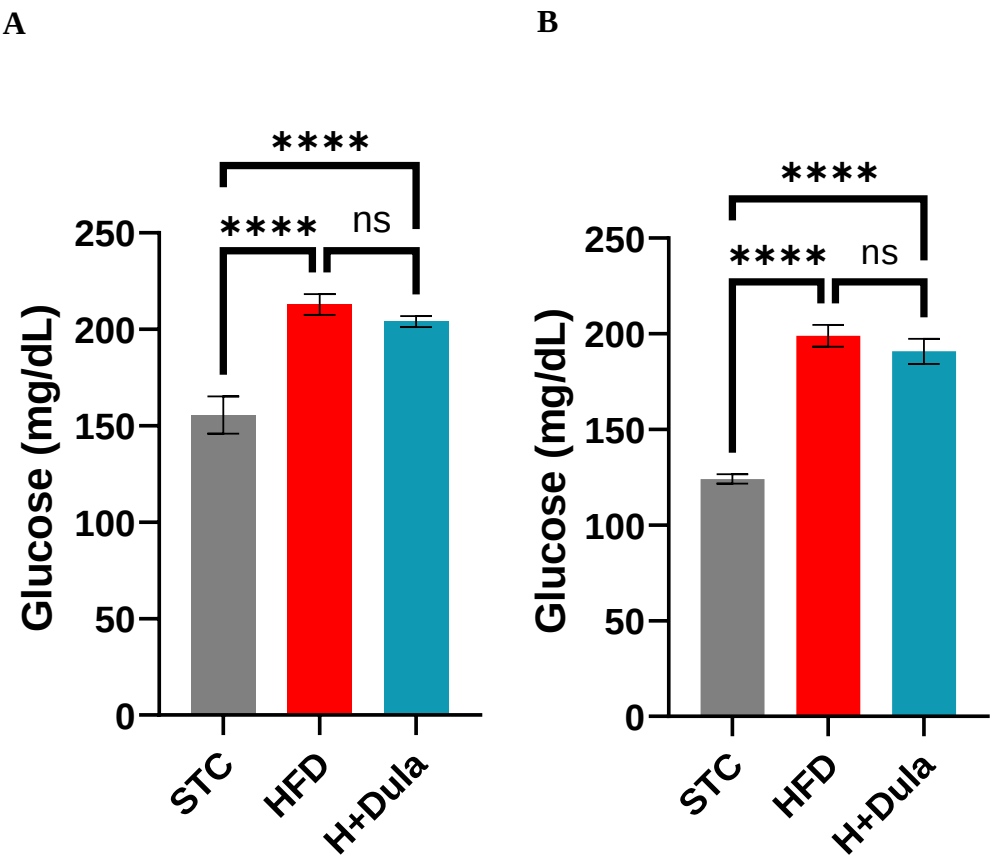

Figure 5. High-fat diet mice has reduced glucose tolerance in both fast and fed state.

Mice were fed with standard chow or high-fat diet for 12 weeks before dulaglutide treatment. Comparison of tail vein blood glucose changes between STC, HFD and H+Dula group in 16-hours fasting (A) and fed state before treatment (B). Data represents means ± SEM, n = 6 – 9 mice per group. *** $P < 0.001$, **** $P < 0.0001$ and ns = not significant.

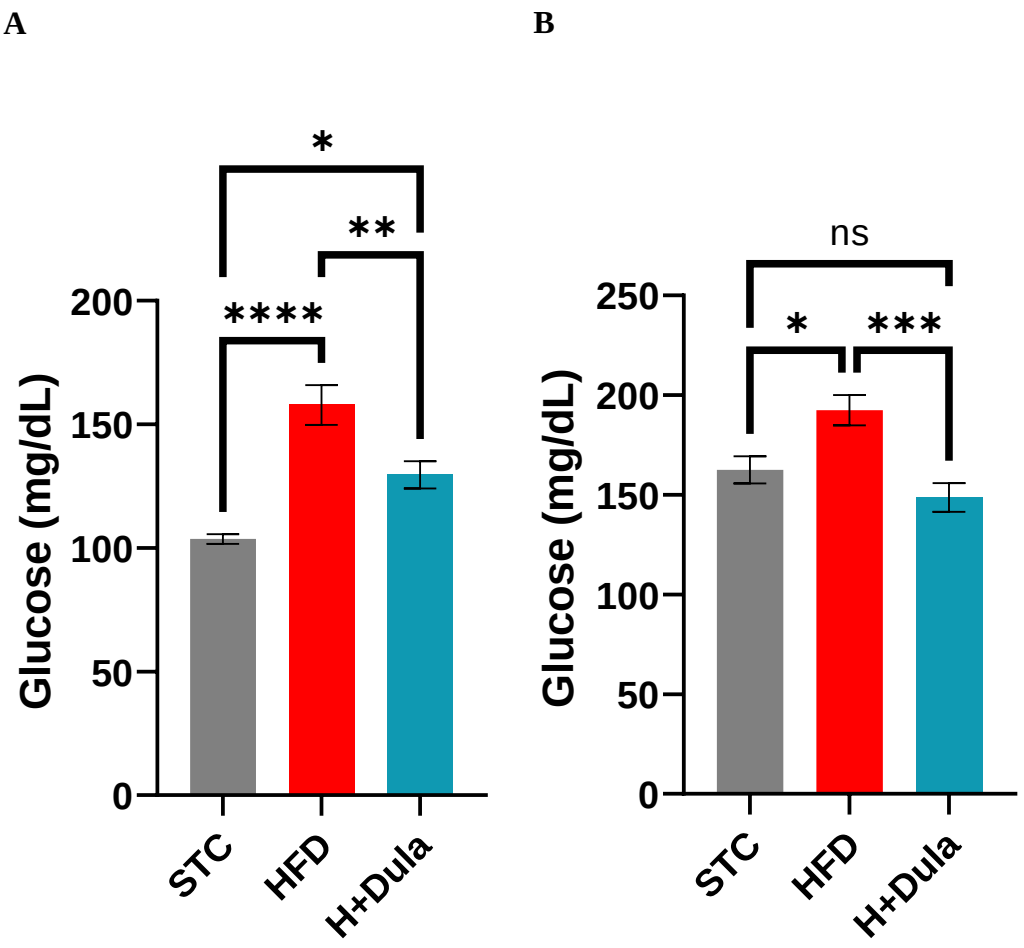

Figure 6. Dulaglutide treated mice has improved glucose tolerance in both fast and fed state as compared to high-fat diet mice

Mice were fed with standard chow or high-fat diet for 12 weeks. After dulaglutide treatment for 4 weeks, tail vein blood glucose changes between STC, HFD and H+Dula group in 16-hours fasting **(A)** and fed state **(B)** compared. Data represents means ± SEM, n = 6 – 9 mice per group. * $P < 0.05$, ** $P < 0.01$, *** $P < 0.001$ and **** $P < 0.0001$.

5.3. Dulaglutide improves glucose tolerance

We further assessed the glucose tolerance of mice by intraperitoneally injected glucose tolerance test (IPGTT) and calculated the AUC and compared between groups before and after treatment of dulaglutide. Figure 7 shows the blood glucose concentration of mice in different group throughout the 180 min test and the AUC before treatment showed a high blood glucose after 15 min of glucose injection and that the blood glucose remained higher than STC till 120 min before gradually returning to concentrations similar to STC. The calculated AUC showed that both HFD and H+Dula groups before treatment has an increased area after 12 weeks of high-fat diet as compared to STC lean control; indicating high-fat diet reduced glucose tolerance (Figure 7B).

After treatment with dulaglutide for 4 weeks, IPGTT was performed and overall, HFD and H+Dula grouped mice showed higher increase in blood glucose as compared to STC group after glucose injection however, the increase in blood glucose was lower in H+Dula as compared to HFD from 15 min to 180 min (Figure 8A). AUC was calculated and showed HFD and H+Dula group have increased area as compared to STC but H+Dula group showed a significantly reduced AUC after treatment as compared to the HFD group (Figure 8B).

A

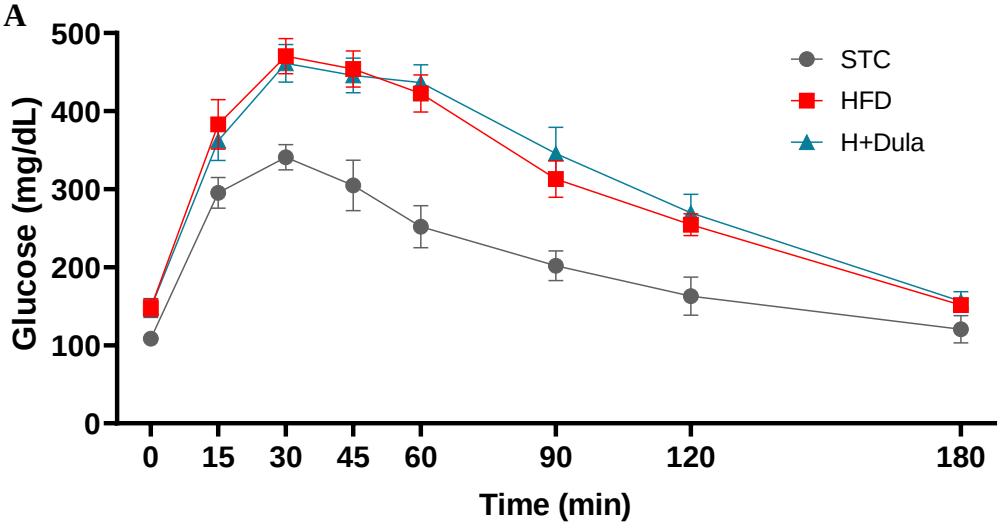
Glucose (mg/dL)
500
400
300
200
100
0
0
15
30
45
60
90
120
180
Time (min)
STC
HFD
H+Dula

B

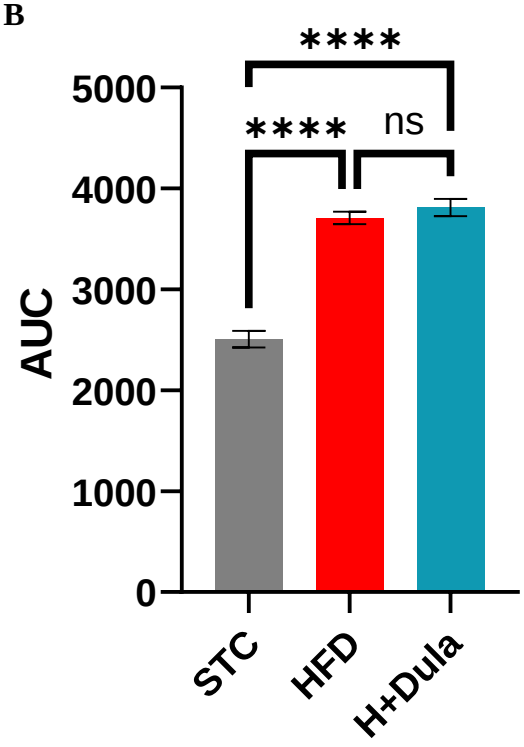
****
****
ns
AUC
5000
4000
3000
2000
1000
0
STC
HFD
H+Dula

Figure 7. High-fat diet fed mice has a reduced glucose tolerance

Mice were fed with standard chow or high-fat diet for 12 weeks. High-fat diet mice were then randomly separated into HFD or H+Dula. Before treatment with dulaglutide, mice were fast for 16-hours and were subjected to 180 minutes IPGTT **(A)**. Glucose tolerance between groups were compared by AUC **(B)**. Data represents means ± SEM, n = 6 – 9 mice per group. **** $P < 0.0001$ and ns = not significant.

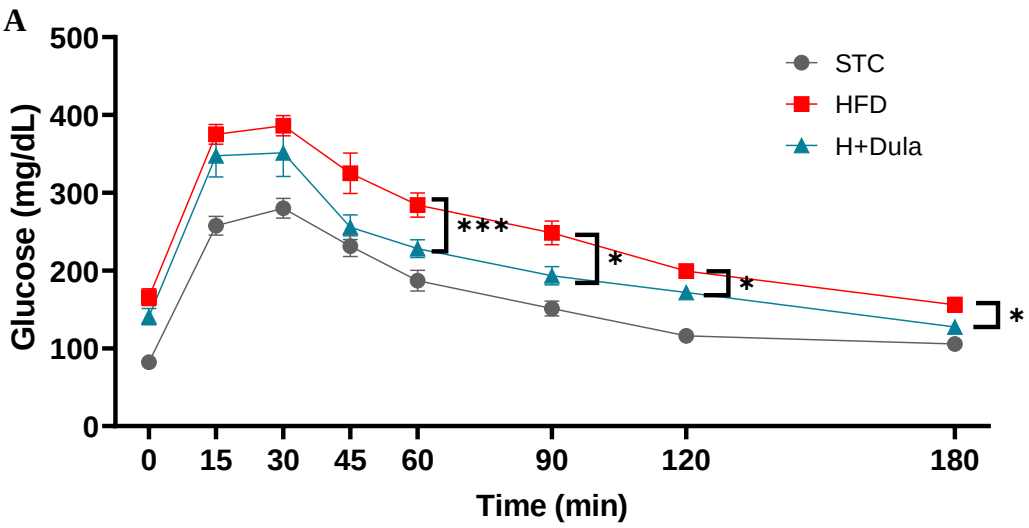
A
500
400
300
200
100
0
Glucose (mg/dL)
0
15
30
45
60
90
120
180
Time (min)
STC
HFD
H+Dula
***
*
*
*

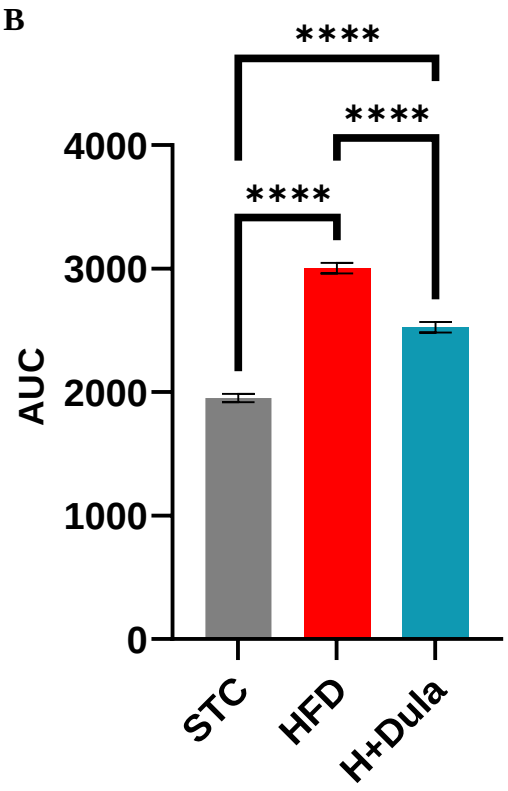
B
****
****
****
4000
3000
2000
1000
0
AUC
STC
HFD
H+Dula

Figure 8. Dulaglutide treated mice has improved glucose tolerance as compared to high-fat diet mice

Mice were fed with standard chow or high-fat diet for 12 weeks. High-fat diet mice were then randomly separated into HFD or H+Dula. After 4-weeks treatment with dulaglutide, mice were fast for 16-hours and were subjected to 180 minutes IPGTT **(A)**. Glucose tolerance between groups were compared by AUC **(B)**. Data represents means ± SEM, n = 6 – 9 mice per group. * $P < 0.05$, ** $P < 0.01$, *** $P < 0.001$ and **** $P < 0.0001$.

5.4. Validation of kidney function after dulaglutide treatment

To investigate the kidney function before and after treatment of dulaglutide in mice, 24 h urine was collected, weighted and further analysed for urinary albumin and creatinine by ELISA.

Before treatment, 12 weeks of high-fat diet let to a decrease in total volume of urine excreted after 24 h in both HFD and H+Dula group as compared to STC group (Figure 9A). ELISA urinary albumin and creatinine concentration between HFD and H+Dula groups as compared to STC control is significantly increased (Figure 9B).

After 4 weeks treatment with dulaglutide, H+Dula group showed a significantly higher total volume of urine excreted after 24 h as compared to HFD group. HFD group continued to show a reduced volume of urine excreted as compared to STC group (Figure 10A). H+Dula group showed significant reduction in urinary albumin as compared to HFD group. HFD group as expected, continued to show an increase in urinary albumin without treatment (Figure 10B).

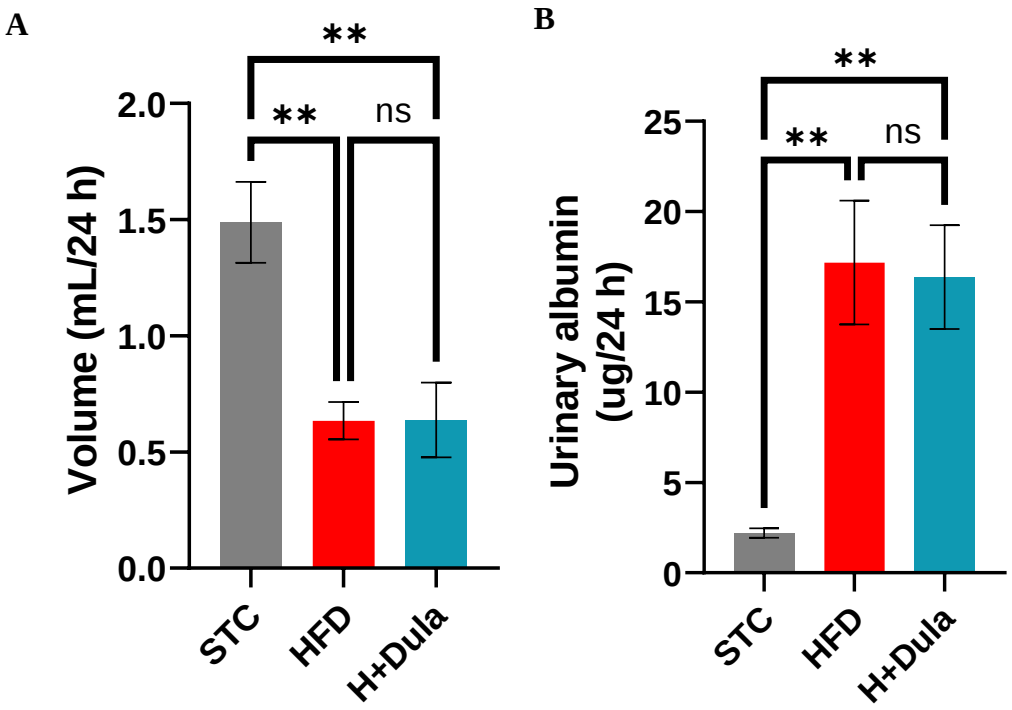

Figure 9. Urine analysis after high-fat diet showed increased albuminuria

Mice were fed with standard chow or high-fat diet for 12 weeks before dulaglutide treatment. 24-hour urine was collected in metabolic cages. Urine volume was measured **(A)** and urinary albumin **(B)**. Data represents means ± SEM, n = 6 – 9 mice per group. ** $P < 0.01$ and ns = not significant.

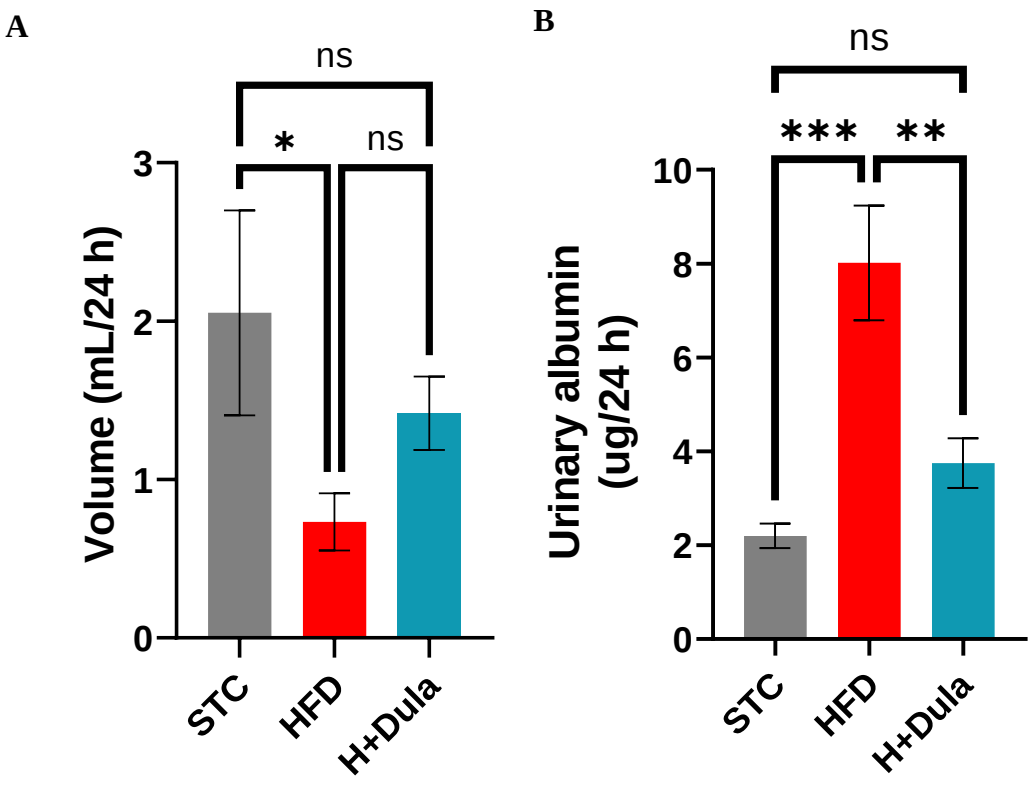

Figure 10. Dulaglutide reduced albuminuria when compared to the HFD group

Mice were fed with standard chow or high-fat diet for 12 weeks and the treatment group was given dulaglutide for 4 weeks. 24-hour urine was collected in metabolic cages. Urine volume was measured **(A)** and urinary albumin **(B)**. Data represents means ± SEM, n = 6 – 9 mice per group. * $P < 0.05$, ** $P < 0.01$, *** $P < 0.001$ and ns = not significant.

5.5. Validation of changes in body composition after dulaglutide treatment

To investigate the body composition of mice before and after dulaglutide treatment. NMR spectrum was acquired and compared among the STC, HFD and H+Dula groups. The weight of body fat, lean body mass and fluid mass were measured in grams and as a ratio over individual mouse body weight. The ratio of body fat over lean body mass in grams was also calculated.

After 12-weeks of high-fat diet, there is an increase in the net weight, in grams, of body fat, lean body mass and fluid mass in the HFD and H+Dula groups compared with STC lean control group. For body fat, the HFD and H+Dula groups when compared to the STC group show significant increase by 6.46 and 6.35 times with both P value of < 0.0001 respectively (Figure 11A). For lean body mass, the HFD and H+Dula groups when compared to the STC group show significant increase by 1.11 and 1.09 times with P value of 0.0034 and 0.039 respectively (Figure 11B). For fluid mass, the HFD and H+Dula groups when compared to the STC group show significant increase by 3.76 and 3.70 times with both P value of < 0.0001 respectively (Figure 11C). There is no significant difference between the HFD and H+Dula groups as compared to STC group for body fat, lean body mass and fluid mass with P value of 0.85, 0.67 and 0.78 respectively.

Similar results are shown for data measured as a percentage relative to body weight. The lean body mass data showed a more significant and drastic change in lean body mass relative to body weight when compared between HFD and H+Dula groups with STC group. For body fat, the HFD and H+Dula groups when compared to the STC group show significant increase by 3.86 and 3.85 times with both P value of < 0.0001 respectively (Figure 11D). For lean body, the HFD and H+Dula groups when compared to the STC group show significant increase by 2.42 and 2.41 times with both

P value < 0.0001 respectively (Figure 11E). There are significant differences between the HFD and H+Dula groups as compared to STC group for body fat, lean body mass and fluid mass with P value of 0.96, 0.99 and 0.87 respectively (Figure 11F).

Fat and lean ratio of each mouse was calculated and plotted by their group and is shown in Figure 11G. Analysis between HFD and H+Dula groups with STC revealed significant increase in the fat and lean ratio after 12 weeks of high-fat diet both by 5.77 times with P value of < 0.0001. There is no significant difference between the HFD and H+Dula with P value of 0.99.

After 4 weeks of dulaglutide treatment in H+Dula group, the body compositions of mice were measured and further compared between the HFD and STC groups. For body fat, the HFD and H+Dula groups when compared to the STC group show significant increase by 5.03 and 3.80 times both have a P value of <0.0001 respectively. There is a significant lower amount of body fat when compared between the HFD with the H+Dula group by a reduction of 0.76 times and with a P value of 0.014 (Figure 12A). For lean body mass, the HFD and H+Dula groups when compared to the STC group show no significant differences with P value of 0.16 and 0.8871 respectively. There is a slight increase in lean body mass trend in between HFD and STC groups. The lean body mass in dulaglutide treated H+Dula group was lower when compared to HFD with P value of 0.23 (Figure 12B). For fluid mass, the HFD and H+Dula groups when compared to the STC group show significant increase by 2.36 and 2.06 times respectively and both have a P value of <0.0001. The fluid mass in dulaglutide treated H+Dula group was significantly lower when compared to HFD with P value of 0.022 (Figure 12C).

Similar results are shown for data measured as a percentage relative to body weight after dulaglutide treatment. For body fat, the HFD and H+Dula groups when compared to the STC group show significant increase by 3.07 and 2.69 times both have a P value of <0.0001. There is a difference in body fat when compared between the HFD with the H+Dula group by a reduction of 0.88 times and with a P value of 0.1342 (Figure 12D). For lean body mass, the HFD and H+Dula groups when compared with STC show a significant decrease in lean body mass ratio, both with a P value of <0.0001. There is a slight increase in lean body mass ratio in H+Dula group when compared with the HFD group however, there is no statistical difference with P value of 0.058 (Figure 12E). For fluid mass, the HFD and H+Dula groups when compared to the STC group show significant increase by 1.45 and 1.47 times both have a P value of <0.0001. There is no significance between the HFD and H+Dula group with P value of 0.7293 (Figure 12F).

Fat and lean ratio of each mouse was further calculated and plotted by their group and is shown in Figure G. Analysis between HFD and H+Dula groups with STC revealed significant increase in the fat and lean ratio after 4 weeks of dulaglutide treatment by 4.78 and 3.80 times with both P values of < 0.0001. There is a lower fat lean ratio in H+Dula group when compared with HFD group however, there is no significant difference between them with P value of 0.07.

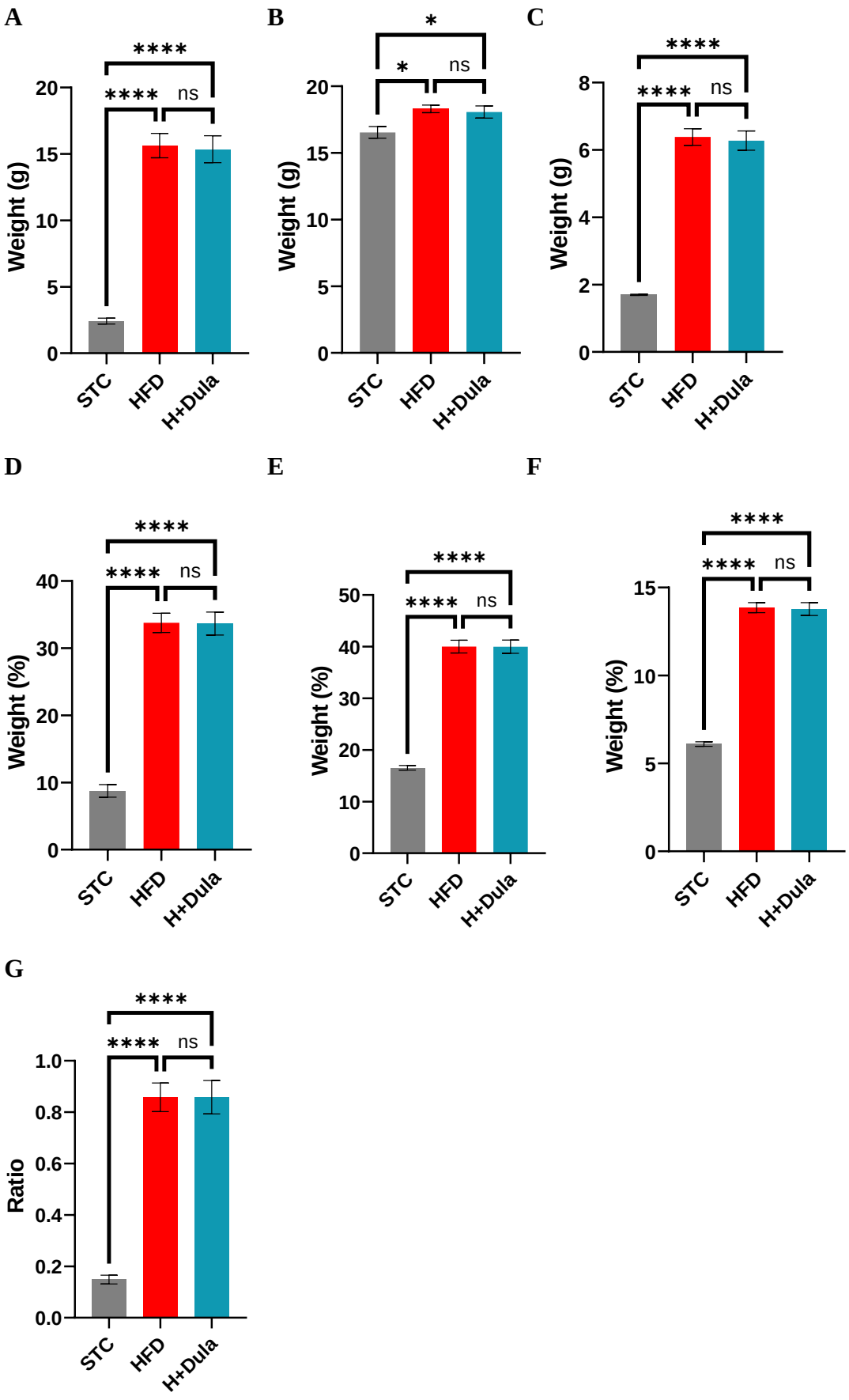
A
B
C
D
E
F
G
Weight (g)
Weight (%)
Ratio
****
ns
*
STC
HFD
H+Dula

Figure 11. ^{1}H nuclear magnetic resonance revealed mice body composition was altered after high-fat diet feeding.

Mice were fed with standard chow or high-fat diet for 12 weeks before dulaglutide treatment. Comparison of body composition was performed using ^{1}H nuclear magnetic resonance (^{1}H-NMR). Parameters including fat **(A and D)**, lean body **(B and E)** masses and fluid **(C and F)** were measured by weight and as a percentage of overall body weight respectively. Fat and lean body mass ratio was also calculated **(G)**. Data represents means ± SEM, n = 6 – 9 mice per group. * $P < 0.05$, ** $P < 0.01$, **** $P < 0.0001$ and ns = not significant

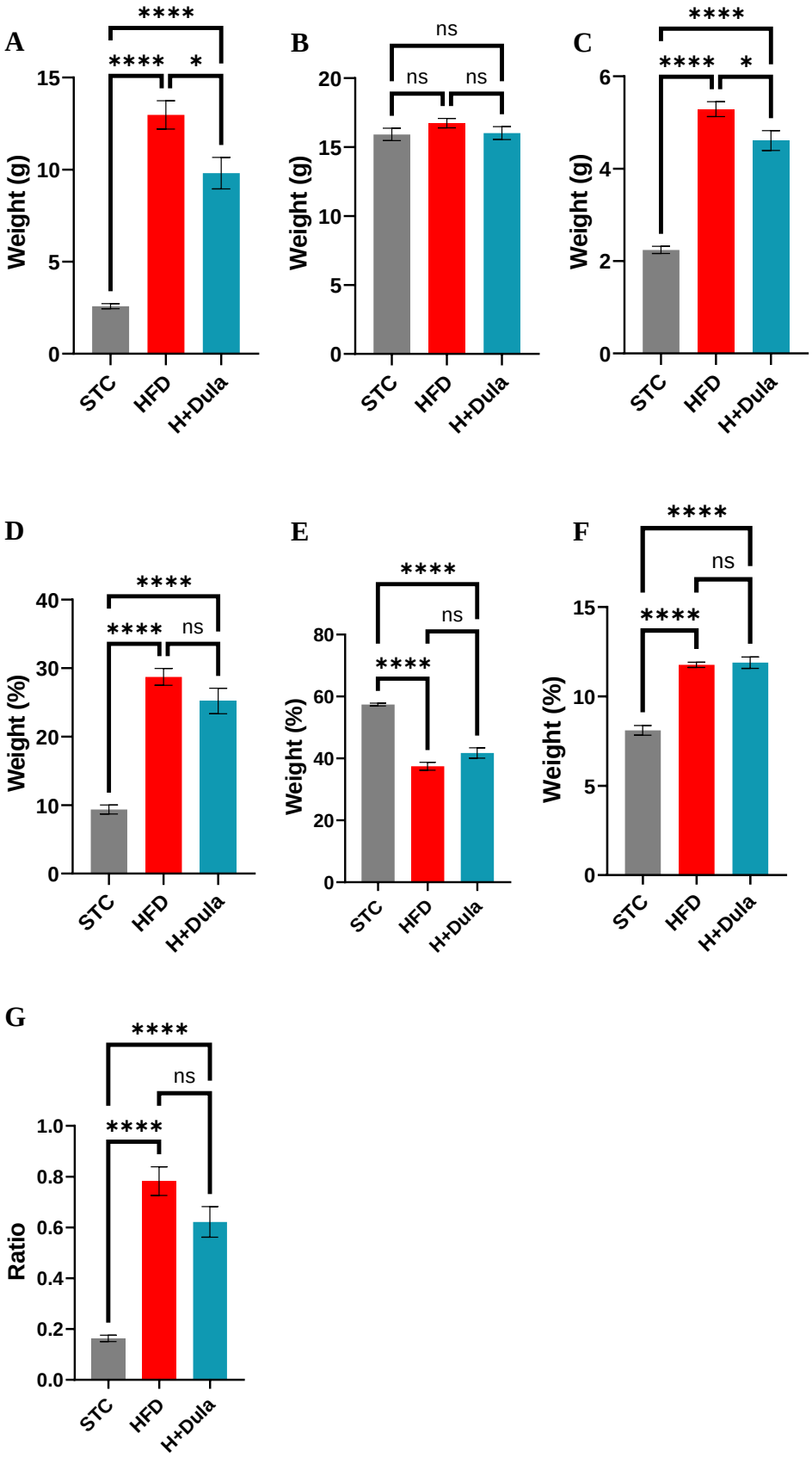
A
B
C
D
E
F
G
Weight (g)
Weight (%)
Ratio
STC
HFD
H+Dula
****
*
ns

Figure 12. ^{1}H nuclear magnetic resonance revealed short-term treatment of dulaglutide led to mild changes in body mass composition from high-fat diet feeding but are not statistically significant when normalized to body weight.

Mice were fed with standard chow or high-fat diet for 12 weeks. After dulaglutide treatment for 4 weeks, comparison of body composition was performed using ^{1}H nuclear magnetic resonance (^{1}H-NMR). Parameters including fat **(A and D)**, lean body **(B and E)** masses and fluid **(C and F)** were measured by weight and as a percentage of overall body weight respectively. Fat and lean body mass ratio was also calculated **(G)**. Data represents means ± SEM, n = 6 – 9 mice per group. * $P < 0.05$, **** $P < 0.0001$ and ns = not significant

5.6. Evaluation of metabolic organ parameters

To investigate changes in metabolic organ after 4 weeks dulaglutide, mice were sacrificed and major metabolic organs, including the kidney, liver and adipose tissue were harvested and weighted.

The kidney weight among STC, HFD and H+Dula remained relatively consistent. The average kidney weight in HFD group was slightly higher when compared with STC and H+Dula group however, there is no significant differences between them with P value of 0.54 and 0.29 respectively (Figure 13A). To investigate the kidney mass relative to overall body mass, the kidney weight was normalized individually with each mouse. There is a higher kidney mass over body weight ratio when STC group is compared to the HFD and H+Dula group, both with P value of < 0.0001. After treatment, H+Dula group shows a higher kidney mass over body weight ratio however, the difference is not statistically significant with P value of 0.25 (Figure 13B). Adipose tissue weight was significantly increased in HFD and H+Dula groups when compared with STC group by 7.88 and 6.67 times respectively with both P value of < 0.0001. Adipose tissue weight was lower in the dulaglutide treated H+Dula group as compared to HFD group however, there is no significant difference between them with a P value of 0.06 (Figure 13C). The liver weight in HFD group was significantly increased as compared with STC group by 1.51 times with P value of 0.02. There is a significantly lower liver weight in H+Dula group when compared with HFD by 0.74 times with a P value of 0.028. There is no significant difference between STC and H+Dula groups with P value of 0.052 (Figure 13D).

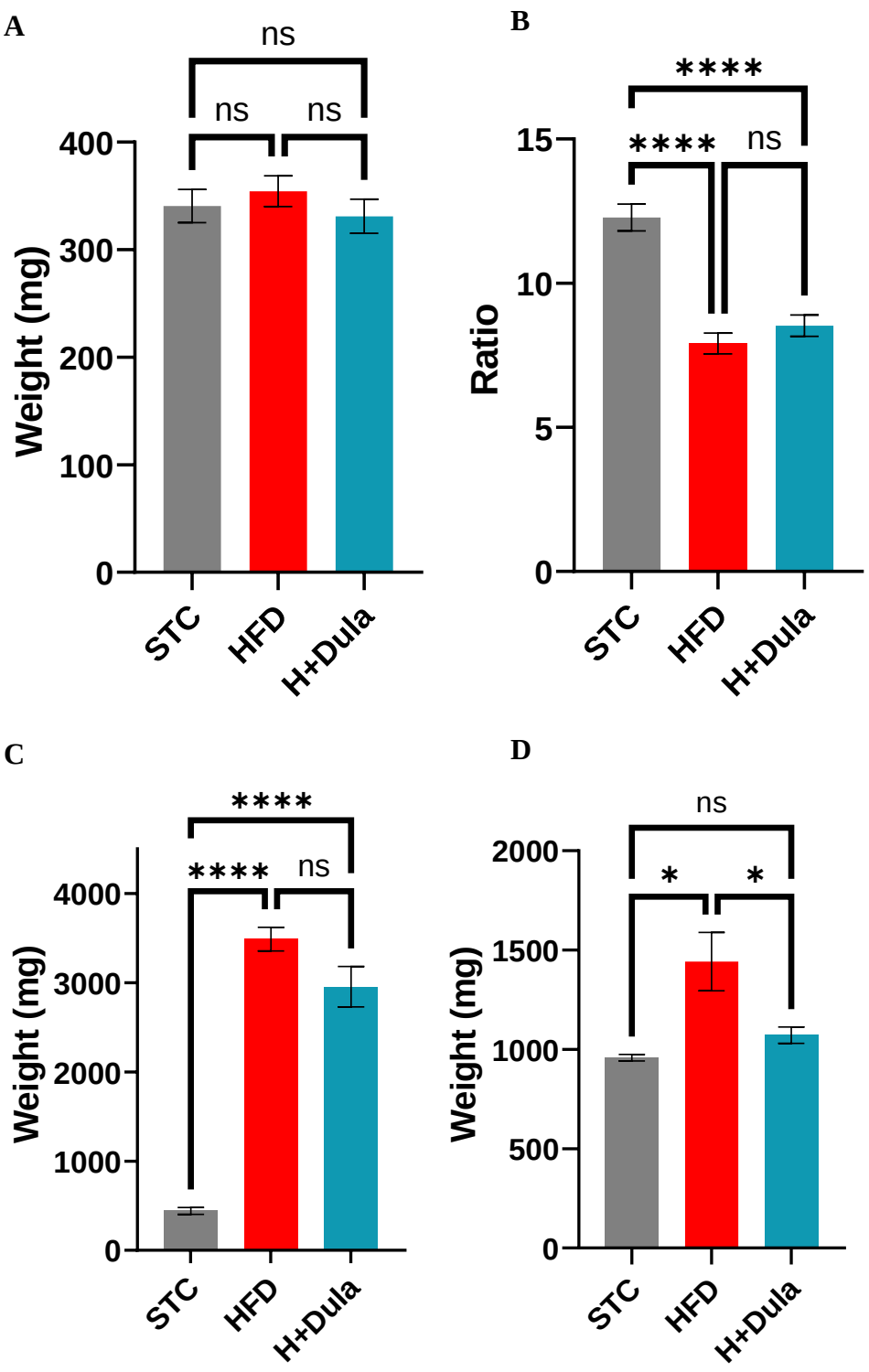
A
ns
ns
ns
Weight (mg)
400
300
200
100
0
STC
HFD
H+Dula
B
****
****
ns
Ratio
15
10
5
0
STC
HFD
H+Dula
C
****
****
ns
Weight (mg)
4000
3000
2000
1000
0
STC
HFD
H+Dula
D
ns
*
*
Weight (mg)
2000
1500
1000
500
0
STC
HFD
H+Dula

Figure 13. 4-weeks treatment with dulaglutide has not altered organ parameters significantly

After 4-weeks treatment with dulaglutide, mice were sacrificed and major metabolic organs were weighed. Effects of dulaglutide treatment on STC, HFD and H+Dula on total kidney weight **(A)**, ratio of kidney weight over body weight **(B)**, adipose tissue weight **(C)** and liver weight **(D)**. Data represents means ± SEM, n = 6 – 9 mice per group. * $P < 0.05$, **** $P < 0.0001$ and ns = not significant

5.7. Energy metabolism and animal behaviour analysis

To investigate the energy metabolism and behaviour of mice after 12 weeks high-fat diet and before 4 weeks dulaglutide treatment, each mouse was placed in individual metabolic cages for measurements including, volume of oxygen intake, volume of carbon dioxide produced, food intake, water intake, energy expenditure and movement by indirect calorimetry. RER was also calculated.

After 12 weeks high-fat diet feeding, the volume of oxygen consumed by mice in HFD and H+Dula was compared. Cumulative oxygen consumption in 24 h, during the 12 h dark cycle and during 12 h light cycle was calculated. It can be seen that dulaglutide treated group H+Dula shows a higher oxygen consumption when compared to HFD among the different conditions however, there are no significant differences between the two groups in a 24 h full cycle, dark cycle and light cycle; their P values are 0.19, 0.21 and 0.18 respectively (Figure 14A). The volume of carbon dioxide produced was also measured. There is a slightly higher volume of carbon dioxide produced among the three conditions however, there are no significant differences between the two groups in a 24 h full cycle, dark cycle and light cycle; their P values are 0.24, 0.24 and 0.27 respectively (Figure 14B**)**. Total food intake was measured and compared between the two groups. There are no significant differences between the two groups in a 24 h full cycle, dark cycle and light cycle; their P value is 0.81, 0.55 and 0.27 respectively **(**Figure 14C**)**. Total water intake was measured and compared between the two groups. There is a slightly lower water intake in H+Dula group in 24 h full cycle and dark cycle however, there are no significant differences between the two groups in a 24 h full cycle, dark cycle and light cycle with their P value is 0.15, 0.084 and 0.92 respectively **(**Figure 14D**)**. The total movement of each mouse was measured based on the total beams broken. There are no significant differences between HFD

and H+Dula groups in 24 h full cycle, dark cycle and light cycle with P value of 0.70, 0.50 and 0.91 respectively **(**Figure 14E**)**. Energy expenditure was measured between the HFD and H+Dula groups in 24 h full cycle, dark cycle and light cycle. There is a slightly higher overall energy expenditure in H+Dula group but the difference is not significant with P value of 0.20, 0.21 and 0.19 respectively **(**Figure 14F**)**. The calculated RER was compared between the HFD and H+Dula groups in 24 h full cycle, dark cycle and light cycle. There are slight differences in RER between the two groups however, their differences are not significant with P values of 0.65, 0.90 and 0.24 respectively **(**Figure 14G**)**.

After dulaglutide drug treatment for 4 weeks, the mice metabolic and behavioural parameters were measured. Cumulative oxygen consumption in H+Dula group is lower than compared to HFD group consumption in 24 h, during the 12 h dark cycle and during 12 h light cycle. There are significant differences between the three conditions with all P value of < 0.0001 **(**Figure 15A**)**. Similar trends are seen in total volume of carbon dioxide produced. There is a lower total volume of carbon dioxide produced in H+Dula group as compared to the HFD group. There are significant differences between the two groups when compared among the three conditions; the P values of all three conditions are < 0.0001 **(**Figure 15B**)**. Both food and water intake were reduced after dulaglutide treatment in 24 h, during the 12 h dark cycle and during 12 h light cycle. Overall 24 h food and water intake were lower in H+Dula group as compared to HFD group by 0.44 and 0.45 times with both P value of < 0.0001. There are significant differences in both food and water intake for 12 h dark cycle between HFD and H+Dula groups with both P value of < 0.0001. Food intake during 12 h light cycle showed significant difference between HFD and H+Dula group with P value of 0.0042. However, for water intake, there is no significant difference between the two

groups in 12 h light cycle, with P value of 0.074 **(**Figure 15C and D**)**. There is an overall higher amount of movement in H+Dula group as compared to HFD group. The difference is significant and has a P value of 0.025. Mice in H+Dula group show significant higher activity level in the 12 h light cycle and not in 12 h dark cycle. The P value are 0.31 and 0.52 respectively (Figure 15E). Energy expenditure was lower in H+Dula group as compared with HFD group in 24 h full cycle, dark cycle and light cycle conditions **(**Figure 15F**)**. The changes are significant and all have a P value of < 0.0001. The calculated RER was compared between the HFD and H+Dula groups in 24 h full cycle, dark cycle and light cycle. There are clear differences in RER between the two groups. There is a significant difference between the two groups and the ratio is lower in H+Dula group. The calculated P value for the different conditions are all <0.0001 **(**Figure 15G**)**.

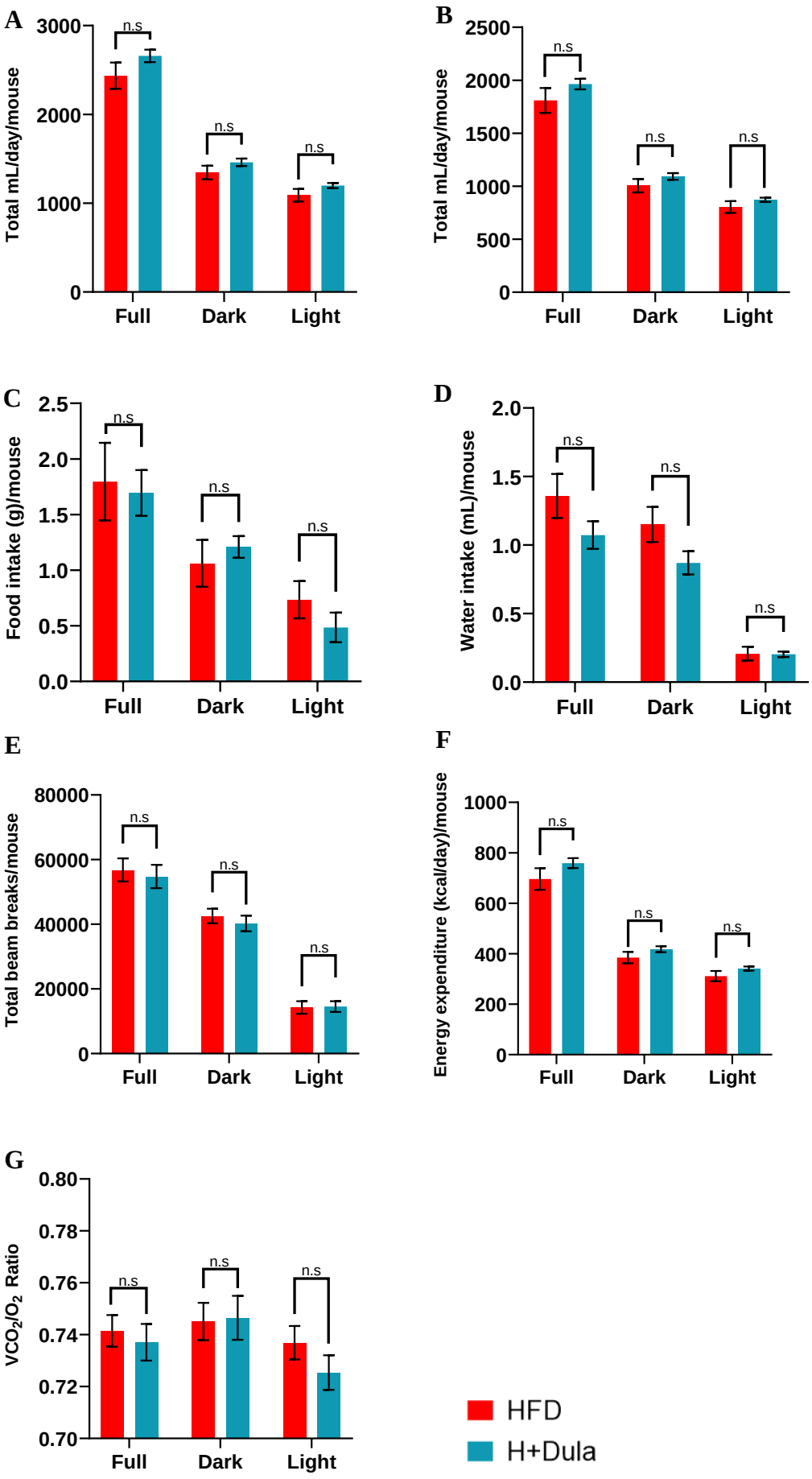
A
Total mL/day/mouse
3000
2000
1000
0
n.s
n.s
n.s
Full
Dark
Light
B
Total mL/day/mouse
2500
2000
1500
1000
500
0
n.s
n.s
n.s
Full
Dark
Light
C
Food intake (g)/mouse
2.5
2.0
1.5
1.0
0.5
0.0
n.s
n.s
n.s
Full
Dark
Light
D
Water intake (mL)/mouse
2.0
1.5
1.0
0.5
0.0
n.s
n.s
n.s
Full
Dark
Light
E
Total beam breaks/mouse
80000
60000
40000
20000
0
n.s
n.s
n.s
Full
Dark
Light
F
Energy expenditure (kcal/day)/mouse
1000
800
600
400
200
0
n.s
n.s
n.s
Full
Dark
Light
G
VCO2/O2 Ratio
0.80
0.78
0.76
0.74
0.72
0.70
n.s
n.s
n.s
Full
Dark
Light
HFD
H+Dula

Figure 14. Baseline of metabolic caging analysis of energy metabolism of mice fed with high-fat diet for 12 weeks before dulaglutide treatment are unchanged.

Mice were fed with standard chow or high-fat diet for 12 weeks before dulaglutide treatment. Metabolic caging analysis of energy metabolism was performed. Mice were placed in individual cages for 24-hours to acclimatize prior to metabolic measurements for 24-hours. Volume of oxygen **(A)** and carbon dioxide **(B)**, food intake **(C)**, water intake **(D)**, movement by total beams broken over 24-hours **(E)** and energy expenditure **(F)**. Respiratory exchange ratio (RER) **(G)** was calculated by volume of carbon dioxide over volume of oxygen over 24-hours. Data represents means ± SEM, n = 6 – 9 mice per group. ns = not significant

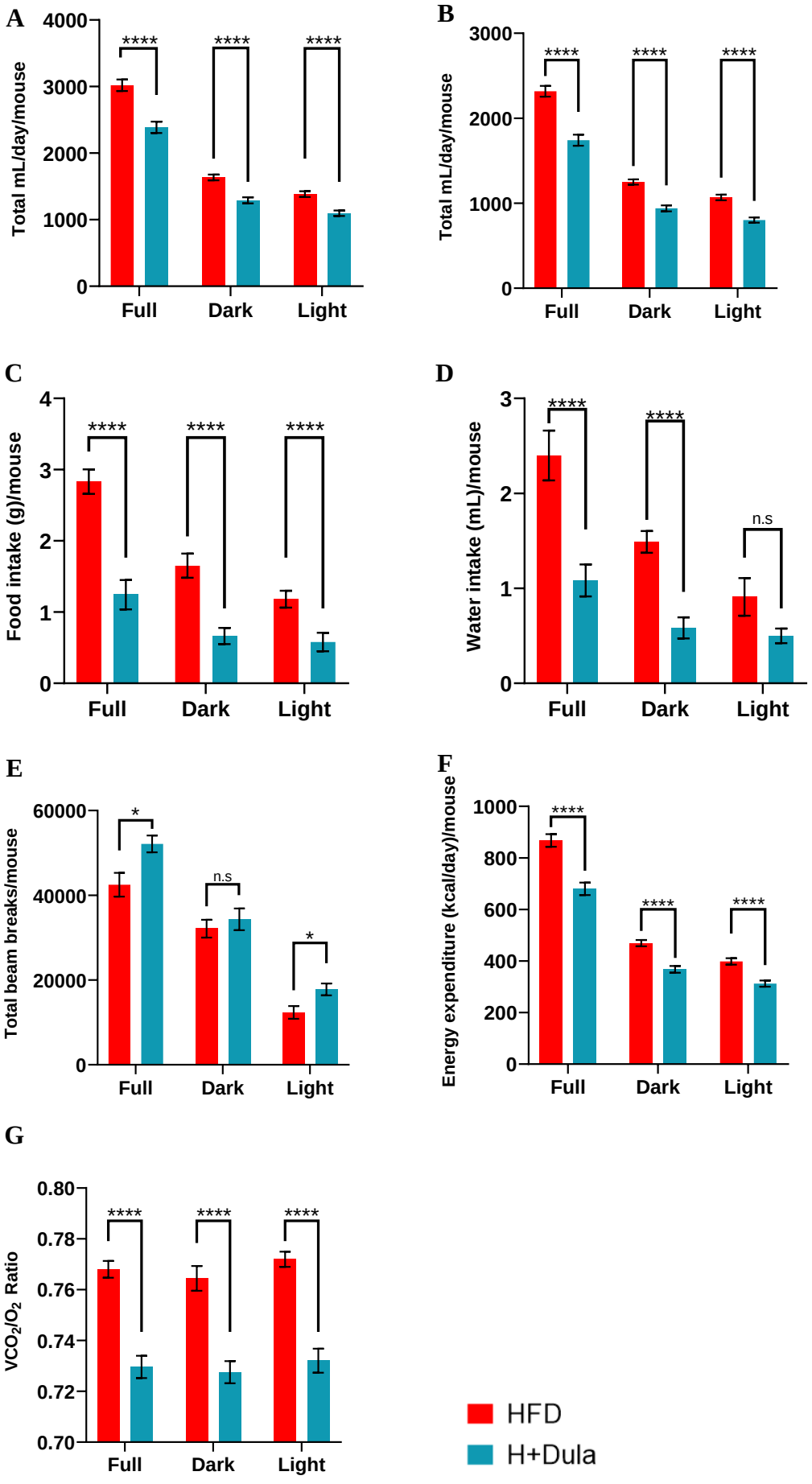
A
Total mL/day/mouse
4000
3000
2000
1000
0
****
****
****
Full
Dark
Light
B
Total mL/day/mouse
3000
2000
1000
0
****
****
****
Full
Dark
Light
C
Food intake (g)/mouse
4
3
2
1
0
****
****
****
Full
Dark
Light
D
Water intake (mL)/mouse
3
2
1
0
****
****
n.s
Full
Dark
Light
E
Total beam breaks/mouse
60000
40000
20000
0
*
n.s
*
Full
Dark
Light
F
Energy expenditure (kcal/day)/mouse
1000
800
600
400
200
0
****
****
****
Full
Dark
Light
G
VCO2/O2 Ratio
0.80
0.78
0.76
0.74
0.72
0.70
****
****
****
Full
Dark
Light
HFD
H+Dula

Figure 15. Dulaglutide altered the energy and behaviour of mice fed with high-fat diet for 12 weeks with 4-weeks dulaglutide treatment.

Mice were fed with standard chow or high-fat diet for 12 weeks. After 4 weeks of dulaglutide treatment, metabolic caging analysis of energy metabolism was performed. Mice were placed in individual cages for 24-hours to acclimatize prior to metabolic measurements for 24-hours. Volume of oxygen **(A)** and carbon dioxide **(B)**, food intake **(C)**, water intake **(D)**, movement by total beams broken over 24-hours **(E)** and energy expenditure **(F)**. Respiratory exchange ratio (RER) **(G)** was calculated by volume of carbon dioxide over volume of oxygen over 24-hours. Data represents means ± SEM, n = 6 – 9 mice per group. * $P < 0.05$, ****, $P < 0.0001$ and ns = not significant

5.8. Studies of morphological changes in mouse renal parenchyma

To investigate the morphological change in kidney cross sections after 4 weeks of dulaglutide treatment among STC, HFD and H+Dula groups, H&E and PASM staining were performed and the morphology of the kidney tissue was examined by light microscopy.

The representative optical micrographs of the H&E stained renal cross sections among STC, HFD and H+Dula groups are shown in Figure 16A. An examination of the optical micrographs of the STC control and HFD groups reveals an increase in the area of isometric vacuolization of the renal tubules, as indicated by the black arrow. The comparison between the HFD and the H+Dula groups show smaller number of vacuoles and size of the vacuoles by area. PASM staining was also performed and is mainly used to stain for basement membrane in the glomerulus. A further examination via PASM staining reveals an enlargement in glomeruli when comparing the HFD group with STC control group (Figure 16B). Image analysis was performed to measure the glomeruli area per cell ratio and the result reveals that there is a significantly larger area per cell ratio in the HFD group when compared between the STC and HFD groups by 6.80 times with P value < 0.0001. The comparison between the HFD and the H+Dula groups shows a significantly smaller area per cell ratio in the dulaglutide treated group H+Dula with P value < 0.0001. Despite there is a smaller area per cell ratio in the glomerulus after 4 weeks dulaglutide treatment, the area per cell ratio remains to be significantly higher in the H+Dula group when compared to the STC group by 4.45 times with P value of < 0.0001 (Figure 16C).

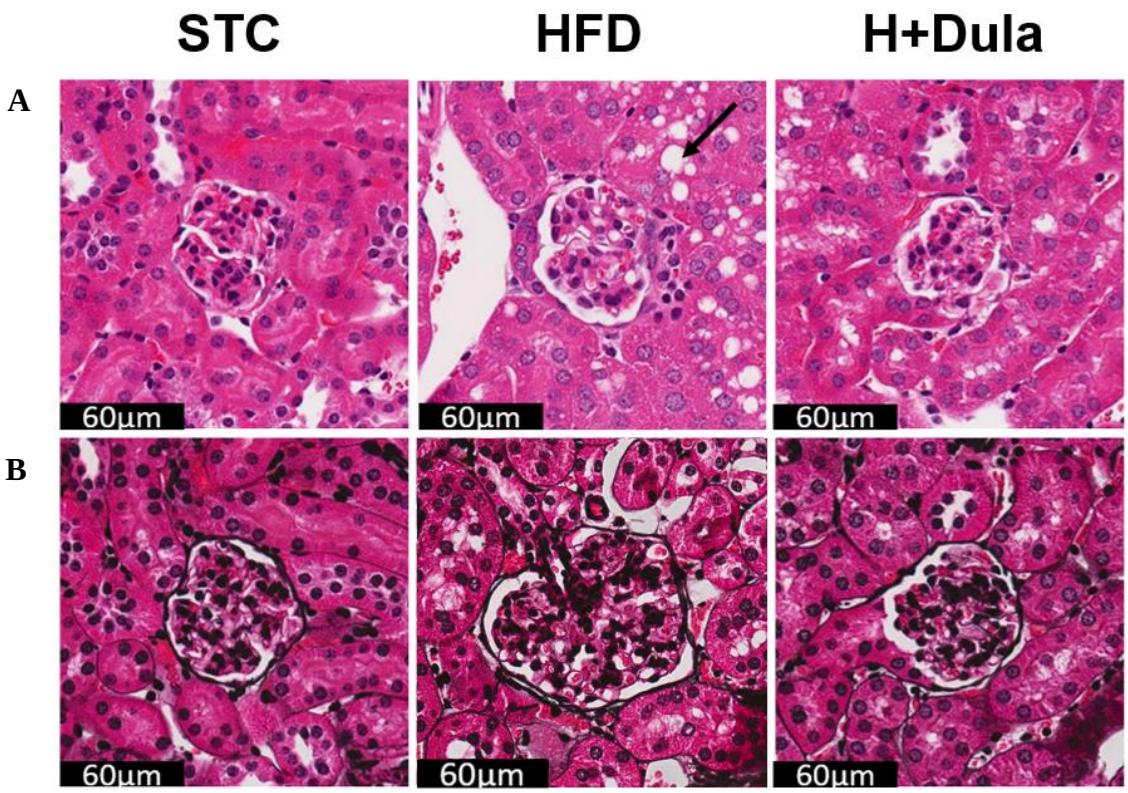
STC
HFD
H+Dula
A
B
60µm
60µm
60µm
60µm
60µm
60µm

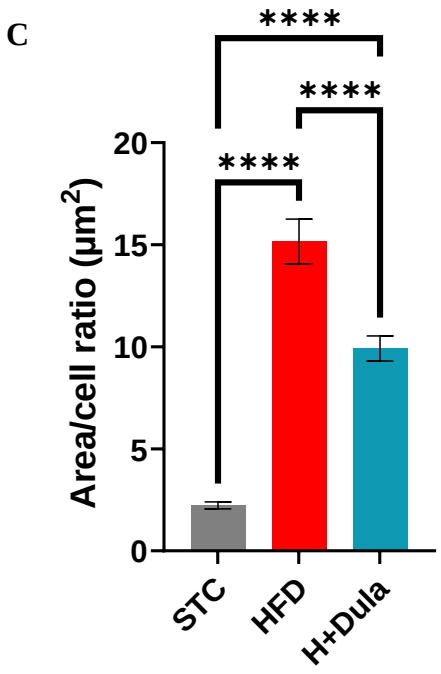
C
****
****
****
Area/cell ratio (µm2)
20
15
10
5
0
STC
HFD
H+Dula

Figure 16. Dulaglutide improved renal morphological changes by reduction of renal parenchymal vacuolization, Bowman's space, basement membrane thickness and total glomeruli area.

STC, HFD and H+Dula treatment mice were sacrificed after 16-hour fasting. Mice kidney were harvested and histopathological assessments were performed. Representative images of H&E **(A)** and PASM **(B)** staining of kidney are shown. Glomerular area was calculated by image analysis **(C)**. Data represents means ± SEM, n = 6 – 9 mice per group. **** $P < 0.0001$

5.9. Evaluation of ectopic lipid accumulation in metabolic organs

To investigate the neutral lipid content in kidney and liver cross sections after 4 weeks of dulaglutide treatment among STC, HFD and H+Dula groups, ORO staining was performed and the neutral lipid content of the kidney and liver tissue was examined by light microscopy and quantified using image analysis.

The representative optical micrographs of the ORO stained renal cross sections among STC, HFD and H+Dula groups are shown in Figure 17A. An examination of the renal optical micrographs of the STC control and HFD groups reveals a higher amount of neutral lipid staining specifically in the renal tubules. Comparison between the HFD and H+Dula group show lower staining intensity in the renal tubule regions. Image analysis was performed to measure the neutral lipid staining and the result reveals that there is a significantly higher amount of neutral lipid staining in the HFD group when compared between the STC and HFD groups by 67.89 times with P value < 0.0001. The comparison between the HFD and the H+Dula groups shows a significantly lower amount of neutral lipid staining in the dulaglutide treated group H+Dula with P value < 0.0001. Although there is a lower amount of neutral lipid staining in the renal tubule regions after 4 weeks dulaglutide treatment, the amount of staining remains to be significantly higher in the H+Dula group when compared to the STC group by 27.28 times with P value of < 0.0001 (Figure 17C).

The representative optical micrographs of the ORO stained liver cross sections among STC, HFD and H+Dula groups are shown in Figure 17B. An examination of the liver optical micrographs of the STC control and HFD groups reveals a higher amount of neutral lipid staining specifically in the liver. Comparison between the HFD and the H+Dula group show similar staining intensity in the liver. Image analysis was performed to measure the neutral lipid staining and the result reveals that there is a

significantly higher amount of neutral lipid staining in the HFD group when compared between the STC and HFD groups by 1.57 times with P value < 0.0001. The comparison between the HFD and the H+Dula groups shows no significant differences in the amount of neutral lipid staining in the dulaglutide treated group H+Dula with P value 0.70. The comparison of neutral lipid staining in liver between the STC and the H+Dula groups show that there is a 1.54 times higher amount of staining in the H+Dula group and the difference has a P value of < 0.0001 (Figure 17D).

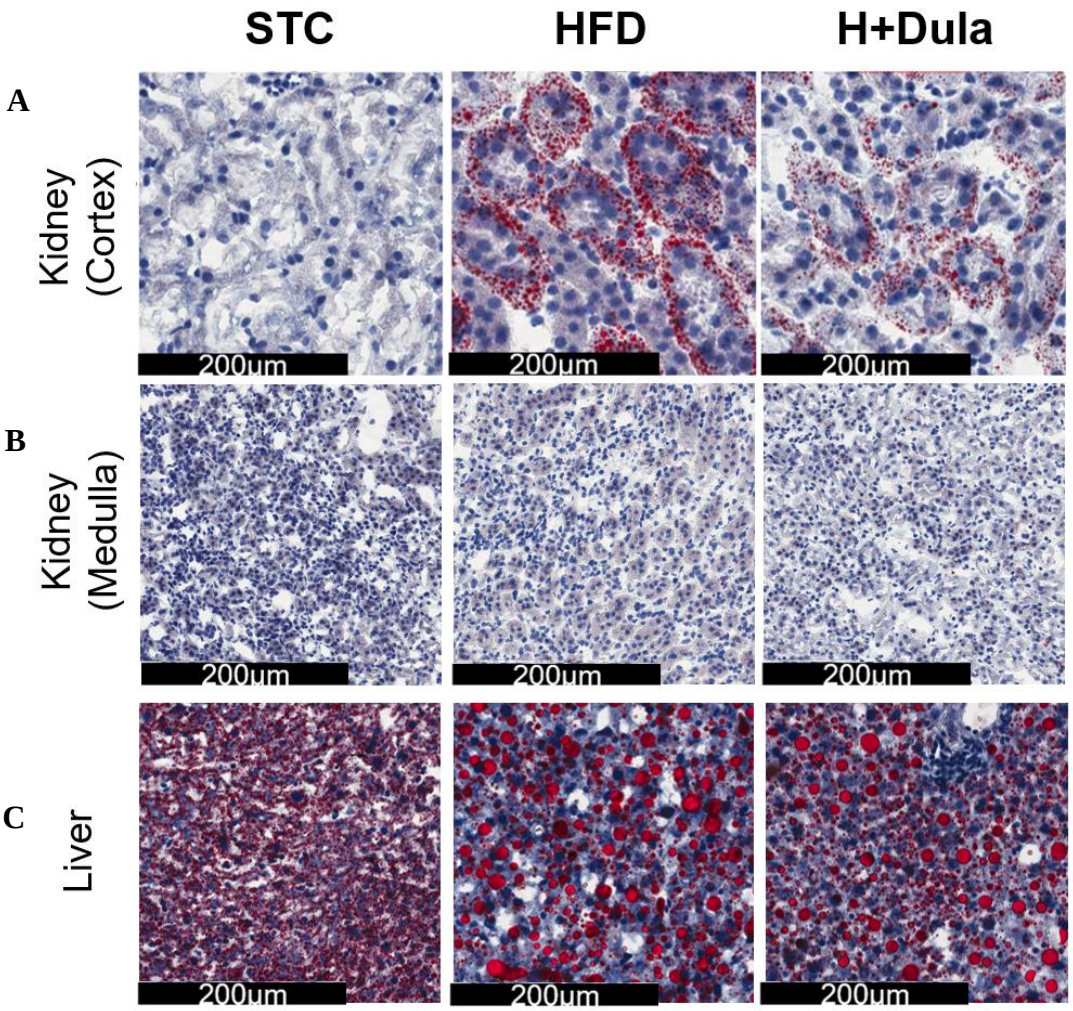
STC
HFD
H+Dula
A
Kidney (Cortex)
B
Kidney (Medulla)
C
Liver
200um

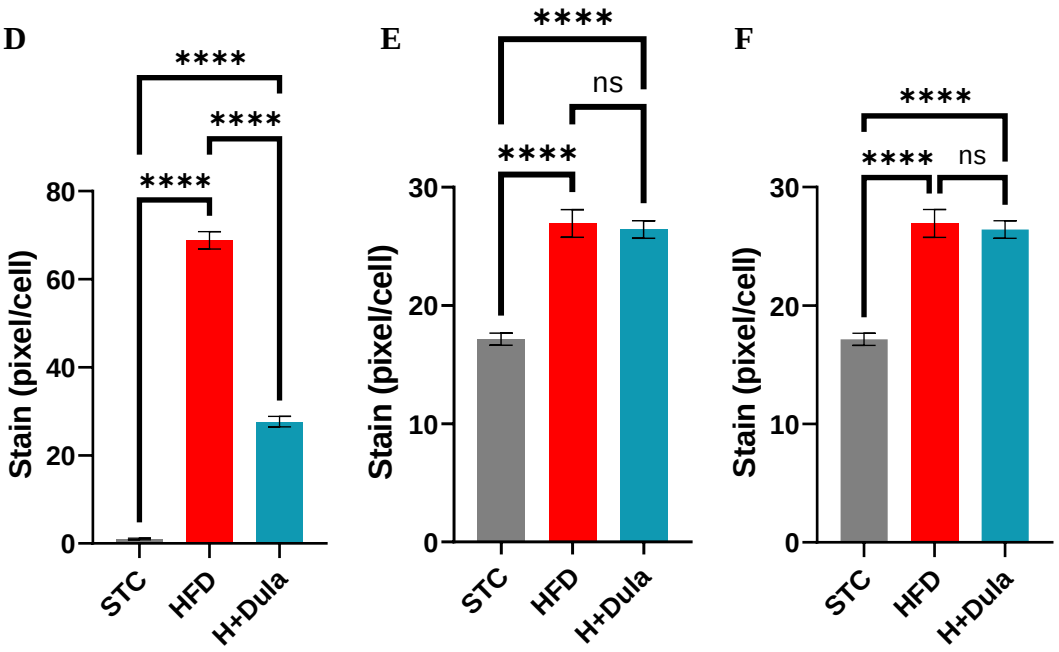
D
E
F
Stain (pixel/cell)
****
ns
STC
HFD
H+Dula

Figure 17. Dulaglutide improved renal ectopic lipid accumulation in renal parenchymal but not in the liver.

STC, HFD and H+Dula mice were sacrificed after 16-hour fasting. Mice kidney and liver were harvested and histopathological assessments were performed. Representative images of Oil red o staining of the kidney cortex, medulla and liver are shown. Neutral lipid stain was quantified by image analysis. Data represents means ± SEM, n = 6 – 9 mice per group. **** $P < 0.0001$ and ns = not significant

5.10. GLP-1R expression analysis after dulaglutide treatment

To investigate the expression of GLP-1R in kidney cross sections and to identify alterations in protein expression among STC, HFD and H+Dula groups after 4 weeks of dulaglutide treatment. Immunohistochemical staining was performed and the protein expression of GLP-1R in kidney tissue was examined by light microscopy and quantified using image analysis.

The representative optical micrographs of the GLP-1R stained by IHC in the renal cross sections among STC, HFD and H+Dula groups are shown in Figure 18A. An examination of the renal optical micrographs reveals that GLP-1R expression is present and abundantly found in renal tubules but not in the glomerulus among all groups. A further image analysis was performed specifically on renal tubules. Comparison of GLP-1R expression among the groups show no statistically significant expression differences. The P value between the STC group and the HFD group, the STC group and the H+Dula group and the HFD and the H+Dula group are 0.93, 0.85 and 0.76 respectively (Figure 18B).

The kidney from standard chow fed mice were used to determine the specificity and sensitivity of the GLP-1R antibody by ABclonal. Literature research show GLP-1R has a molecular weight of approximately 53 kDa (Alvarez *et al.*, 2005). Western blot analysis of the kidney showed expression of GLP-1R present and has a clear band between the 42 and 57 kDa markers. No additional non-specific bands were seen (Figure 19A). Additional Glyceraldehyde 3-phosphate dehydrogenase (GAPDH) was probed, as a control, on a separate membrane and the results show clearly the positive protein loading (Figure 19B).

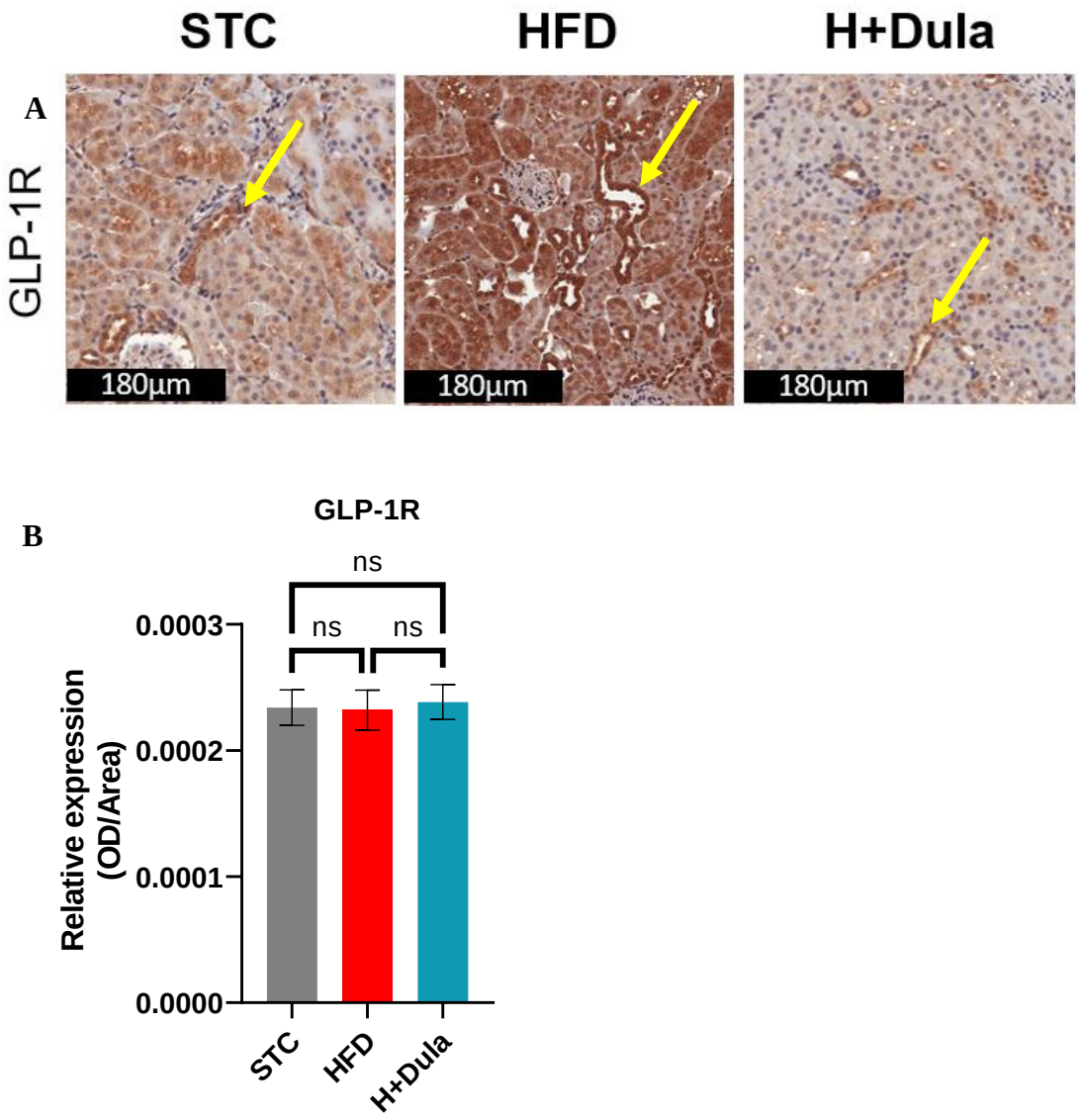

Figure 18. GLP-1R protein expression is unaltered after 12- weeks high-fat diet and with 4-weeks dulaglutide treatment in renal tubules.

STC, HFD and H+Dula treatment mice were sacrificed after 16-hour fasting. IHC staining of GLP-1R was performed on mice kidney **(A)**. Representative images of GLP-1R of kidney are shown. The chromogen DAB was quantified in renal tubules specifically by image analysis **(B)**. Data represents means ± SEM, n = 6 – 9 mice per group. ns = not significant

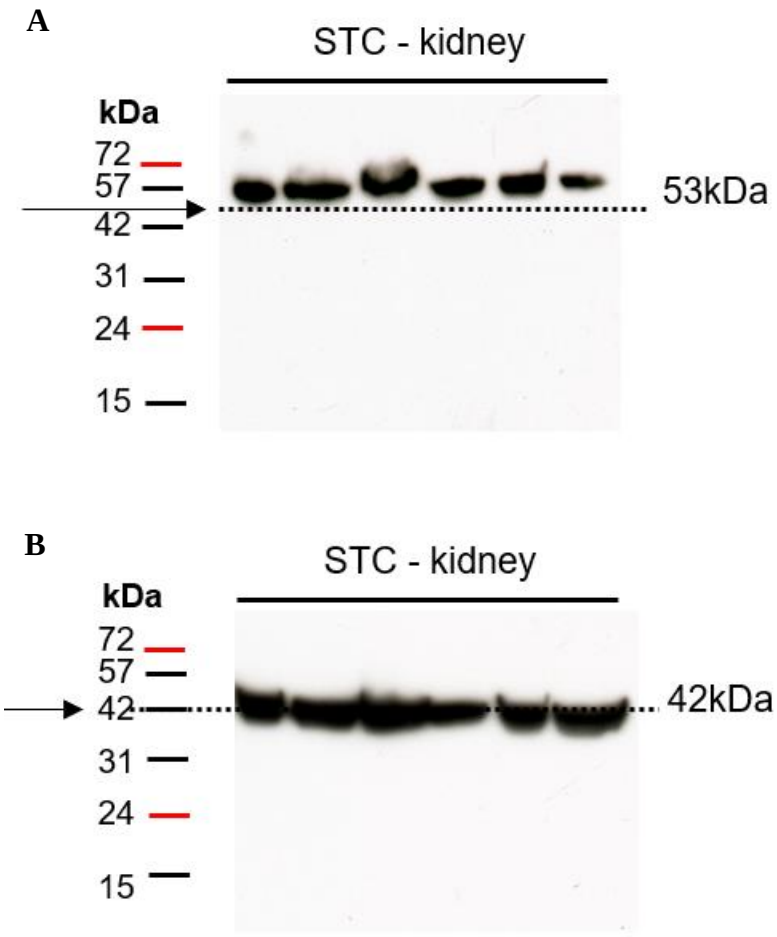

Figure 19. Antibody validation of glucagon-like peptide-1 receptor antibody via Western blot

The expression of GLP-1R in standard chow fed mice was measured by Western blot to identify the specificity of the GLP-1R antibody based on the molecular weight **(A)**. GAPDH was probed as a control **(B)**.

5.11. Determination of kidney injury marker expression after dulaglutide treatment

To investigate the expression of KIM-1 in kidney cross sections among STC, HFD and H+Dula groups after 4 weeks of dulaglutide treatment. Immunohistochemical staining was performed and the protein expression of KIM-1 in kidney tissue was examined by light microscopy and quantified using image analysis.

The representative optical micrographs of the KIM-1 stained by IHC in the renal cross sections among STC, HFD and H+Dula groups are shown in Figure 20A. An examination of the renal optical micrographs reveals that KIM-1 expression is present and abundantly found in renal tubules, specifically in proximal tubules, but not in the glomerulus among all groups. A further image analysis was performed specifically on renal tubules. Comparison of KIM-1 expression between the STC group and the HFD group show statistically significant expression difference. There is a higher expression in the HFD group by 6.95 times with P value of < 0.0001. Comparison of HFD group with H+Dula group show a decrease in expression by 0.11 times with a P value of < 0.0001. Between the STC group and the H+Dula group also show significant differences with a P value of < 0.0001 (Figure 20B).

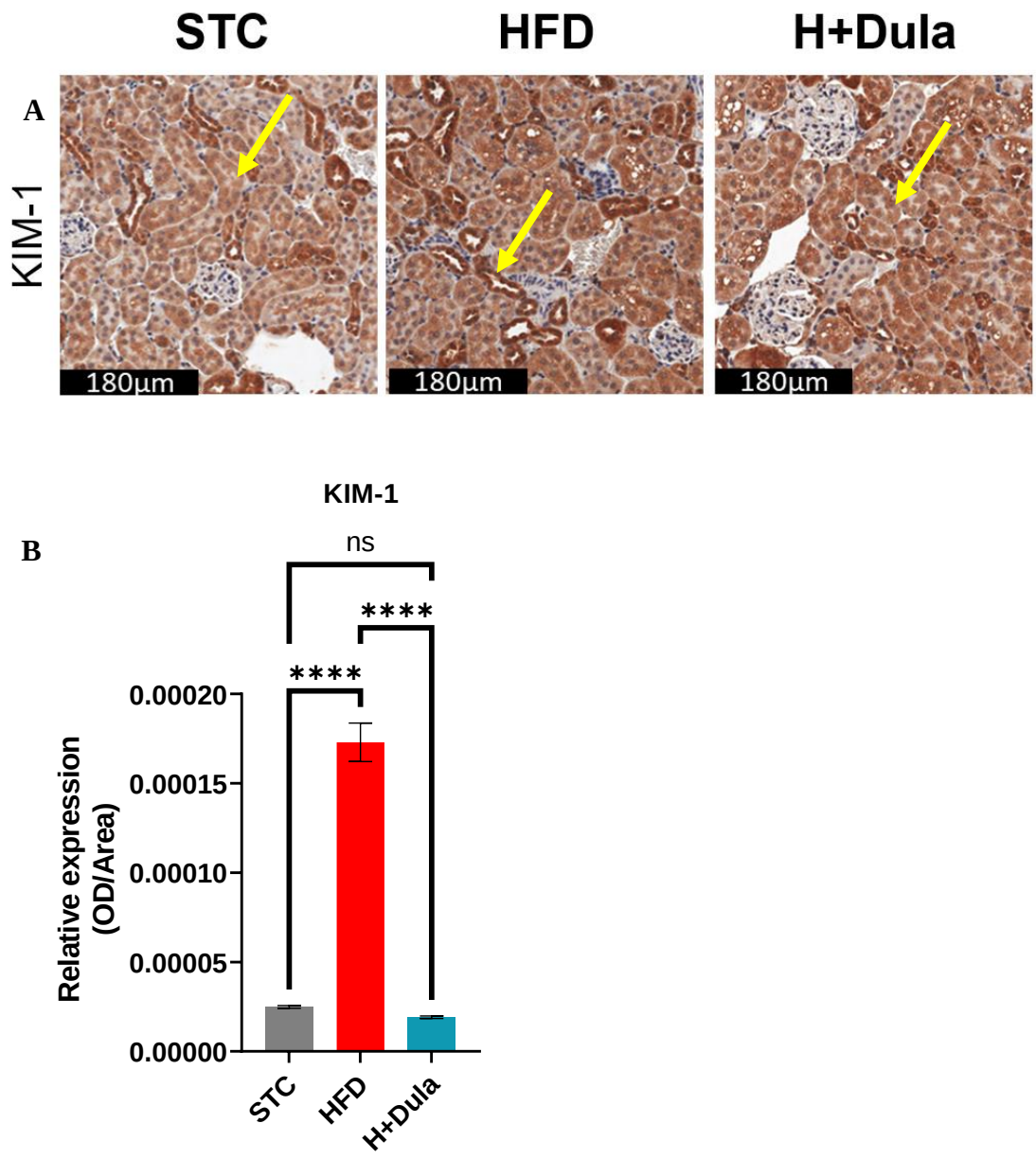

Figure 20. Dulaglutide reduced kidney damage by immunohistochemical staining of kidney injury molecule-1.

STC, HFD and H+Dula mice were sacrificed after 16-hour fasting. Immunohistochemical (IHC) staining of kidney injury molecule-1 (KIM-1) was performed on mice kidney. Representative images of KIM-1 of kidney are shown **(A)**. The chromogen 3,3'-Diaminobenzidine (DAB) was quantified by image analysis **(B)**.

Data represents means ± SEM, n = 6 – 9 mice per group. **** $P < 0.0001$ and ns = not significant

5.12. Kidney lipidome analysis using UHPLC/ESI-QTOF-MS

To investigate the lipidome changes in kidney cross sections among the STC, HFD and H+Dula groups, kidney lipid profiles were obtained from positive and negative electrospray ionization (ESI) modes of UHPLC/ESI-QTOF-MS for non-targeted lipidomic analysis. The raw data collected were imported into Progenesis QI software for peak alignment, peak extraction, and normalization before subsequent multivariate analysis was performed using SIMCA software. PCA was performed and the positive and negative dataset scores plot were plotted for the general visualization of interrelations and separation among the STC control, HFD and H+Dula groups. PLS-DA was performed and the positive and negative dataset scores plot were plotted to further facilitate the detection and differentiation of potential compounds of interest among the three groups. Whilst the OPLS-DA was also applied and allowed a complete separation between the HFD and H+Dula groups to further highlight the differential compounds. PCA score plots show that the lipidomic profiles of all groups under both positive and negative conditions are clustered and separated Pooled quality control samples were injected at regular intervals between data collection to ensure the stability and reliability of UHPLC/ESI-QTOF-MS acquired data. The QC samples are clearly clustered and positioned near the centre of the PCA scores plot indicating high stability and reliability of the UHPLC/ESI-QTOF-MS and data acquired. The HFD and H+Dula groups are separated from the STC control group (Figure 21A and B). A further analysis of the profiles by PLS-DA shows a clear separation among all groups. In addition, the PLS-DA positive ESI mode scores plot data are R^2X_{cum} = 0.534, R^2Y_{cum} = 0.990 and Q^2_{cum} = 0.792 whilst the negative ESI mode scores plot data are R^2X_{cum} = 0.561, R^2Y_{cum} = 0.990 and Q^2_{cum} = 0.885 (Figure 21C and D). Furthermore, an OPLS-DA analysis, which was performed on mass spectra and normalized

abundance obtained from the HFD and H+Dula groups, shows a significant separation between these two groups **(Figure X)**. The OPLS-DA positive ESI mode scores plot data are R^2X_{cum} = 0.563, R^2Y_{cum} = 0.999 and Q^2_{cum} = 0.706 whilst the negative ESI mode scores plot data are R^2X_{cum} = 0.414, R^2Y_{cum} = 0.975 and Q^2_{cum} = 0.614 (Figure 21E and F).

The results indicate that there are significant differences in kidney lipidome among the three groups. There is a clear separation of the STC group from the HFD group based on PCA scores plot indicating lipidome changes occur after 16 weeks high-fat diet feeding. There is also separation between the HFD and H+Dula groups based on PCA scores plot and this indicates that 4 weeks dulaglutide treatment have an effect on kidney lipidome.

ESI +

ESI -

PCA

PLS-DA

OPLS-DA

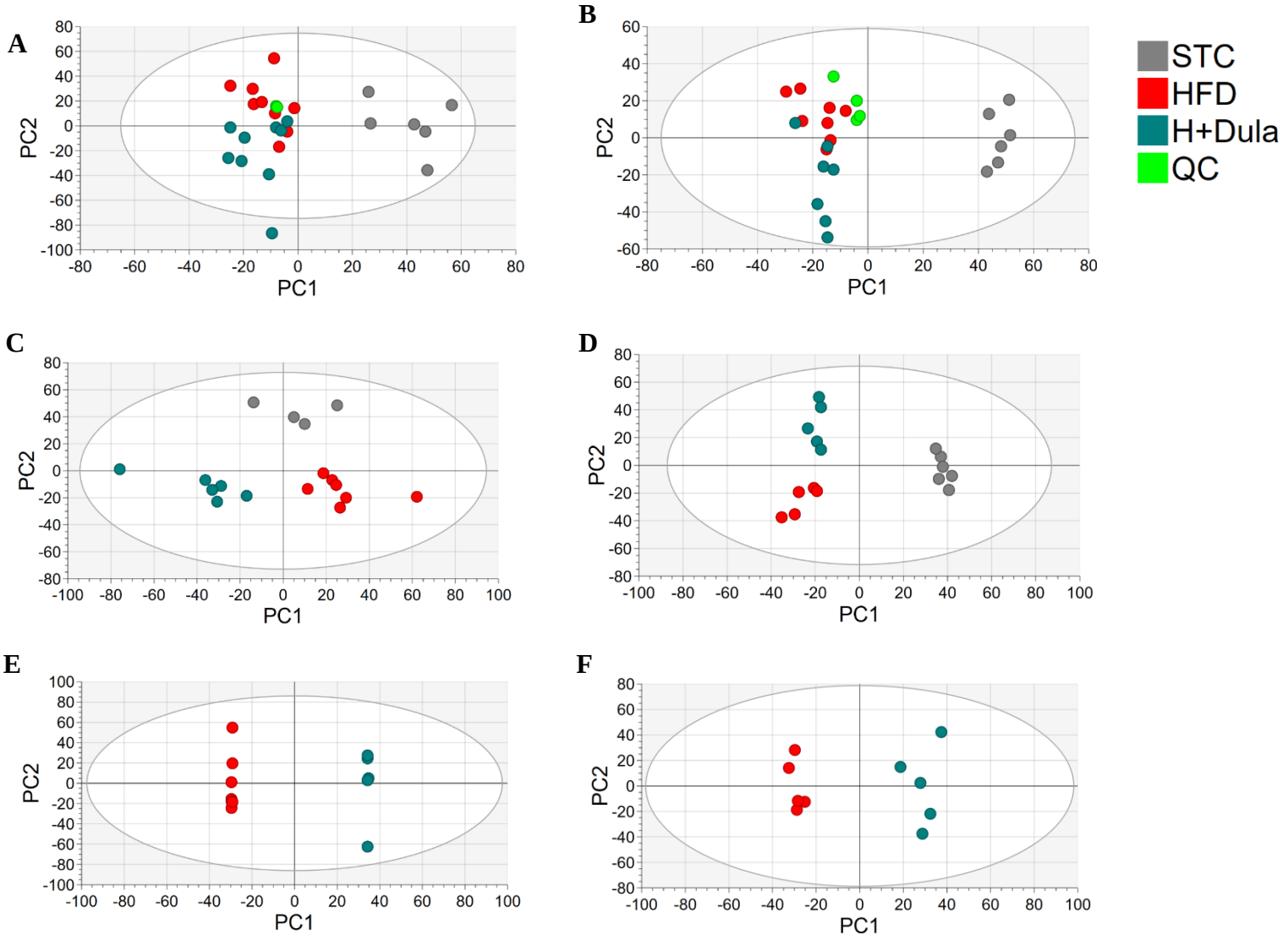

Figure 21. The different grouped mice are distinctly separated by their kidney lipidome in both positive and negative mode.

Kidney lipids were extracted, semi-quantified and identified using UHPLC/ESI-QTOF-MS in positive and negative ESI modes for the visualization using score plot of PCA **(A and B)**, PLS-DA **(C and D)** and OPLS-DA **(E and F)** respectively. All samples were pooled together to form the QC sample. Positive PLS-DA score plot: $R^2X_{(cum)}$ = 0.534, $R^2Y_{(cum)}$ = 0.990, $Q^2_{(cum)}$ = 0.792; negative PLS-DA score plot: $R^2X_{(cum)}$ = 0.561, $R^2Y_{(cum)}$ = 0.990, $Q^2_{(cum)}$ = 0.885. Positive OPLS-DA score plot: $R^2X_{(cum)}$ = 0.563, $R^2Y_{(cum)}$ = 0.999, $Q^2_{(cum)}$ = 0.706; negative OPLS-DA score plot: $R^2X_{(cum)}$ = 0.414, $R^2Y_{(cum)}$ = 0.975, $Q^2_{(cum)}$ = 0.614.

5.13. Determination of differential lipids and identification

To further investigate the lipidome changes among the HFD and H+Dula groups acquired by UHPLC/ESI-QTOF-MS, VIP plots were used for easy visualization for the selection of differential lipids and they are subsequently identified.

The positive and negative VIP plot are presented and differential lipids were selected based on VIP value of >1.0, which are important contributors to the group separation in PLS-DA scores plot. The VIP plots are shown in Figure 22A and B respectively. An independent sample t-test of the compounds was performed and compounds with $p < 0.05$ were selected. Compounds with coefficient of variation of < 30 % were also selected in Progenesis QI software. The remaining candidates were used for further analysis. In addition, MS/MS were performed to accurately determine the possible chemical structures of these compounds. We identified 62 compounds of interest with 44 compounds in positive mode and 18 compounds in negative mode. Their names, molecular formulae, ionization modes, mass fragments, retention times, mass errors, p-values and average fold changes are shown in Table 6**.**

Moreover, the 65 identified compounds of interest were further analysed by MetaboAnalyst 5.0 based on the compound's chemical nature and metabolic pathway. It is predicted that there are several altered metabolic pathways after the treatment with dulaglutide in the kidney. Top three altered pathways are glycerophospholipid, sphingolipid and ether lipid metabolisms (Figure 23A). Further lipid set enrichment identified specific altered lipid groups in the order of significance are glycerophosphocholines, sphingolipids, glycerophospholipids, glycerophosphoethanlamines and CL. In addition, CL shows the highest enrichment ratio among the enrichment dataset **(**Figure 23B**)**. Furthermore, the matched pathways from MetaboAnalyst are shown in Figure 23C which includes the pathway topology

analysis with P values and the number of matched lipids from KEGG database. Hits ≥ 2 are considered with high impact.

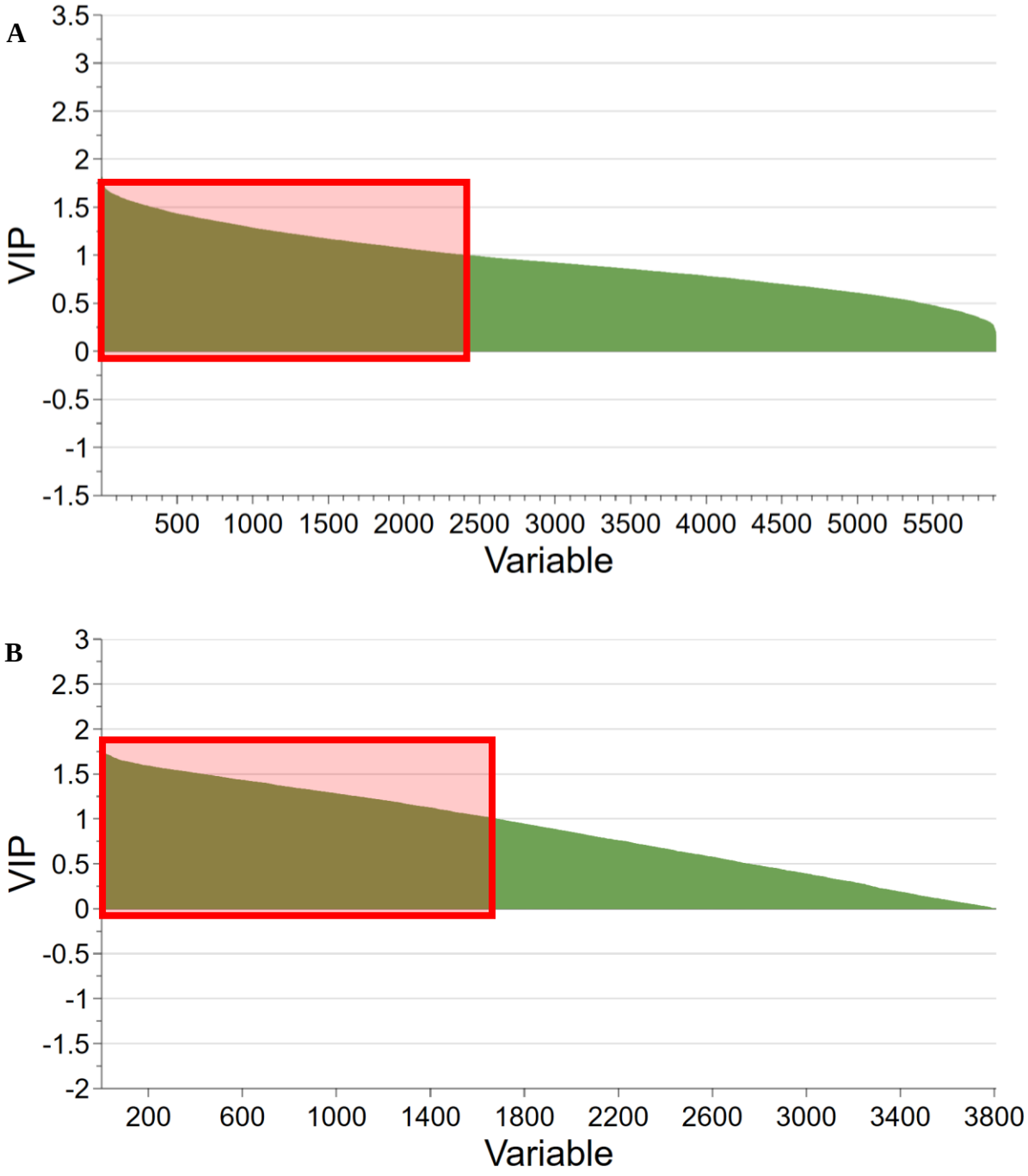

Figure 22. VIP plot identified differential lipid compounds after dulaglutide treatment.

Multivariate analysis was performed between the HFD and H+Dula groups; VIP was plotted for positive **(A)** and negative **(B)** ESI modes data. Lipids with VIP value > 1.0 have greater significance in the differentiation between groups (red box).

Table 6. Identified differential lipids between HFD model over dulaglutide treated mice in kidney tissue obtained by UHPLC/ESI-QTOF-MS in ESI positive and negative mode.

NO.	Abbreviation	Molecular formula	+/-	Adduct form	Mass-to-charge ratio (m/z)	Retention time (min)	Mass error (ppm)	p-value	Fold change (Log_2FC)
1.	Cer(d42:1)	$C_{42}H_{83}NO_3$	+	M+H	650.646	11.42	2.15	0.0133	0.244
2.	Cer(d40:2)	$C_{40}H_{77}NO_3$	-	M+FA-H	664.585	9.36	0.66	0.0428	0.160
3.	CL(72:0)	$C_{81}H_{158}O_{17}P_2$	-	M-H	1464.083	7.03	-4.72	0.0420	0.970
4.	CL(74:3)	$C_{83}H_{156}O_{17}P_2$	-	M-H	1486.079	7.85	2.89	0.0277	0.369
5.	CL(76:1)	$C_{85}H_{164}O_{17}P_2$	-	M+FA-H	1564.146	7.69	2.02	0.0371	-0.210
6.	CL(76:12)	$C_{85}H_{142}O_{17}P_2$	-	M-H	1495.962	11.37	-2.10	0.0487	0.321
7.	CL(78:2)	$C_{87}H_{166}O_{17}P_2$	-	M+Cl	1580.130	7.04	0.54	0.0433	0.240
8.	DG(32:5)	$C_{35}H_{58}O_5$	+	M+H	559.435	6.55	-1.97	0.0245	-0.497
9.	DG(42:8)	$C_{45}H_{72}O_5$	+	M+H	693.544	9.07	-1.98	0.0048	-0.638
10.	DG(38:5)	$C_{41}H_{70}O_5$	+	M+H	643.529	9.23	-1.38	0.0014	-0.348
11.	DG(40:6)	$C_{43}H_{72}O_5$	+	$M+NH_4$	686.570	8.81	-2.77	0.0194	0.525
12.	DG(42:7)	$C_{45}H_{74}O_5$	+	M+H	695.560	9.80	-0.91	0.0488	-0.939

13.	DG(42:9)	$C_{45}H_{70}O_5$	+	M+H	691.528	8.48	-1.82	0.0084	-0.817
14.	Glu-Cer(d30:1)	$C_{36}H_{69}NO_8$	+	M+H	644.510	5.66	1.39	0.0212	-0.196
15.	LysoPC(O-18:0)	$C_{26}H_{56}NO_6P$	+	M+H	510.391	3.90	-1.61	0.0254	0.680
16.	LysoPE(22:0)	$C_{27}H_{56}NO_7P$	+	M+H	538.389	3.78	4.73	0.0391	-0.667
17.	PA(33:2)	$C_{36}H_{67}O_8P$	+	M+H	659.467	6.27	3.69	0.0322	-0.937
18.	PA(41:0)	$C_{44}H_{87}O_8P$	+	M+H	775.623	11.49	1.81	0.0217	-1.658
19.	PC(34:2)	$C_{42}H_{80}NO_8P$	+	M+H	758.572	6.96	3.12	0.0097	0.360
20.	PC(40:5)	$C_{48}H_{86}NO_8P$	+	M+Na	858.596	8.04	-2.85	0.0489	0.652
21.	PC(42:10)	$C_{50}H_{80}NO_8P$	-	M-H	852.558	4.72	3.38	0.0064	-0.596
22.	PC(P-38:5)	$C_{46}H_{82}NO_7P$	-	M+Cl	826.554	6.01	2.56	0.0199	0.545
23.	PC(P-40:4)	$C_{48}H_{88}NO_7P$	+	M+Na	844.621	7.08	2.25	0.0127	0.466
24.	PC(40:5)	$C_{48}H_{86}NO_8P$	+	M+H	836.617	6.98	0.22	0.0271	-0.719
25.	PC(P-38:5)	$C_{46}H_{82}NO_7P$	+	M+H	792.591	6.94	0.86	0.0179	-0.362
26.	PC(P-40:5)	$C_{48}H_{86}NO_7P$	+	M+H	820.622	7.83	1.21	0.0195	-0.633
27.	PC(42:10)	$C_{50}H_{80}NO_8P$	+	M+H	854.570	5.51	0.93	0.0487	0.502
28.	PC(o-38:0)	$C_{46}H_{94}NO_7P$	+	M+H	804.684	10.95	-0.25	0.0093	1.297
29.	PC(o-44:4)	$C_{52}H_{98}NO_7P$	+	M+H	880.719	12.17	4.06	0.0263	1.024
30.	PC(P-36:0)	$C_{44}H_{88}NO_7P$	+	M+Na	796.620	8.28	1.35	0.0020	0.402
31.	PC(P-38:4)	$C_{46}H_{84}NO_7P$	+	M+H	794.605	7.21	-1.23	0.0260	-0.470

32.	PC(P-40:6)	$C_{48}H_{84}NO_7P$	+	M+H	818.605	6.88	-0.87	0.0289	-0.356
33.	PC(P-38:1)	$C_{46}H_{90}NO_7P$	+	M+Na	822.637	8.16	3.12	0.0111	-0.533
34.	PE(34:2)	$C_{39}H_{74}NO_8P$	+	M+H	716.523	7.23	0.11	0.0055	0.264
35.	PE(P-34:2)	$C_{39}H_{74}NO_7P$	-	M+Cl	734.492	6.63	3.94	0.0206	-0.350
36.	PE(38:5)	$C_{43}H_{76}NO_8P$	-	M-H	764.520	7.03	-4.10	0.0417	0.210
37.	PE(38:0)	$C_{43}H_{86}NO_8P$	+	M+H	776.614	9.73	-3.00	0.0408	0.721
38.	PE(40:8)	$C_{45}H_{74}NO_8P$	+	M+H	788.524	8.19	2.36	0.0086	0.790
39.	PE(P-36:2)	$C_{41}H_{78}NO_7P$	+	M+H	728.559	8.65	-0.02	0.0281	0.427
40.	PE(P-38:4)	$C_{43}H_{78}NO_7P$	-	M+Cl	786.524	6.81	3.79	0.0082	0.194
41.	PE(P-42:2)	$C_{47}H_{90}NO_7P$	+	M+H	812.656	13.70	3.54	0.0263	1.318
42.	PE-NMe(32:5)	$C_{38}H_{66}NO_8P$	+	M+H	696.463	3.90	4.83	0.0260	0.728
43.	PG(36:3)	$C_{42}H_{77}O_{10}P$	-	M-H	771.517	5.51	-0.94	0.0333	-0.393
44.	PG(34:2)	$C_{40}H_{75}O_{10}P$	-	M-H	745.502	5.45	-0.67	0.0148	-0.891
45.	PG(36:2)	$C_{42}H_{79}O_{10}P$	-	M-H	773.533	6.09	-1.09	0.0231	-0.354
46.	PG(38:6)	$C_{44}H_{75}O_{10}P$	-	M-H	793.499	4.73	-4.45	0.0164	-0.348
47.	PG(36:4)	$C_{42}H_{75}O_{10}P$	-	M-H	769.503	5.46	0.08	0.0451	0.685
48.	PI(38:3)	$C_{47}H_{85}O_{13}P$	+	M+H	889.580	7.07	-0.34	0.0466	0.558
49.	PI(40:5)	$C_{49}H_{85}O_{13}P$	-	M-H	911.564	6.53	-1.42	0.0406	-0.420
50.	PS(P-28:0)	$C_{34}H_{66}NO_9P$	+	M+Na	686.439	2.72	4.03	0.0403	0.961

51.	PS(37:1)	$C_{43}H_{82}NO_{10}P$	+	M+H	804.572	6.51	-3.89	0.0067	-0.325
52.	PS(32:0)	$C_{38}H_{74}NO_{10}P$	-	M-H	734.499	6.79	2.25	0.0359	-0.610
53.	SM(d36:1)	$C_{41}H_{83}N_2O_6P$	+	M+H	731.608	7.79	1.92	0.0229	-0.222
54.	SM(d36:2)	$C_{41}H_{81}N_2O_6P$	+	M+K	767.544	8.17	-3.85	0.0036	0.478
55.	TG(48:4)	$C_{51}H_{90}O_6$	+	M+H	799.681	11.65	0.02	0.0093	0.986
56.	TG(52:6)	$C_{55}H_{94}O_6$	+	$M+NH_4$	868.739	12.67	0.20	0.0240	-0.399
57.	TG(54:9)	$C_{57}H_{92}O_6$	+	$M+NH_4$	890.724	11.83	1.09	0.0184	-0.741
58.	TG(49:2)	$C_{52}H_{96}O_6$	+	M+Na	839.710	13.61	-0.35	0.0363	-0.457
59.	TG(50:5)	$C_{53}H_{92}O_6$	+	M+Na	847.678	11.97	-0.68	0.0370	-0.941
60.	TG(60:12)	$C_{63}H_{98}O_6$	+	$M+NH_4$	968.770	12.17	-0.08	0.0011	-0.782
61.	TG(62:13)	$C_{65}H_{100}O_6$	+	$M+NH_4$	994.785	12.14	-0.51	0.0017	-1.237
62.	TG(62:14)	$C_{65}H_{98}O_6$	+	$M+NH_4$	992.770	11.51	-0.24	0.0057	-1.735

A

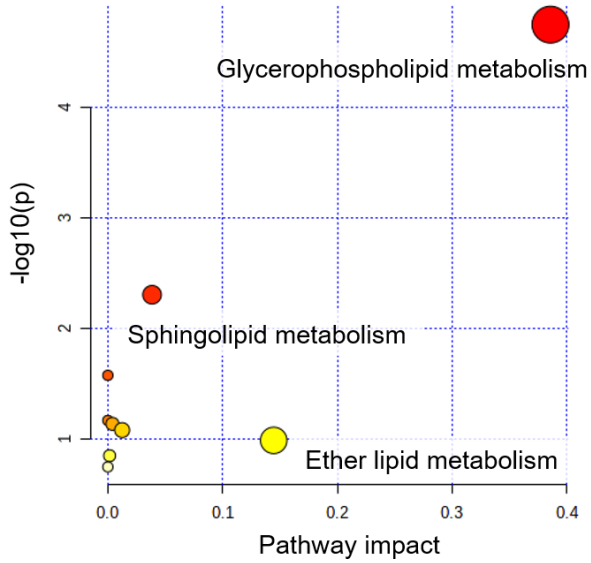

B

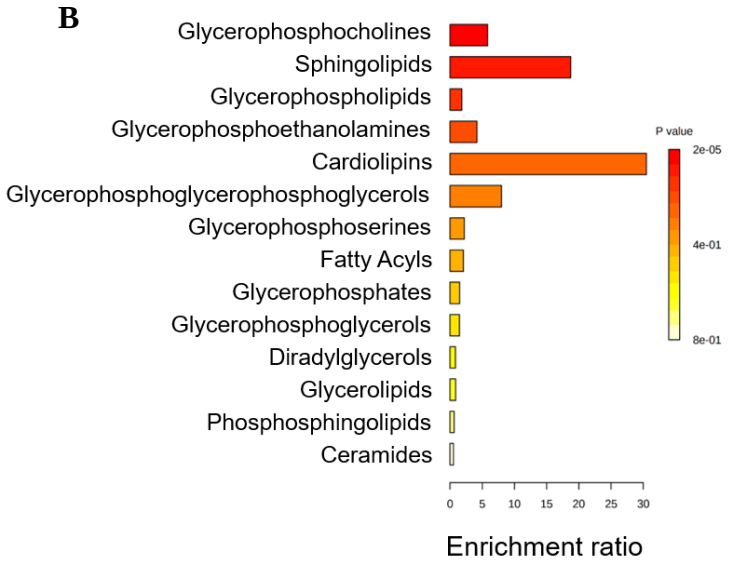

C

Pathway	*Total*	*Expected*	*Hits*	*Raw p*	*-LOG10(p)*	*FDR*	*Impact*
Glycerophospholipid metabolism	36	0.19124	4	1.80E-05	4.744	0.001515	0.38583
Sphingolipid metabolism	21	0.11155	2	0.004932	2.307	0.20715	0.03854
Linoleic acid metabolism	5	0.02656	1	0.026314	1.5798	0.7368	0
alpha-Linolenic acid metabolism	13	0.069057	1	0.067158	1.1729	1	0

Glycosylphosphatidylinositol (GPI)-anchor biosynthesis	14	0.074369	1	0.072156	1.1417	1	0.00399
Glycerolipid metabolism	16	0.084993	1	0.082083	1.0857	1	0.01246
Ether lipid metabolism	20	0.10624	1	0.10166	0.99286	1	0.14458
Phosphatidylinositol signalling system	28	0.14874	1	0.13972	0.85476	1	0.00152
Arachidonic acid metabolism	36	0.19124	1	0.17635	0.75361	1	0

Figure 23. Lipid pathway analysis and set enrichment show altered metabolism after dulaglutide treatment.

Pathway topology analysis by MetaboAnalyst 5.0 and KEGG database was performed. Pathway analysis overview and table of matched pathways between HFD and H+Dula grouped mice are shown **(A)**. Further lipid data were enriched to identify specific lipid types changes involved after dulaglutide treatment **(B)**. The additional information provided from the matched pathway topology analysis is shown **(C)**. The top matched pathways and its impact values are shown. Pathways with more than 2 hits are considered.

5.14. Spatial visualization of kidney lipidome after dulaglutide treatment

To investigate lipid alterations spatially in kidney cross section among the STC, HFD and H+Dula groups, MALDI-MSI was performed in both positive and negative mode by acquiring mass spectra systematically at a spatial resolution of 100 μm to evaluate the changes in the level of lipid species from kidney tissue. Prior to data acquisition, the DHB matrix applied was deposited evenly on all kidney tissue and was check microscopically to guarantee fair analysis of acquired data afterwards.

MALDI images of mouse kidney sections are shown in Figure 24. The left kidney from each mouse was trimmed and sectioned at 8 μm thick using a cryostat. Three representative levels were taken and are of 40 μm in thickness apart. A DHB matrix was used to acquire the mass spectral data systematically to calculate and observe the lipidome changes in the different renal compartments. All spectra were normalized by root-mean-square method. The results showed an alteration in the abundance of specific lipid groups, such as triglyceride (TG), phosphatidylinositol (PI), phosphatidylcholine (PC) and CL. Previous observations from ORO staining suggested that most lipids are found present in the cortex region of the kidney; hence, subsequent analysis was conducted in the cortex region of the kidney.

Spatial distribution of TG (52:2) are shown in Figure 24A, which represents the TGs in the kidney cortex regions of the three groups. Unlike the distributions of PCs and CLs, high abundance of TGs is observed in the HFD kidney cortex. It is a major type of lipid involved in ectopic lipid accumulation [28]. Low abundance of TG is found in the outer medulla of cortex region of the STC control. After high-fat diet feeding, TG abundance increased dramatically in the cortex region and also in the outer medulla of the HFD group with P value of <0.0001. After treatment with dulaglutide decreased signal intensities of TG are observed mainly in the cortex region with P value of

<0.0001. In summary, normalized intensities of TG (52:2) in the kidney cortex regions show a significant increase in TG after high-fat diet feeding and a significant reduction after dulaglutide treatment; however, the short treatment duration may have prevented a complete recovery of the TG deposited in the cortex, showing consistence with the ORO staining results.

The abundance of PI is shown in Figure 24B, and it is mainly accumulated in the cortex region of the kidney sections in the STC group. Using PI (38:4) as the representative distribution of PIs, there is a significantly lower abundance of PI in the HFD group as compared with the STC group with P value of <0.0001. Furthermore, the comparison between the HFD group and the H+Dula group shows that there is a significantly higher abundance of PI in the dulaglutide treated group with a P value of <0.0001. As PIs play a vital role in cell polarization and are presently found in proximal tubules, the higher abundance in the H+Dula group may contribute to improved tubule functions.

Remarkably, most identified PCs show a general decrease in abundance after the high-fat diet for 12 weeks, as compared with the STC lean control with P value of 0.0003. The H+Dula group shows a mild recovery of PC abundance as compared with the HFD group (Figure 24C). We specifically selected PC (38:7) as an example of all PCs to determine the difference in the PC abundance within the cortex region of each kidney cross section from each group. The normalized intensities of the ions at m/z = 804.6 from the kidney cortex region of the HFD group are much lower as compared with those from the kidney cortex region of the STC control group, suggesting a much lower PC abundance in the kidney cortex region of the HFD group. Interestingly, the figure also shows that there is a significant increase in the abundance of PC after dulaglutide treatment in the H+Dula group when compared with the HFD group.

The distribution of CL is shown in Figure 24D. The abundance of CL in cortex regions of the kidney sections is similar to that of PC shown in Figure 24C. Using CL (74:2) as a representative distribution of CLs, Figure 24D reveals a high abundance of CL in the cortex region of mouse kidney of the STC control as compared with that of the HFD group. The reduction of CL in the HFD group was ameliorated after the treatment with dulaglutide. The normalized intensities show statistically significant difference among the HFD, STC lean control, and H+Dula groups.

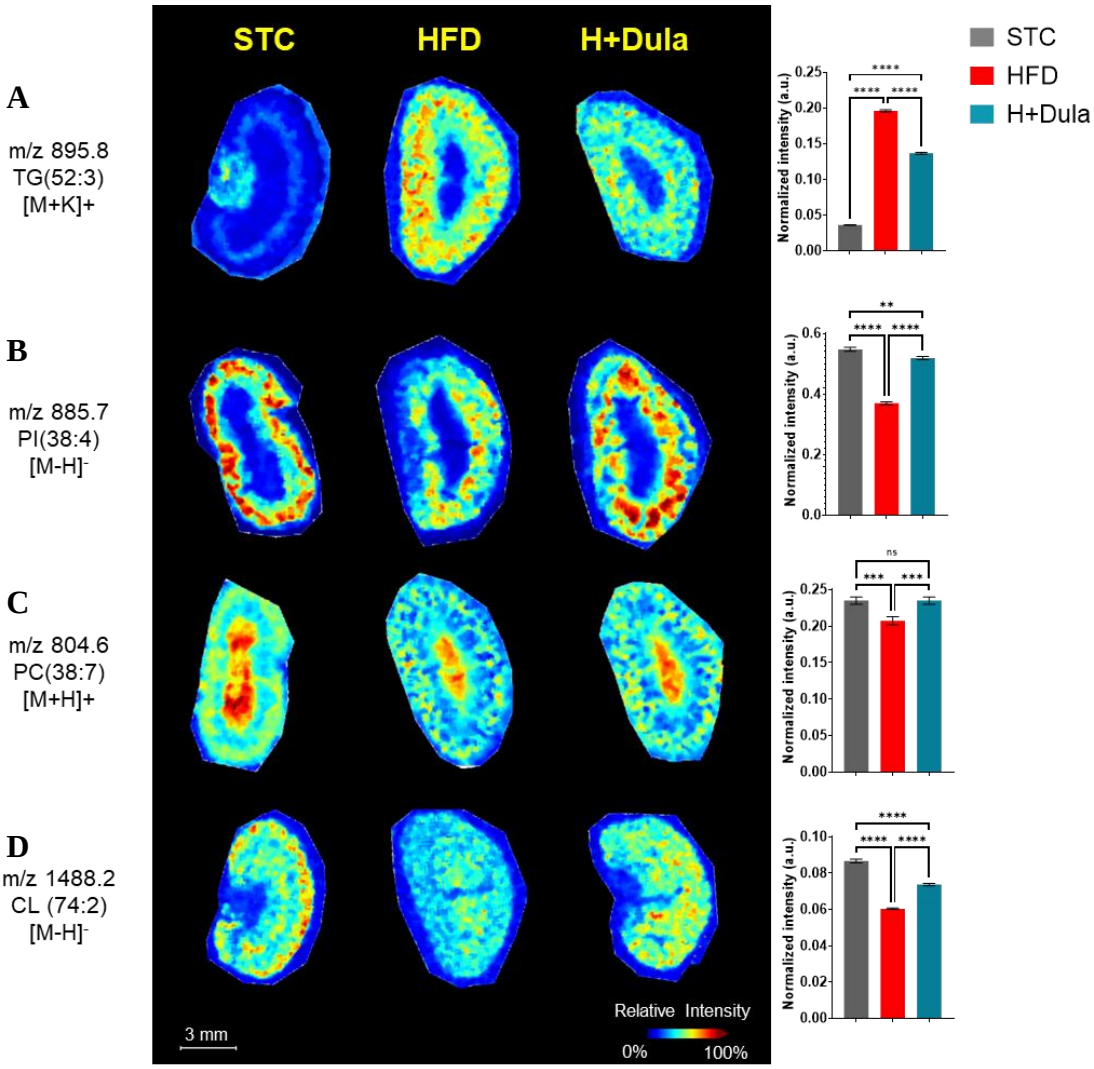
A
m/z 895.8
TG(52:3)
[M+K]+
B
m/z 885.7
PI(38:4)
[M-H]-
C
m/z 804.6
PC(38:7)
[M+H]+
D
m/z 1488.2
CL (74:2)
[M-H]-
STC
HFD
H+Dula
3 mm
Relative Intensity
0%
100%
Normalized intensity (a.u.)
STC
HFD
H+Dula

Figure 24. Dulaglutide treatment altered kidney lipid content and abundance especially in the kidney cortex.

Dulaglutide can trigger the spatial redistribution of lipids in the kidneys of high-fat diet-fed mice visualized by MALDI-MSI. MALDI-MSI acquired images of mouse kidney sections obtained at a spatial resolution of 100 μm. Alterations in lipid content of TG, PI, PC and CL in the kidney cortex after dulaglutide treatment are visualized by MALDI-MSI. Spatial visualization of **(A**) TG(52:3), [M+K]+, m/z 895.8 was performed in positive mode. **(B)** PI(38:4), [M-H]-, m/z 885.7 was performed in negative mode. **(C)** PC(38:7), [M+H]+, m/z 804.6) was performed in positive mode and **(D)** CL(74:2), [M+H]-, m/z 1488.2 was performed in negative mode. Bar chart of normalized intensities was plotted and used to calculate changes. Data represents means ± SEM, n = 6 – 9 mice per group. **** $P < 0.0001$ and ns = not significant

5.15. Validation of the involvement of dulaglutide in cardiolipin synthesis pathway

To confirm the changes in cardiolipin abundance observed by UHPLC/ESI-QTOF-MS and MALDI-MSI, the gene expression related to cardiolipin synthesis was measured using qRT-PCR.

CL abundance in homogenized kidney tissues and cross-sectional kidney sections were determined by UHPLC/ESI-QTOF-MS and MALDI-MSI, respectively. The results show an overall reduction in CL abundance, especially within the kidney cortex regions of the HFD group. As mentioned previously, a normal functional kidney requires high amounts of energy, which are produced by the mitochondria; however, the reduction of CL has a negative impact on the mitochondria function and activity [29]. As CL abundance was significantly increased in the H+Dula group; to confirm the increase of CL and its effects, which are associated with the CL synthesis pathway, we measured mRNA expression of major enzymes involved in this process. An overview of CL synthesis pathway was determined and lipid data involved in CL synthesis were obtained from UHPLC/ESI-QTOF-MS experiments. Lipids with increased or decreased abundance are highlighted in red and green, respectively (Figure 25A). Cytidine diphosphate diacylglycerol synthetase 1 (CDS1), phosphatidylglycerol phosphate synthase (PGPS), cardiolipin synthase (CLS), tafazzin (TAZ) and acyl-CoA:lysocardiolipin acyltransferase 1 (ALCAT1) were quantified using RT-qPCR.

CDS1 gene expression was measured and there is no significant difference between the STC group and the HFD group with P value of 0.95. There is a higher gene expression in the H+Dula group when compared with the STC and HFD group. The

differences are significant with a P value of 0.0106 and 0.0091 respectively (Figure 25B).

For PGPS, the gene expression was measured and compared among the three groups. There is no significant gene expression in the HFD group when compared with the STC group with P value of 0.1902. The H+Dula group was compared with the HFD group and shows a significantly higher gene expression with P value of 0.0254. There is a significantly higher expression when compared between the STC group and H+Dula group with P value of 0.0010 (Figure 25C).

For CLS, the gene expression was measured and compared among the three groups. There is no significant gene expression in the HFD group when compared with the STC group with P value of 0.6955. The H+Dula group was compared with the HFD group and shows a significantly higher gene expression with P value of 0.0061. There is a higher expression when comparing between the STC group and H+Dula group but with no significant difference, with a P value of 0.0522 (Figure 25D).

For TAZ, the gene expression was measured and compared among the three groups. There is no significant difference in gene expression in the HFD group when compared with the STC group with P value of 0.9702. The H+Dula group was compared with the HFD group and shows a significantly higher gene expression with P value of 0.028. There is a significantly higher expression when compared between the STC group and H+Dula group with P value of 0.0219 (Figure 25E).

For ALCAT1, the gene expression was measured and compared among the three groups. There is a mild higher gene expression in the HFD group when compared with the STC group with P value of 0.1784. The H+Dula group was compared with the

HFD group and shows slightly lower gene expression with P value of 0.8292 (Figure 25F).

Overall, the gene expression of CDS1, PGPS, CLS and TAZ show significant increases in mRNA expression (Figure 25B, C, D and E) in H+Dula group when compared with the HFD group along with a reduction of CL precursor lipid groups, such as PA and PG. Whilst ALCAT1 showed a slightly higher gene expression in the HFD group, the H+Dula group show very little difference in gene expression after drug treatment.

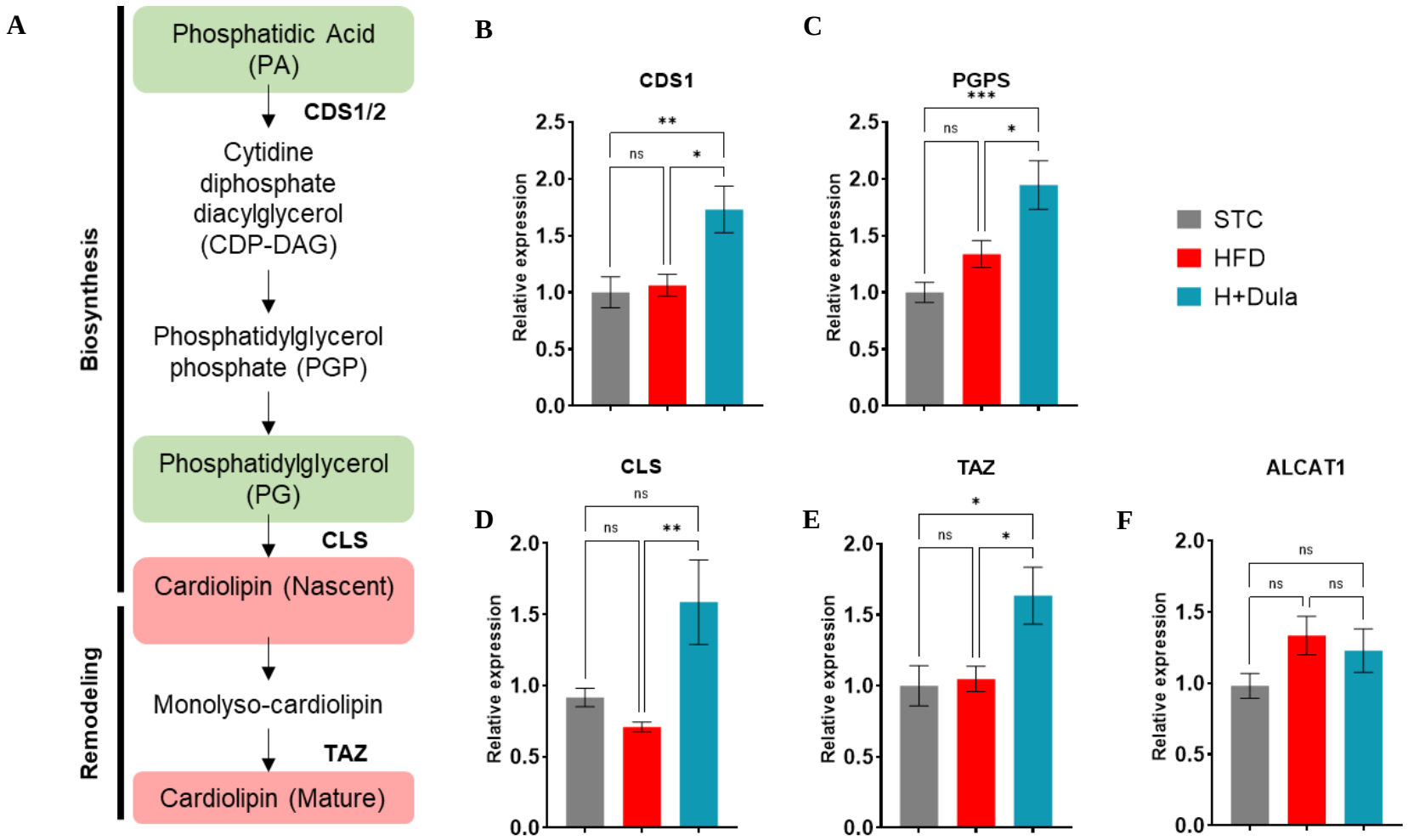
A
Biosynthesis
Remodeling
Phosphatidic Acid (PA)
CDS1/2
Cytidine diphosphate diacylglycerol (CDP-DAG)
Phosphatidylglycerol phosphate (PGP)
Phosphatidylglycerol (PG)
CLS
Cardiolipin (Nascent)
Monolyso-cardiolipin
TAZ
Cardiolipin (Mature)
B
CDS1
C
PGPS
D
CLS
E
TAZ
F
ALCAT1
Relative expression
ns
*
**
***
STC
HFD
H+Dula

Figure 25. mRNA expressions of key enzymes involved in cardiolipin synthesis was elevated after dulaglutide treatment

Gene expressions of enzymes involved in cardiolipin synthesis were quantified after dulaglutide treatment using RT-qPCR. **(A)** Overview of cardiolipin biosynthesis pathway. Lipid groups with increased and decreased abundance from UHPLC/ESI-QTOF-MS data are highlighted in red and green respectively. The mRNA level of enzymes involved in CL biosynthesis and remodelling includes CDS1 **(B)**, PGPS **(C)**, CLS **(D)**, TAZ **(E)** and ALCAT1 **(F)** were measured in kidney tissue samples by qPCR. All measurements are normalized to GAPDH, and are shown relative to STC group, which were set arbitrary to 1. Data represents means ± SEM, n = 6 – 9 mice per group. * $P < 0.05$, ** $P < 0.01$, *** $P < 0.001$ and ns = not significant

5.16. Quantification of mitochondrial DNA, PGC-1α and its downstream gene expressions

To determine whether 4 weeks of dulaglutide treatment may have an effect on mitochondrial number and its biogenesis, qRT-PCR was performed to quantify the mRNA gene expression changes.

The mitochondrial DNA (mtDNA) was measured and was normalized to the genomic DNA (gDNA). Their ratio was calculated as a measure of relative mtDNA and is compared among the STC, HFD and H+Dula groups. After high-fat diet for 16 weeks, comparing the HFD group with the STC group showed a significantly lower mtDNA content by 0.38 times with a P value of 0.0053. The H+Dula group was compared with the HFD group and shows a significantly higher mtDNA content with P value of 0.041 (Figure 26A).

For peroxisome proliferator-activated receptor gamma coactivator 1-alpha (PGC-1α), the gene expression was measured and compared among the three groups. There is a significantly lower gene expression in the HFD group when compared with the STC group with P value of 0.001. The H+Dula group was compared with the HFD group and shows a significantly higher gene expression with P value of 0.0243. There is a significantly lower expression when compared between the STC group and H+Dula group with P value of 0.03 (Figure 26B).

For nuclear respiratory factor 1 (NRF1), the gene expression was measured and compared among the three groups. There is a mild increase in gene expression in the HFD group when compared with the STC group with P value of 0.8753. The H+Dula group was compared with the HFD group and shows a significantly higher gene expression with P value of 0.0494. There is a significantly higher expression when

compared between the H+Dula group and STC group with P value of 0.0274 (Figure 26C).

For mitochondrial transcription factor A (TFAM), the gene expression was measured and compared among the three groups. There is a mild increase in gene expression in the HFD group when compared with the STC group with P value of 0.7248. The H+Dula group was compared with the HFD group and shows a significantly higher gene expression with P value of 0.0196. There is a significantly higher expression when compared between the H+Dula group and STC group with P value of 0.0069 (Figure 26D).

For gluconeogenic phosphoenolpyruvate carboxykinase (PEPCK), the gene expression was measured and compared among the three groups. There is a mild increase in gene expression in the HFD group when compared with the STC group with P value of 0.4306. The H+Dula group was compared with the HFD group and shows similar gene expression with P value of 0.99. There is a higher expression when compared between the H+Dula group and STC group with P value of 0.3920 (Figure 26E).

For NADH-ubiquinone oxidoreductase chain 5 protein (ND5), the gene expression was measured and compared among the three groups. There is an increase in gene expression in the HFD group when compared with the STC group with P value of 0.2551. The H+Dula group was compared with the HFD group and shows lower gene expression with P value of 0.0534. There is a lower expression when compared between the H+Dula group and STC group with P value of 0.7073 (Figure 26F).

For cytochrome b (CYTB), the gene expression was measured and compared among the three groups. There is a mild increase in gene expression in the HFD group when

compared with the STC group with P value of 0.86. The H+Dula group was compared with the HFD group and shows lower gene expression with P value of 0.3534. There is a lower expression when compared between the H+Dula group and STC group with P value of 0.72 (Figure 26G).

For cytochrome oxidase III (CoxIII), the gene expression was measured and compared among the three groups. There is a similar gene expression in the HFD group when compared with the STC group with P value of 0.9915. The H+Dula group was compared with the HFD group and shows lower gene expression with P value of 0.8865. There is a lower expression when compared between the H+Dula group and STC group with P value of 0.9443 (Figure 26H).

Overall, there is a lower mitochondria content in high-fat diet fed mice. Dulaglutide treated mice showed higher mitochondria content. This pattern is similar to PGC-1α gene expression. There is also a higher expression of downstream transcriptional factors associated with PGC-1α in the H+Dula group. However, the gene expressions of key mitochondrial biogenesis markers did not show significant increase and therefore may not play a role in mitochondrial restoration via biosynthesis.

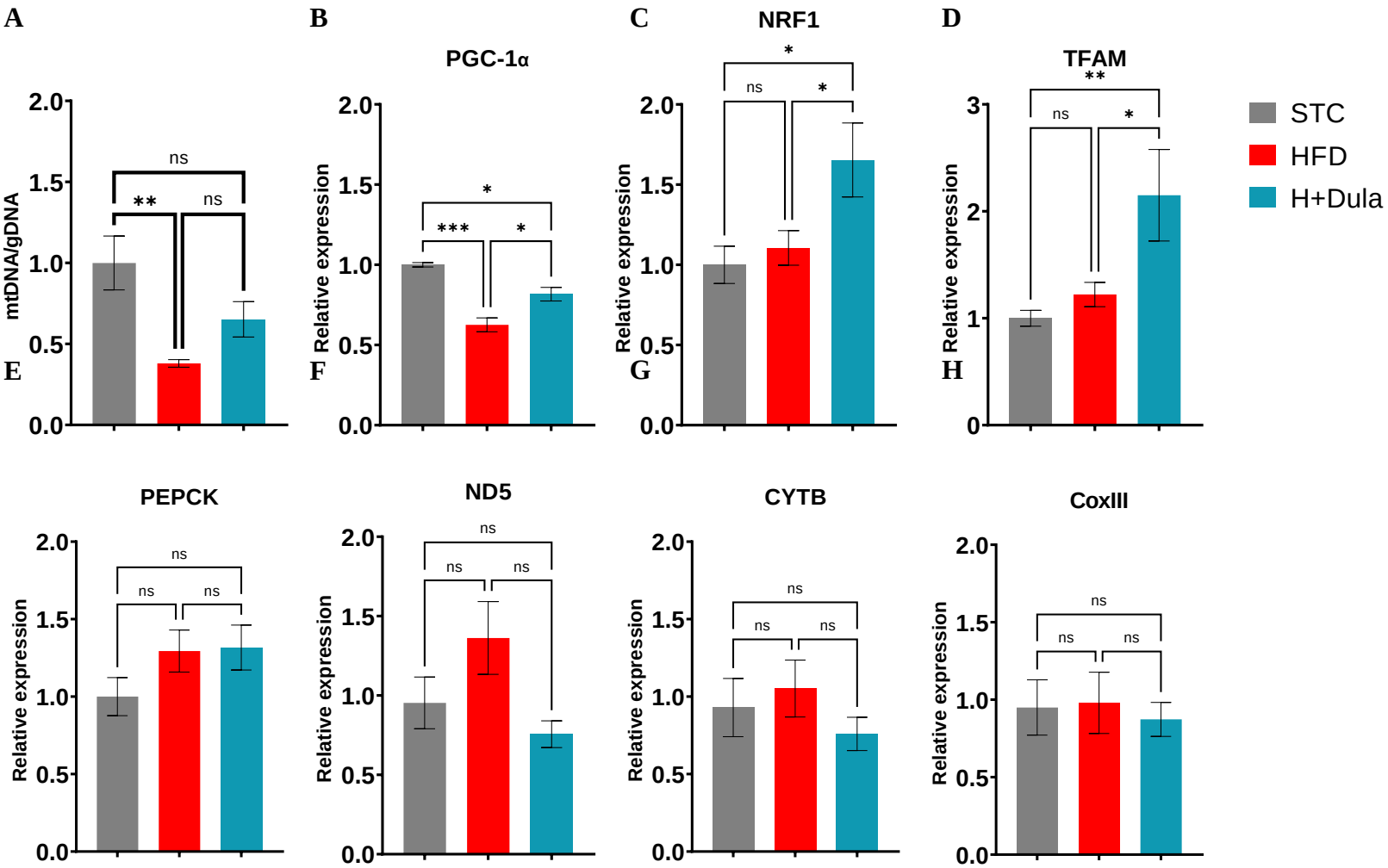
A
B
C
NRF1
D
TFAM
PGC-1α
mtDNA/gDNA
Relative expression
STC
HFD
H+Dula
E
F
G
H
PEPCK
ND5
CYTB
CoxIII
ns
*
**
***

Figure 26. Dulaglutide treatment increases mtDNA but not via mitochondrial biogenesis

Gene expression of the ratio between mitochondrial DNA (mtDNA) and genomic DNA (gDNA) was performed to compare the mitochondria number among different groups **(A)**. The gene expression of peroxisome proliferator-activated receptor gamma coactivator 1-alpha (PGC-1α) was quantified as a measure of mitochondrial biogenesis **(B)**. The nuclear respiratory factor 1 (NRF1) **(C)** and mitochondrial transcription factor A (TFAM) **(D)** are downstream transcriptional activators. Their gene expressions are influenced by the activation of PGC-1α transcriptional network. The gene expression of key mitochondrial biogenesis markers including gluconeogenic phosphoenolpyruvate carboxykinase (PEPCK) **(E)**, NADH-ubiquinone oxidoreductase chain 5 protein (ND5) **(F)**, cytochrome b (CYTB) **(G)** and cytochrome oxidase III (CoxIII) **(H)** are quantified. All measurements are normalized to GAPDH, and are shown relative to STC group, which were set arbitrary to 1. Data represents means ± SEM, n = 6 – 9 mice per group. * $P < 0.05$, ** $P < 0.01$, $P < 0.001$ and ns = not significant

5.17. Quantification of key enzymes involved in cardiolipin synthesis pathway gene expressions in the liver

To determine whether 4 weeks of dulaglutide treatment may have an effect on key enzymes involved in cardiolipin synthesis in the liver, qRT-PCR was performed to quantify the mRNA gene expression changes.

CDS1 gene expression was measured and there is no significant difference among the three groups. Comparison between the STC group and the HFD group has a P value of 0.9367. There is no difference between the HFD and H+Dula group with a P value of 0.99. There is a slightly higher expression in H+Dula group when compared to STC group with a P value of 0.94 (Figure 27A).

PGPS gene expression was measured and there is no significant difference among the three groups. Comparison between the STC group and the HFD group has a P value of 0.9336. There is no difference between the HFD and H+Dula group with a P value of 0.9024. There is expression difference in H+Dula group when compared to STC group with a P value of 0.99 (Figure 27B).

CLS gene expression was measured and there is no significant difference between HFD group and treatment group. Comparison between the STC group and the HFD group show a significantly lower expression in the HFD group, and has a P value of 0.0384. There is slight increase in expression when comparing between the H+Dula and HFD group with a P value of 0.72. There is expression difference, but not significant, in H+Dula group when compared to STC group with a P value of 0.1374 (Figure 27C).

TAZ gene expression was measured and there is no significant difference among the three groups. Comparison between the HFD group with the STC group has a relatively

lower expression a P value of 0.27. There is no difference between the HFD and H+Dula group with a P value of 0.99. There is relative low expression in H+Dula group when compared to STC group with a P value of 0.30 (Figure 27D).

ALCAT1 gene expression was measured and there is no significant difference among the three groups. Comparison between the HFD group and the STC group has no significant difference with a P value of 0.9876. There is a mild higher expression between the H+Dula and HFD group with a P value of 0.8564. There is a slightly higher expression in H+Dula group when compared to STC group with a P value of 0.82 (Figure 27E).

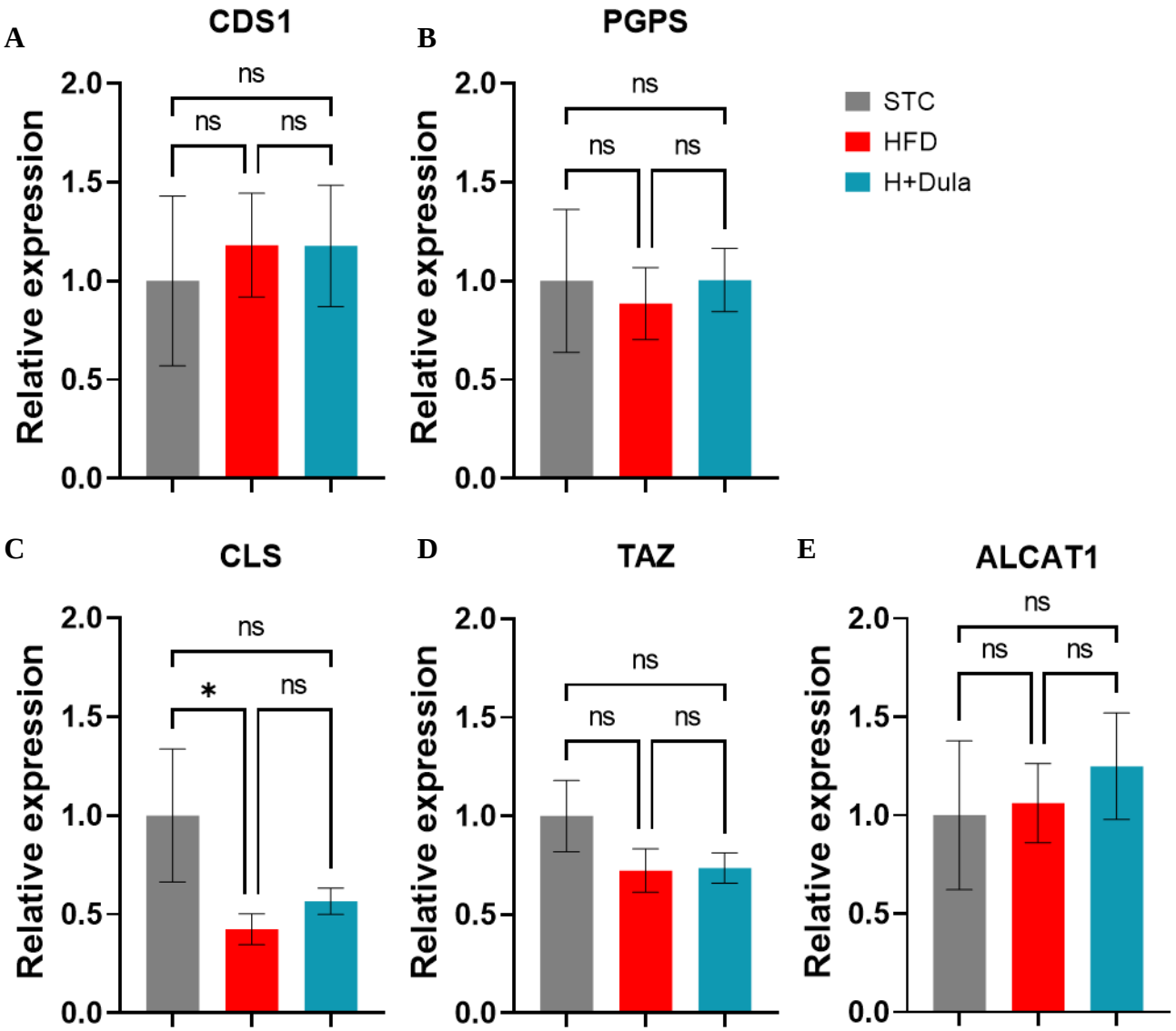
A
CDS1
B
PGPS
C
CLS
D
TAZ
E
ALCAT1
Relative expression
2.0
1.5
1.0
0.5
0.0
ns
*
STC
HFD
H+Dula

Figure 27. Dulaglutide treatment does not alter mRNA expressions of key enzymes involved in cardiolipin synthesis in the liver

The mRNA level of enzymes involved in CL biosynthesis and remodelling includes CDS1 **(A)**, PGPS **(B)**, CLS **(C)**, TAZ **(D)** and ALCAT1 **(E)** were measured in the liver tissue samples by qPCR. All measurements are normalized to GAPDH, and are shown relative to STC group, which were set arbitrary to 1. Data represents means ± SEM, n = 6 – 9 mice per group. * $P < 0.05$ and ns = not significant

6. Discussion

6.1. Dulaglutide attenuated renal morphological changes, body composition and glucose tolerance

To examine the effects of short-term treatment of dulaglutide on high-fat diet-induced renal dysfunction mouse model. High-fat diet was used to mimic obesity and type-2 diabetes mellitus with metabolic syndrome, such as hyperglycaemia and dyslipidaemia to initiate renal injury (Sun *et al.*, 2020). We found that mice fed with high-fat diet for 12 weeks showed increased body weight, increased fasting glucose, and a reduced glucose tolerance. Consistent with previous findings, dulaglutide treatment reversed body weight gain, reduction of glucose tolerance, and dyslipidaemia in high-fat diet-treated mice (Coskun *et al.*, 2018, Edwards and Minze, 2015). Furthermore, high-fat diet-induced mice caused kidney morphological changes, including the formation of cytoplasmic vacuolization of the renal tubules, mesangial expansion and thickened basement membrane, leading to impaired renal function (An *et al.*, 2015). Mitochondria, endoplasmic reticulum, and lysosome are important cytoplasmic components for normal functioning of the cell and its composition is altered in diabetic kidney due to increased cellular stress (Pourghasem *et al.*, 2015, Seely *et al.*, 2018). Moreover, a high-fat diet led to ectopic lipid accumulation in renal tubules which is a common metabolic syndrome found in DKD (Nishi *et al.*, 2019). The extra storage and imbalance of excessive lipids in the tubules will lead to lipotoxicity which can further induce inflammation, leading to fibrosis and ESRD (Wada and Makino, 2013). Overall, we are the first to show dulaglutide-treated mouse kidneys have reduced ectopic lipid accumulation, and not in the liver, possibly exhibiting anti-inflammatory effects in a similar manner as other GLP-1R agonists (Wang *et al.*, 2018).

6.2. Albuminuria and kidney injury are reduced after dulaglutide treatment irrelevant to GLP-1R expression

To examine the effect of dulaglutide on renal function and outcomes, renal function test and IHC staining are performed. KIM-1, was first identified to be elevated patient renal biopsies diagnosed with ischemic acute tubular necrosis (Han *et al.*, 2002). A previous RCT study has shown that KIM-1 expression in the histology from renal biopsies show a negatively correlation with PTC function (Bank *et al.*, 2017). The use of KIM-1 as a kidney injury marker has been well documented and is believed to be a sensitive and specific marker for acute kidney injury (Yin and Wang, 2016). In our study, there is a high KIM-1 expression in the HFD group and was reduced after treatment, suggesting that dulaglutide when simultaneously fed can suppress the effect of diet-induced DKD. The positive effects of glucagon-like peptide-1 receptor agonist on diabetic kidney disease renoprotection is well established. However, the expression of GLP-1R in the kidney is controversial as indicated previously that GLP-1R is expressed in the renal cortex and proximal tubules as proposed by Schlatter *et al*. (23) whilst it is mainly expressed in the kidney vasculature as suggested by Pyke *et al.* and Jensen *et al.* (Schlatter *et al.*, 2007, Pyke *et al.*, 2014, Jensen *et al.*, 2015). In this study, we demonstrated that GLP-1R is expressed in the renal tubules, especially distal tubules, and not in the glomerulus or renal vasculature. No significant changes in GLP-1R expression after high-fat diet and dulaglutide treatment in the renal tubules suggest that Overall, GLP-1R downregulation in diabetic kidney disease is not responsible for the reduced kidney function. Weekly treatment of dulaglutide for 4 weeks significantly improved renal function and renal composite parameters including urine volume, urinary albumin and urinary albumin creatinine ratio, and ameliorated renal morphological changes induced by high-fat diet.

6.3. Renal function improvement is not a secondary effect of changes in body composition and behaviour

In order to confirm whether renal function improvement is the primary improvement after dulaglutide treatment and not secondary, mice body behaviour and ^{1}H-NMR spectrometry were used. GLP-1 is known to regulate food intake and satiety, resulting in lower energy expenditure (Flint *et al.*, 2000). It is also understood that GLP-1RAs is associated with reduction in fat body mass (Shah and Vella, 2014). Previous study has shown that GLP-1 may induce AMP-activated protein kinase activation which acts as metabolic sensors to regulate important homeostatic systems including mitochondrial biosynthesis and fatty acid oxidation (Ruderman *et al.*, 2010). In our study, metabolic caging analysis of energy metabolism revealed that H+Dula group mice showed a lower food and water intake. H+Dula grouped mice also showed a lower RER when compared to HFD group. ^{1}H-NMR spectrometry was performed on mice after dulaglutide treatment and the body composition of mice in the H+Dula group showed a slightly lower fat body mass. Lean body mass and fluid weight was not altered throughout the treatment suggesting that our short-term treatment of dulaglutide did not significantly alter the overall body composition of mice. The ratio of fat and lean body mass revealed a mild reduction, but not significantly. Therefore, the attenuated renal function improvements observed in this study may be considered as the primary improvement and not as a secondary effect due to the reduction of obesity.

6.4. Dulaglutide reduced liver and adipose tissue weight by increasing satiety in mice

To identify whether high-fat diet feeding may alter key metabolic organ parameters, the kidneys, liver and adipose tissue were weighed after the mice are sacrificed. It is known that the consumption of high-fat diets can cause harmful effects on the liver which includes the ectopic lipid accumulation and hepatic insulin resistance (Longato *et al.*, 2012, Park *et al.*, 2005). End point metabolic organs were weighed and revealed a significant lower liver weight and a lower adipose tissue weight. Kidney weight and the ratio of kidney weight over body weight showed no significant changes in the H+Dula group when compared with HFD group. All of these phenotypes are due to dulaglutide, as a GLP-1 mimic, exerting a delayed gastric emptying and also increasing the satiety in mice. Leading to an overall reduction in food intake thereby reducing circulating glucose and fatty acids for infiltration into hepatocytes. Overall, these results demonstrate that dulaglutide, a GLP-1R agonist, can reduce the weight of liver and adipose tissue but not the kidney and that dulaglutide may plays an important role in renoprotection and function restoration possibly by altering lipid metabolism pathways.

6.5. Dulaglutide can alter the kidney lipidomes in high-fat diet mice

In order to identify possible alterations in lipid pathways in the kidney after dulaglutide treatment, a UHPLC/ESI-QTOF-MS based untargeted lipidomic method was performed with multivariate statistical analysis for kidney lipidome profiling.

Lipid enrichment was performed on the identified differential lipid compounds and most significant lipid types with high enrichment ratios, including glycerophospholipids, glycerophosphocholines, glycerophosphethanlamines and CL. These lipid groups are part of glycerophospholipid metabolism which was also predicted by pathway analysis with strong impact. Glycerophospholipids which are abundantly found in cell membranes to form the phospholipid bilayer acting as a cell barrier are also featured and involved in a range of physiological roles, including cellular growth, cell-cell interaction from attachment to mitigation, acting as a signalling molecule for recognition, transduction and cell survival (Gai *et al.*, 2021). Previous studies have shown that glycerophospholipid metabolism is altered in the obese with T2DM, resulting in changing the composition and abundance of glycerophospholipids (Rauschert *et al.*, 2016, Wolfgang, 2021). These lipidome changes, which are also observed in CKD and ESRD patients with dyslipidaemia, further contribute to the pathophysiological development of these diseases (Afshinnia *et al.*, 2018). As the kidney has a high metabolic rate with high-energy consumption, there is a high demand for energy (Bhargava and Schnellmann, 2017). Renal tubules, which are responsible for reabsorption of water and metabolites, including albumin, glucose, and other ions and electrolytes, undergo fatty acid metabolism, in which β-oxidation is the main process generating up to 129 ATP per fatty acid chain in the mitochondria to meet the energy demand (Koeppen and Stanton, 2012). However, as part of DKD development, dyslipidaemia, impairment of fatty acid transport and

altered metabolism in the obese has resulted in ectopic lipid accumulation in the renal tubules, (Herman-Edelstein *et al.*, 2014, Yang *et al.*, 2018, Zager *et al.*, 2005). It is also known that abnormal accumulation of lipids in non-adipose organs leads to lipotoxic pathological changes in DKD progression (Tamilarasan *et al.*, 2012, Gai *et al.*, 2019) and may be responsible for subsequent mitochondrial dysfunction. Although both lipotoxicity and mitochondrial dysfunction are known as independent contributors to DKD progression, the cause or the consequence remains to be explored.

The typical mitochondrial membrane, which is composed of glycerophospholipids that can undergo esterification with amino acids to form a range of glycerophospholipid subtypes, including PC, PI, phosphatidylserine (PS), phosphatidylethanolamine (PE) and CL (Hasan *et al.*, 2011, Blanco and Blanco, 2017). They were found present in the inner mitochondrial membrane by contributing to membrane stability and proper function of the oxidative phosphorylation system. Our UHPLC/ESI-QTOF-MS results showed that among lipids, which are involved in glycerophospholipid metabolism after high-fat diet, CL and PE showed increased abundance whilst phosphatidic acid (PA) and phosphatidylglycerol (PG) revealed decreased abundance. After treatment, these changes were reversed, suggesting that dulaglutide improves renal function by attenuating lipidome changes. Furthermore, CL is a mitochondrial-specific lipid, which shows a positive correlation with ATP synthase activity (Santiago *et al.*, 1973) and is known to play a critical role in mitochondrial cristae structure and metabolism (Szeto, 2014b). Previous study has shown that there is a decrease in CL abundance in the kidney of non-alcoholic steatohepatitis mouse model (Hayasaka *et al.*, 2016). In our study, there was an increase in the CL abundance in the cortex region of the kidney after dulaglutide treatment. The increase in the CL abundance may potentially revert mitochondrial damage and attenuate CL-protein

interactions, especially in the respiratory complexes III and IV, which are essential for energy production in renal tubules (Paradies *et al.*, 2014). Moreover, CL and its oxidation products are known to exhibit cardiolipin-mediated cellular signalling which may regulate important functions such as apoptosis and mitophagy in aging (Patil and Greenberg, 2013, Dudek, 2017). Our lipid enrichment data also showed that CL had the highest enrichment ratio. This increase in CL may reinstate its binding to cytochrome bc1 complex found on complex III to maintain structural integrity for normal electron transport function. Moreover, the physical properties of CL allow mitochondrial ridges to be formed, allowing protons to be trapped, maintaining a proton gradient essential for ATP synthesis via ATP synthase (Paradies *et al.*, 2014).

6.6. Dulaglutide increases mtDNA via increasing expression of key enzymes involved in cardiolipin synthesis pathway in the kidney but not in the liver

To further confirm the increase of the CL content, we assessed the gene expression involved in CL synthesis. Our results clearly showed that dulaglutide could stimulate the mRNA expression of enzymes involved in the biosynthesis of CL. PA and PG, which are upstream lipid intermediate involved in CL biosynthesis, were decreased in abundance. The finished product of CL synthesis is immature CLs. These CLs require further remodelling by reacylation to become their mature forms for function by TAZ (Houtkooper *et al.*, 2009). We further assessed the mRNA expression of TAZ, which showed a significant increase. This further suggests that dulaglutide may stimulate CL biosynthesis and remodelling, leading to increased mature CL abundance. ALCAT1 is known to cause pathological remodelling of CL, our data shows a mild increase in ALCAT1 gene expression in the HFD group and a slight lowering in the H+Dula group however, the changes are not significant.

As mentioned previously, CL is highly associated with the mitochondria and its biosynthesis may be involved in the regulation of mitochondrial content and quality (Schlame and Greenberg, 2017). To assess whether the increase in CL abundance has led to an increase in mitochondrial biosynthesis, we measured the relative expression ratio of mitochondria DNA (mtDNA) over genomic DNA (gDNA) for relative comparison among the groups. Our data show a higher ratio of mtDNA to gDNA in the H+Dula group when compared with the HFD group suggesting a higher mitochondrial content after drug treatment. As PGC-1α is known as the master regulator of mitochondrial biogenesis (Quan *et al.*, 2020, Li *et al.*, 2011), we further examined and quantified the mRNA gene expressions of it and its downstream traditional factors including NRF1 and TFAM (Wu *et al.*, 1999). Our data show a

significantly higher gene expression of these genes and therefore dulaglutide treatment may potentially increase mitochondrial biosynthesis as a result of increased cardiolipin presence. To validate this, we measured the gene expressions of mitochondria specific transcripts including ND5, CYTB, CoxIII and PEPCK that were used in previous study for the study of mitochondrial biogenesis (Heinonen *et al.*, 2015, Li *et al.*, 2011). Interestingly, the mitochondrial biomarkers show no significant changes for PEPCK, CYTB and CoxIII and instead a significant decrease in ND5 gene expression. The data indicates that despite there is an increase in PGC-1α and its network of transcriptional activators, overall key mitochondrial biosynthesis did not increase, suggesting that dulaglutide did not improve renal function by increased mitochondrial biogenesis.

Furthermore, it is well known that GLP-1R is not expressed in hepatocytes (Richards *et al.*, 2014, Pyke *et al.*, 2014), as it is an important metabolic organ involved in lipid regulation (Chao *et al.*, 2019), ORO staining was performed on the liver and ectopic lipid accumulation remained after 4-week dulaglutide treatment, similar to previous report (Hupa-Breier *et al.*, 2021). We further validated whether key enzymes involved in cardiolipin synthesis was improved, our results indicate that mRNA gene expressions of CDS1, PGPS, CLS, TAZ and ALCAT1 show no significant changes. Our data here suggests that dulaglutide enhances key enzymes involved in cardiolipin synthesis by the activation of GLP-1R and has been shown in the kidney cortex region of mice in the H+Dula group.

Overall, our data demonstrates that dulaglutide treatment can increase mtDNA in the kidney by the increase of cardiolipin abundance. The gene expression of key enzymes involved in cardiolipin synthesis pathway were upregulated in the kidney of the treatment group but not in the liver.

7. Conclusions

In summary, we presented a study showing that diet-induced obese mice treated with dulaglutide exhibited attenuated kidney function, reduced ectopic lipid accumulation and damage in renal tubules with improvement in pathomorphological changes. GLP-1R was shown to be expressed in renal tubules and not in the glomerulus or vasculature regions. Importantly, our UHPLC/ESI-QTOF-MS untargeted lipidomic approach showed that the changes in kidney lipidome after treatment with dulaglutide are associated with glycerophospholipid metabolism. Lipids, especially CLs, which are involved in glycerophospholipid metabolism, showed increased abundance by increasing the mRNA expression of key cardiolipin synthesis enzymes in the kidney (Figure 28). CLs are strongly correlated with ATP synthase activity, preservation of respiratory complexes, and their physiological function in the mitochondria. Although the association of lipotoxicity and mitochondrial dysfunction in the development of DKD requires further exploration, our lipidomic system has shed light on identifying potential lipid pathways and biomarkers for future evaluation and potential mechanistic research.

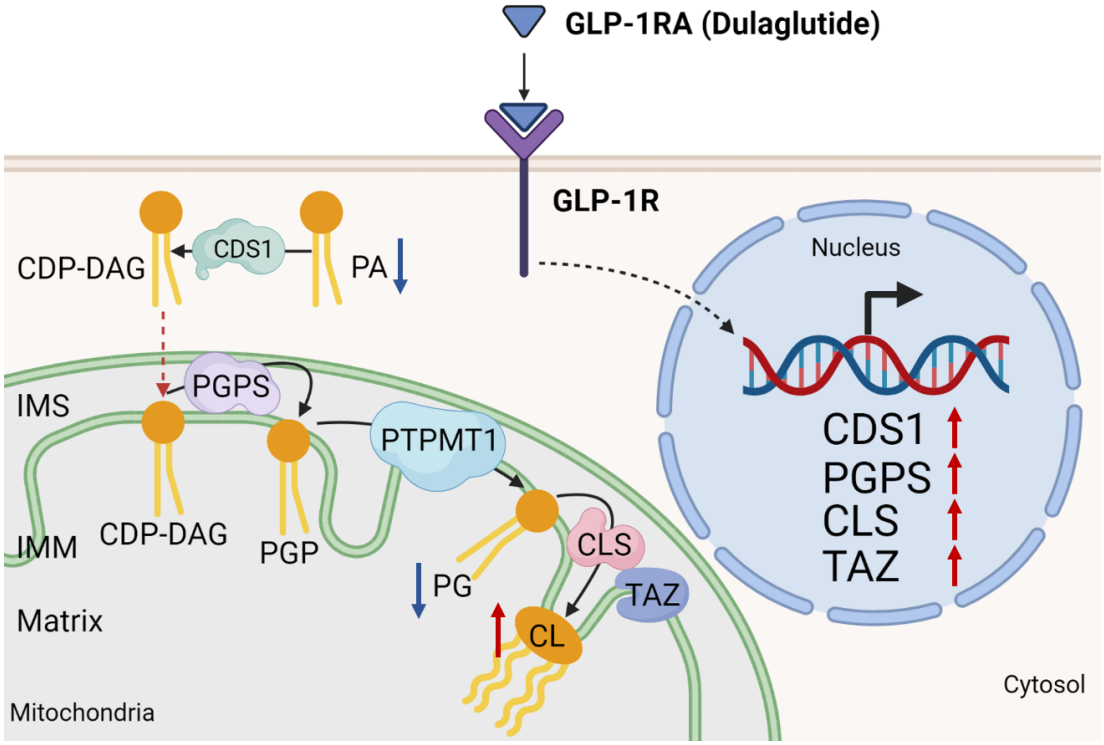

Figure 28. An overview of the metabolic pathway after dulalgutide treatment in the kidney

An overview of the metabolic pathway related to after dulaglutide treatment. Activation of GLP-1R by dulaglutide led to the reduction in abundance of PA and PG and an increase in abundance of CL by increasing the gene transcription of key cardiolipin synthesis enzymes including CDS1, PGPS, CLS and TAZ. PTPMT1, protein tyrosine phosphatase mitochondrial 1; IMS, inner mitochondrial space; IMM, inner mitochondrial membrane. Red arrow ↑ denotes increased abundance and blue arrow ↓ denotes reduced abundance based on UHPLC/ESI-QTOF-MS.

8. References

1. Afshinnia, F., Rajendiran, T. M., Soni, T., et al. 2018. Impaired beta-Oxidation and Altered Complex Lipid Fatty Acid Partitioning with Advancing CKD. *J Am Soc Nephrol,* 29**,** 295-306.
2. Agnoli, G. C. & Garutti, C. 1976. [Renal water-electrolyte excretion and its control mechanisms. Current status of knowledge]. *Minerva Med,* 67**,** 3673-702.
3. Altaf, Q. A. & Tahrani, A. A. 2015. Chapter 23 - Obstructive Sleep Apnea and Diabetic Microvascular Complications. *In:* WATSON, R. R. (ed.) *Modulation of Sleep by Obesity, Diabetes, Age, and Diet.* San Diego: Academic Press.
4. Alvarez, E., Martinez, M. D., Roncero, I., et al. 2005. The expression of GLP-1 receptor mRNA and protein allows the effect of GLP-1 on glucose metabolism in the human hypothalamus and brainstem. *J Neurochem,* 92**,** 798-806.
5. An, Y., Xu, F., Le, W., et al. 2015. Renal histologic changes and the outcome in patients with diabetic nephropathy. *Nephrol Dial Transplant,* 30**,** 257-66.
6. Ansary, T. M., Nakano, D. & Nishiyama, A. 2019. Diuretic Effects of Sodium Glucose Cotransporter 2 Inhibitors and Their Influence on the Renin-Angiotensin System. *Int J Mol Sci,* 20.
7. Bank, J. R., Van Der Pol, P., Vreeken, D., et al. 2017. Kidney injury molecule-1 staining in renal allograft biopsies 10 days after transplantation is inversely correlated with functioning proximal tubular epithelial cells. *Nephrol Dial Transplant,* 32**,** 2132-2141.
8. Barker, M. & Rayens, W. 2003. Partial least squares for discrimination. *Journal of Chemometrics,* 17**,** 166-173.

9. Berry, C. E. & Hare, J. M. 2004. Xanthine oxidoreductase and cardiovascular disease: molecular mechanisms and pathophysiological implications. *J Physiol,* 555**,** 589-606.
10. Bhargava, P. & Schnellmann, R. G. 2017. Mitochondrial energetics in the kidney. *Nat Rev Nephrol,* 13**,** 629-646.
11. Blanco, A. & Blanco, G. 2017. Chapter 5 - Lipids. *In:* BLANCO, A. & BLANCO, G. (eds.) *Medical Biochemistry.* Academic Press.
12. Bobulescu, I. A., Lotan, Y., Zhang, J., et al. 2014. Triglycerides in the human kidney cortex: relationship with body size. *PLoS One,* 9**,** e101285.
13. Bomback, A. S. & Toto, R. 2009. Dual blockade of the renin-angiotensin-aldosterone system: beyond the ACE inhibitor and angiotensin-II receptor blocker combination. *Am J Hypertens,* 22**,** 1032-40.
14. Bonnet, F., Deprele, C., Sassolas, A., et al. 2001. Excessive body weight as a new independent risk factor for clinical and pathological progression in primary IgA nephritis. *Am J Kidney Dis,* 37**,** 720-7.
15. Brenner, B. M., Cooper, M. E., De Zeeuw, D., et al. 2001. Effects of losartan on renal and cardiovascular outcomes in patients with type 2 diabetes and nephropathy. *N Engl J Med,* 345**,** 861-9.
16. Briffa, J. F., Grinfeld, E., Jenkin, K. A., et al. 2015. Diet induced obesity in rats reduces NHE3 and Na(+) /K(+) -ATPase expression in the kidney. *Clin Exp Pharmacol Physiol,* 42**,** 1118-26.
17. Burgoine, T., Sarkar, C., Webster, C. J., et al. 2018. Examining the interaction of fast-food outlet exposure and income on diet and obesity: evidence from 51,361 UK Biobank participants. *Int J Behav Nutr Phys Act,* 15**,** 71.

18. Buscemi, J., Rybak, T. M., Berlin, K. S., et al. 2017. Impact of food craving and calorie intake on body mass index (BMI) changes during an 18-month behavioral weight loss trial. *J Behav Med,* 40**,** 565-573.
19. Chao, H. W., Chao, S. W., Lin, H., et al. 2019. Homeostasis of Glucose and Lipid in Non-Alcoholic Fatty Liver Disease. *Int J Mol Sci,* 20.
20. Chernushevich, I. V., Loboda, A. V. & Thomson, B. A. 2001. An introduction to quadrupole-time-of-flight mass spectrometry. *J Mass Spectrom,* 36**,** 849-65.
21. Chong, J., Wishart, D. S. & Xia, J. 2019. Using MetaboAnalyst 4.0 for Comprehensive and Integrative Metabolomics Data Analysis. *Curr Protoc Bioinformatics,* 68**,** e86.
22. Collins, F. S. & Fink, L. 1995. The Human Genome Project. *Alcohol Health Res World,* 19**,** 190-195.
23. Coskun, T., Sloop, K. W., Loghin, C., et al. 2018. LY3298176, a novel dual GIP and GLP-1 receptor agonist for the treatment of type 2 diabetes mellitus: From discovery to clinical proof of concept. *Molecular Metabolism,* 18**,** 3-14.
24. Coughlan, M. T., Thorburn, D. R., Penfold, S. A., et al. 2009. RAGE-induced cytosolic ROS promote mitochondrial superoxide generation in diabetes. *J Am Soc Nephrol,* 20**,** 742-52.
25. Crajoinas, R. O., Oricchio, F. T., Pessoa, T. D., et al. 2011. Mechanisms mediating the diuretic and natriuretic actions of the incretin hormone glucagon-like peptide-1. *Am J Physiol Renal Physiol,* 301**,** F355-63.
26. Cranford, T. L., Enos, R. T., Velazquez, K. T., et al. 2016. Role of MCP-1 on inflammatory processes and metabolic dysfunction following high-fat feedings in the FVB/N strain. *Int J Obes (Lond),* 40**,** 844-51.

27. Dettmer, K., Aronov, P. A. & Hammock, B. D. 2007. Mass spectrometry-based metabolomics. *Mass Spectrom Rev,* 26**,** 51-78.
28. Doyle, M. E. & Egan, J. M. 2007. Mechanisms of action of glucagon-like peptide 1 in the pancreas. *Pharmacol Ther,* 113**,** 546-93.
29. Dudek, J. 2017. Role of Cardiolipin in Mitochondrial Signaling Pathways. *Front Cell Dev Biol,* 5**,** 90.
30. Dugan, L. L., You, Y. H., Ali, S. S., et al. 2013. AMPK dysregulation promotes diabetes-related reduction of superoxide and mitochondrial function. *J Clin Invest,* 123**,** 4888-99.
31. Edwards, K. L. & Minze, M. G. 2015. Dulaglutide: an evidence-based review of its potential in the treatment of type 2 diabetes. *Core Evid,* 10**,** 11-21.
32. Eid, A. A., Gorin, Y., Fagg, B. M., et al. 2009. Mechanisms of podocyte injury in diabetes: role of cytochrome P450 and NADPH oxidases. *Diabetes,* 58**,** 1201-11.
33. Espinoza, R., Gracida, C., Cancino, J., et al. 2006. Effect of obese living donors on the outcome and metabolic features in recipients of kidney transplantation. *Transplant Proc,* 38**,** 888-9.
34. Færgestad, E. M., Langsrud, Ø., Høy, M., et al. 2009. 4.08 - Analysis of Megavariate Data in Functional Genomics. *In:* BROWN, S. D., TAULER, R. & WALCZAK, B. (eds.) *Comprehensive Chemometrics.* Oxford: Elsevier.
35. Farah, L. X. S., Valentini, V., Pessoa, T. D., et al. 2016. The physiological role of glucagon-like peptide-1 in the regulation of renal function. 310**,** F123-F127.
36. Fiehn, O. 2001. Combining genomics, metabolome analysis, and biochemical modelling to understand metabolic networks. *Comp Funct Genomics,* 2**,** 155-68.
37. Fiehn, O. 2002. Metabolomics--the link between genotypes and phenotypes. *Plant Mol Biol,* 48**,** 155-71.

38. Fioretto, P. & Mauer, M. 2007. Histopathology of diabetic nephropathy. *Semin Nephrol,* 27**,** 195-207.
39. Flint, A., Raben, A., Rehfeld, J. F., et al. 2000. The effect of glucagon-like peptide-1 on energy expenditure and substrate metabolism in humans. *Int J Obes Relat Metab Disord,* 24**,** 288-98.
40. Forbes, J. M. & Thorburn, D. R. 2018. Mitochondrial dysfunction in diabetic kidney disease. *Nat Rev Nephrol,* 14**,** 291-312.
41. Forstermann, U. & Sessa, W. C. 2012. Nitric oxide synthases: regulation and function. *Eur Heart J,* 33**,** 829-37, 837a-837d.
42. Fried, L. F., Emanuele, N., Zhang, J. H., et al. 2013. Combined angiotensin inhibition for the treatment of diabetic nephropathy. *N Engl J Med,* 369**,** 1892-903.
43. Gai, X., Guo, C., Zhang, L., et al. 2021. Serum Glycerophospholipid Profile in Acute Exacerbation of Chronic Obstructive Pulmonary Disease. *Front Physiol,* 12**,** 646010.
44. Gai, Z., Wang, T., Visentin, M., et al. 2019. Lipid Accumulation and Chronic Kidney Disease. *Nutrients,* 11.
45. Gerstein, H. C., Colhoun, H. M., Dagenais, G. R., et al. 2019. Dulaglutide and renal outcomes in type 2 diabetes: an exploratory analysis of the REWIND randomised, placebo-controlled trial. *Lancet,* 394**,** 131-138.
46. Gieger, C., Geistlinger, L., Altmaier, E., et al. 2008. Genetics meets metabolomics: a genome-wide association study of metabolite profiles in human serum. *PLoS Genet,* 4**,** e1000282.
47. Goligorsky, M. S., Brodsky, S. V. & Noiri, E. 2002. Nitric oxide in acute renal failure: NOS versus NOS. *Kidney Int,* 61**,** 855-61.

48. Gullans, S. R., Harris, S. I. & Mandel, L. J. 1984. Glucose-dependent respiration in suspensions of rabbit cortical tubules. *J Membr Biol,* 78**,** 257-62.
49. Han, W. K., Bailly, V., Abichandani, R., et al. 2002. Kidney Injury Molecule-1 (KIM-1): a novel biomarker for human renal proximal tubule injury. *Kidney Int,* 62**,** 237-44.
50. Hasan, S. S., Yamashita, E., Ryan, C. M., et al. 2011. Conservation of lipid functions in cytochrome bc complexes. *J Mol Biol,* 414**,** 145-62.
51. Hayasaka, T., Fuda, H., Hui, S. P., et al. 2016. Imaging Mass Spectrometry Reveals a Decrease of Cardiolipin in the Kidney of NASH Model Mice. *Anal Sci,* 32**,** 473-6.
52. Heinonen, S., Buzkova, J., Muniandy, M., et al. 2015. Impaired Mitochondrial Biogenesis in Adipose Tissue in Acquired Obesity. *Diabetes,* 64**,** 3135-45.
53. Herman-Edelstein, M., Scherzer, P., Tobar, A., et al. 2014. Altered renal lipid metabolism and renal lipid accumulation in human diabetic nephropathy. *J Lipid Res,* 55**,** 561-72.
54. Horton, J. D., Goldstein, J. L. & Brown, M. S. 2002. SREBPs: activators of the complete program of cholesterol and fatty acid synthesis in the liver. *J Clin Invest,* 109**,** 1125-31.
55. Houtkooper, R. H., Rodenburg, R. J., Thiels, C., et al. 2009. Cardiolipin and monolysocardiolipin analysis in fibroblasts, lymphocytes, and tissues using high-performance liquid chromatography–mass spectrometry as a diagnostic test for Barth syndrome. *Analytical biochemistry,* 387**,** 230-237.
56. Huang, X., Dai, F. F., Gaisano, G., et al. 2013. The identification of novel proteins that interact with the GLP-1 receptor and restrain its activity. *Mol Endocrinol,* 27**,** 1550-63.

57. Hupa-Breier, K. L., Dywicki, J., Hartleben, B., et al. 2021. Dulaglutide Alone and in Combination with Empagliflozin Attenuate Inflammatory Pathways and Microbiome Dysbiosis in a Non-Diabetic Mouse Model of NASH. *Biomedicines,* 9.

58. Ioannidis, J. P. & Khoury, M. J. 2011. Improving validation practices in "omics" research. *Science,* 334**,** 1230-2.

59. Jackson, K. G., Maitin, V., Leake, D. S., et al. 2006. Saturated fat-induced changes in Sf 60-400 particle composition reduces uptake of LDL by HepG2 cells. *J Lipid Res,* 47**,** 393-403.

60. Jay, A. G., Chen, A. N., Paz, M. A., et al. 2015. CD36 binds oxidized low density lipoprotein (LDL) in a mechanism dependent upon fatty acid binding. *J Biol Chem,* 290**,** 4590-603.

61. Jensen, E. P., Poulsen, S. S., Kissow, H., et al. 2015. Activation of GLP-1 receptors on vascular smooth muscle cells reduces the autoregulatory response in afferent arterioles and increases renal blood flow. *Am J Physiol Renal Physiol,* 308**,** F867-77.

62. Jerums, G., Premaratne, E., Panagiotopoulos, S., et al. 2010. The clinical significance of hyperfiltration in diabetes. *Diabetologia,* 53**,** 2093-104.

63. Jocken, J. W., Langin, D., Smit, E., et al. 2007. Adipose triglyceride lipase and hormone-sensitive lipase protein expression is decreased in the obese insulin-resistant state. *J Clin Endocrinol Metab,* 92**,** 2292-9.

64. Jolliffe, I. T. & Cadima, J. 2016. Principal component analysis: a review and recent developments. *Philos Trans A Math Phys Eng Sci,* 374**,** 20150202.

65. Kanehisa, M., Furumichi, M., Tanabe, M., et al. 2017. KEGG: new perspectives on genomes, pathways, diseases and drugs. *Nucleic Acids Res,* 45**,** D353-D361.

66. Kang, H. M., Ahn, S. H., Choi, P., et al. 2015. Defective fatty acid oxidation in renal tubular epithelial cells has a key role in kidney fibrosis development. *Nat Med,* 21**,** 37-46.

67. Kato, M. & Natarajan, R. 2019. Epigenetics and epigenomics in diabetic kidney disease and metabolic memory. *Nat Rev Nephrol,* 15**,** 327-345.

68. Kawanami, D., Matoba, K., Takeda, Y., et al. 2017. SGLT2 Inhibitors as a Therapeutic Option for Diabetic Nephropathy. *Int J Mol Sci,* 18.

69. Kawanami, D., Matoba, K. & Utsunomiya, K. 2016. Signaling pathways in diabetic nephropathy. *Histol Histopathol,* 31**,** 1059-67.

70. Kawanami, D. & Takashi, Y. 2020. GLP-1 Receptor Agonists in Diabetic Kidney Disease: From Clinical Outcomes to Mechanisms. *Front Pharmacol,* 11**,** 967.

71. Kennedy, D. J., Chen, Y., Huang, W., et al. 2013. CD36 and Na/K-ATPase-alpha1 form a proinflammatory signaling loop in kidney. *Hypertension,* 61**,** 216-24.

72. Khamis, M. M., Adamko, D. J. & El-Aneed, A. 2017. Mass spectrometric based approaches in urine metabolomics and biomarker discovery. *Mass Spectrom Rev,* 36**,** 115-134.

73. Kim, T. J. & Von Dem Knesebeck, O. 2018. Income and obesity: what is the direction of the relationship? A systematic review and meta-analysis. *BMJ Open,* 8**,** e019862.

74. Kincaid-Smith, P. 2004. Hypothesis: obesity and the insulin resistance syndrome play a major role in end-stage renal failure attributed to hypertension and labelled 'hypertensive nephrosclerosis'. *J Hypertens,* 22**,** 1051-5.

75. Klassen, A., Faccio, A. T., Canuto, G. A., et al. 2017. Metabolomics: Definitions and Significance in Systems Biology. *Adv Exp Med Biol,* 965**,** 3-17.

76. Koeppen, B. M. & Stanton, B. A. 2012. *Renal Physiology E-Book: Mosby Physiology Monograph Series*, Elsevier Health Sciences.

77. Kofeler, H. C. & Gross, M. L. 2005. Correction of accurate mass measurement for target compound verification by quadrupole time-of-flight mass spectrometry. *J Am Soc Mass Spectrom,* 16**,** 406-8.

78. Kolovou, G. D., Anagnostopoulou, K. K. & Cokkinos, D. V. 2005. Pathophysiology of dyslipidaemia in the metabolic syndrome. *Postgrad Med J,* 81**,** 358-66.

79. Kooij, A. 1994. A re-evaluation of the tissue distribution and physiology of xanthine oxidoreductase. *Histochem J,* 26**,** 889-915.

80. Kramer, A., Green, J., Pollard, J., Jr., et al. 2014. Causal analysis approaches in Ingenuity Pathway Analysis. *Bioinformatics,* 30**,** 523-30.

81. Kruger, C., Nguyen, T. T., Breaux, C., et al. 2019. Proximal Tubular Cell-Specific Ablation of Carnitine Acetyltransferase Causes Tubular Disease and Secondary Glomerulosclerosis. *Diabetes,* 68**,** 819-831.

82. Lakka, H. M., Laaksonen, D. E., Lakka, T. A., et al. 2002. The metabolic syndrome and total and cardiovascular disease mortality in middle-aged men. *JAMA,* 288**,** 2709-16.

83. Lecocq, J. & Ballou, C. E. 1964. On the Structure of Cardiolipin. *Biochemistry,* 3**,** 976-80.

84. Lee, J. H., Kim, S. C., Han, D. J., et al. 2007. Risk factors for MDRD-GFR of less than 60 mL/min per 1.73 m2 in former kidney donors. *Nephrology (Carlton),* 12**,** 600-6.

85. Lewis, E. J., Hunsicker, L. G., Bain, R. P., et al. 1993. The effect of angiotensin-converting-enzyme inhibition on diabetic nephropathy. The Collaborative Study Group. *N Engl J Med,* 329**,** 1456-62.

86. Li, L., Pan, R., Li, R., et al. 2011. Mitochondrial biogenesis and peroxisome proliferator-activated receptor-gamma coactivator-1alpha (PGC-1alpha) deacetylation by physical activity: intact adipocytokine signaling is required. *Diabetes,* 60**,** 157-67.

87. Li, M. X. & Dewson, G. 2015. Mitochondria and apoptosis: emerging concepts. *F1000Prime Rep,* 7**,** 42.

88. Lin, Y. C., Chang, Y. H., Yang, S. Y., et al. 2018. Update of pathophysiology and management of diabetic kidney disease. *J Formos Med Assoc,* 117**,** 662-675.

89. Longato, L., Tong, M., Wands, J. R., et al. 2012. High fat diet induced hepatic steatosis and insulin resistance: Role of dysregulated ceramide metabolism. *Hepatol Res,* 42**,** 412-27.

90. Mann, J. F., Schmieder, R. E., Mcqueen, M., et al. 2008. Renal outcomes with telmisartan, ramipril, or both, in people at high vascular risk (the ONTARGET study): a multicentre, randomised, double-blind, controlled trial. *Lancet,* 372**,** 547-53.

91. Mann, J. F. E., Orsted, D. D., Brown-Frandsen, K., et al. 2017. Liraglutide and Renal Outcomes in Type 2 Diabetes. *N Engl J Med,* 377**,** 839-848.

92. Maric, C. & Hall, J. E. 2011. Obesity, metabolic syndrome and diabetic nephropathy. *Contrib Nephrol,* 170**,** 28-35.

93. Mcpherson, K. C., Shields, C. A., Poudel, B., et al. 2019. Impact of obesity as an independent risk factor for the development of renal injury: implications from rat models of obesity. *Am J Physiol Renal Physiol,* 316**,** F316-F327.

94. Moncada, S. & Higgs, E. A. 2006. The discovery of nitric oxide and its role in vascular biology. *Br J Pharmacol,* 147 Suppl 1**,** S193-201.

95. Moorhead, J. F., Chan, M. K., El-Nahas, M., et al. 1982. Lipid nephrotoxicity in chronic progressive glomerular and tubulo-interstitial disease. *Lancet,* 2**,** 1309-11.

96. Mori, H., Inoki, K., Masutani, K., et al. 2009. The mTOR pathway is highly activated in diabetic nephropathy and rapamycin has a strong therapeutic potential. *Biochem Biophys Res Commun,* 384**,** 471-5.

97. Musi, N., Hirshman, M. F., Nygren, J., et al. 2002. Metformin increases AMP-activated protein kinase activity in skeletal muscle of subjects with type 2 diabetes. *Diabetes,* 51**,** 2074-81.

98. Nangaku, M. 2004. Hypoxia and tubulointerstitial injury: a final common pathway to end-stage renal failure. *Nephron Exp Nephrol,* 98**,** e8-12.

99. Niki, E., Yoshida, Y., Saito, Y., et al. 2005. Lipid peroxidation: mechanisms, inhibition, and biological effects. *Biochem Biophys Res Commun,* 338**,** 668-76.

100. Nishi, H., Higashihara, T. & Inagi, R. 2019. Lipotoxicity in Kidney, Heart, and Skeletal Muscle Dysfunction. *Nutrients,* 11.

101. Ofei, F. 2005. Obesity - a preventable disease. *Ghana Med J,* 39**,** 98-101.

102. Opazo-Rios, L., Mas, S., Marin-Royo, G., et al. 2020. Lipotoxicity and Diabetic Nephropathy: Novel Mechanistic Insights and Therapeutic Opportunities. *Int J Mol Sci,* 21.

103. Pagliarini, D. J., Calvo, S. E., Chang, B., et al. 2008. A mitochondrial protein compendium elucidates complex I disease biology. *Cell,* 134**,** 112-23.

104. Palm, F., Hansell, P., Ronquist, G., et al. 2004. Polyol-pathway-dependent disturbances in renal medullary metabolism in experimental insulin-deficient diabetes mellitus in rats. *Diabetologia,* 47**,** 1223-1231.

105. Paradies, G., Paradies, V., De Benedictis, V., et al. 2014. Functional role of cardiolipin in mitochondrial bioenergetics. *Biochim Biophys Acta,* 1837**,** 408-17.

106. Park, S. Y., Cho, Y. R., Kim, H. J., et al. 2005. Unraveling the temporal pattern of diet-induced insulin resistance in individual organs and cardiac dysfunction in C57BL/6 mice. *Diabetes,* 54**,** 3530-40.

107. Patil, V. A. & Greenberg, M. L. 2013. Cardiolipin-mediated cellular signaling. *Adv Exp Med Biol,* 991**,** 195-213.

108. Perkovic, V., Jardine, M. J., Neal, B., et al. 2019. Canagliflozin and Renal Outcomes in Type 2 Diabetes and Nephropathy. *N Engl J Med,* 380**,** 2295-2306.

109. Pourghasem, M., Shafi, H. & Babazadeh, Z. 2015. Histological changes of kidney in diabetic nephropathy. *Caspian J Intern Med,* 6**,** 120-7.

110. Pyke, C., Heller, R. S., Kirk, R. K., et al. 2014. GLP-1 receptor localization in monkey and human tissue: novel distribution revealed with extensively validated monoclonal antibody. *Endocrinology,* 155**,** 1280-90.

111. Quan, Y., Xin, Y., Tian, G., et al. 2020. Mitochondrial ROS-Modulated mtDNA: A Potential Target for Cardiac Aging. *Oxid Med Cell Longev,* 2020**,** 9423593.

112. Rauschert, S., Uhl, O., Koletzko, B., et al. 2016. Lipidomics Reveals Associations of Phospholipids With Obesity and Insulin Resistance in Young Adults. *J Clin Endocrinol Metab,* 101**,** 871-9.

113. Ravid, M., Savin, H., Jutrin, I., et al. 1993. Long-term stabilizing effect of angiotensin-converting enzyme inhibition on plasma creatinine and on proteinuria in normotensive type II diabetic patients. *Ann Intern Med,* 118**,** 577-81.

114. Reidy, K., Kang, H. M., Hostetter, T., et al. 2014. Molecular mechanisms of diabetic kidney disease. *J Clin Invest,* 124**,** 2333-40.

115. Richards, P., Parker, H. E., Adriaenssens, A. E., et al. 2014. Identification and characterization of GLP-1 receptor-expressing cells using a new transgenic mouse model. *Diabetes,* 63**,** 1224-33.

116. Roberts, L. D., Souza, A. L., Gerszten, R. E., et al. 2012. Targeted metabolomics. *Curr Protoc Mol Biol,* Chapter 30**,** Unit 30 2 1-24.

117. Rosenberger, C., Khamaisi, M., Abassi, Z., et al. 2008. Adaptation to hypoxia in the diabetic rat kidney. *Kidney Int,* 73**,** 34-42.

118. Ruderman, N. B., Xu, X. J., Nelson, L., et al. 2010. AMPK and SIRT1: a long-standing partnership? *Am J Physiol Endocrinol Metab,* 298**,** E751-60.

119. Santiago, E., Lopez-Moratalla, N. & Segovia, J. F. 1973. Correlation between losses of mitochondrial ATPase activity and cardiolipin degradation. *Biochem Biophys Res Commun,* 53**,** 439-45.

120. Saric, A., Andreau, K., Armand, A. S., et al. 2015. Barth Syndrome: From Mitochondrial Dysfunctions Associated with Aberrant Production of Reactive Oxygen Species to Pluripotent Stem Cell Studies. *Front Genet,* 6**,** 359.

121. Schlame, M. & Greenberg, M. L. 2017. Biosynthesis, remodeling and turnover of mitochondrial cardiolipin. *Biochim Biophys Acta Mol Cell Biol Lipids,* 1862**,** 3-7.

122. Schlatter, P., Beglinger, C., Drewe, J., et al. 2007. Glucagon-like peptide 1 receptor expression in primary porcine proximal tubular cells. *Regul Pept,* 141**,** 120-8.

123. Schmidt, W. E., Siegel, E. G. & Creutzfeldt, W. 1985. Glucagon-like peptide-1 but not glucagon-like peptide-2 stimulates insulin release from isolated rat pancreatic islets. *Diabetologia,* 28**,** 704-7.

124. Scott, R. P. & Quaggin, S. E. 2015. Review series: The cell biology of renal filtration. *J Cell Biol,* 209**,** 199-210.

125. Seely, J. C., Hard, G. C. & Blankenship, B. 2018. Chapter 11 - Kidney. *In:* SUTTIE, A. W. (ed.) *Boorman's Pathology of the Rat (Second Edition).* Boston: Academic Press.

126. Shah, M. & Vella, A. 2014. Effects of GLP-1 on appetite and weight. *Rev Endocr Metab Disord,* 15**,** 181-7.

127. Smith, U. 2015. Abdominal obesity: a marker of ectopic fat accumulation. *J Clin Invest,* 125**,** 1790-2.

128. Solinas, G., Boren, J. & Dulloo, A. G. 2015. De novo lipogenesis in metabolic homeostasis: More friend than foe? *Mol Metab,* 4**,** 367-77.

129. Sun, Y., Ge, X., Li, X., et al. 2020. High-fat diet promotes renal injury by inducing oxidative stress and mitochondrial dysfunction. *Cell Death & Disease,* 11**,** 914.

130. Susztak, K., Ciccone, E., Mccue, P., et al. 2005. Multiple metabolic hits converge on CD36 as novel mediator of tubular epithelial apoptosis in diabetic nephropathy. *PLoS Med,* 2**,** e45.

131. Sweeting, H. N. 2007. Measurement and definitions of obesity in childhood and adolescence: a field guide for the uninitiated. *Nutr J,* 6**,** 32.

132. Szeto, H. H. 2014a. First-in-class cardiolipin-protective compound as a therapeutic agent to restore mitochondrial bioenergetics. *Br J Pharmacol,* 171**,** 2029-50.

133. Szeto, H. H. 2014b. First-in-class cardiolipin-protective compound as a therapeutic agent to restore mitochondrial bioenergetics. *British journal of pharmacology,* 171**,** 2029-2050.

134. Takiyama, Y. & Haneda, M. 2014. Hypoxia in diabetic kidneys. *Biomed Res Int,* 2014**,** 837421.

135. Tamilarasan, K. P., Temmel, H., Das, S. K., et al. 2012. Skeletal muscle damage and impaired regeneration due to LPL-mediated lipotoxicity. *Cell Death Dis,* 3**,** e354.

136. Tanaka, T., Higashijima, Y., Wada, T., et al. 2014. The potential for renoprotection with incretin-based drugs. *Kidney Int,* 86**,** 701-11.

137. Thomas, M. C., Brownlee, M., Susztak, K., et al. 2015. Diabetic kidney disease. *Nat Rev Dis Primers,* 1**,** 15018.

138. Trouwborst, I., Bowser, S. M., Goossens, G. H., et al. 2018. Ectopic Fat Accumulation in Distinct Insulin Resistant Phenotypes; Targets for Personalized Nutritional Interventions. *Front Nutr,* 5**,** 77.

139. Turi, K. N., Romick-Rosendale, L., Ryckman, K. K., et al. 2018. A review of metabolomics approaches and their application in identifying causal pathways of childhood asthma. *J Allergy Clin Immunol,* 141**,** 1191-1201.

140. Tuttle, K. R., Lakshmanan, M. C., Rayner, B., et al. 2018. Dulaglutide versus insulin glargine in patients with type 2 diabetes and moderate-to-severe chronic kidney disease (AWARD-7): a multicentre, open-label, randomised trial. *Lancet Diabetes Endocrinol,* 6**,** 605-617.

141. Veselkov, K., Sleeman, J., Claude, E., et al. 2018. BASIS: High-performance bioinformatics platform for processing of large-scale mass spectrometry imaging data in chemically augmented histology. *Sci Rep,* 8**,** 4053.

142. Wada, J. & Makino, H. 2013. Inflammation and the pathogenesis of diabetic nephropathy. *Clin Sci (Lond),* 124**,** 139-52.

143. Wang, C., Li, L., Liu, S., et al. 2018. GLP-1 receptor agonist ameliorates obesity-induced chronic kidney injury via restoring renal metabolism homeostasis. *PLoS One,* 13**,** e0193473.

144. Wolf, G., Neilson, E. G., Goldfarb, S., et al. 1991. The influence of glucose concentration on angiotensin II-induced hypertrophy of proximal tubular cells in culture. *Biochem Biophys Res Commun,* 176**,** 902-9.

145. Wolfgang, M. J. 2021. Remodeling glycerophospholipids affects obesity-related insulin signaling in skeletal muscle. *J Clin Invest,* 131.

146. Wu, Z., Puigserver, P., Andersson, U., et al. 1999. Mechanisms controlling mitochondrial biogenesis and respiration through the thermogenic coactivator PGC-1. *Cell,* 98**,** 115-24.

147. Xiao, H. H., Sham, T. T., Chan, C. O., et al. 2018. A Metabolomics Study on the Bone Protective Effects of a Lignan-Rich Fraction From Sambucus Williamsii Ramulus in Aged Rats. *Front Pharmacol,* 9**,** 932.

148. Xu, H., Barnes, G. T., Yang, Q., et al. 2003. Chronic inflammation in fat plays a crucial role in the development of obesity-related insulin resistance. *J Clin Invest,* 112**,** 1821-30.

149. Yacoub, R. & Campbell, K. N. 2015. Inhibition of RAS in diabetic nephropathy. *Int J Nephrol Renovasc Dis,* 8**,** 29-40.

150. Yang, J. & Holman, G. D. 2006. Long-term metformin treatment stimulates cardiomyocyte glucose transport through an AMP-activated protein kinase-dependent reduction in GLUT4 endocytosis. *Endocrinology,* 147**,** 2728-36.

151. Yang, W., Luo, Y., Yang, S., et al. 2018. Ectopic lipid accumulation: potential role in tubular injury and inflammation in diabetic kidney disease. *Clin Sci (Lond),* 132**,** 2407-2422.

152. Yin, C. & Wang, N. 2016. Kidney injury molecule-1 in kidney disease. *Ren Fail,* 38**,** 1567-1573.

153. Zager, R. A., Johnson, A. C. & Hanson, S. Y. 2005. Renal tubular triglyercide accumulation following endotoxic, toxic, and ischemic injury. *Kidney Int,* 67**,** 111-21.

154. Zerhouni, E. 2003. Medicine. The NIH Roadmap. *Science,* 302**,** 63-72.

155. Zinman, B., Lachin, J. M. & Inzucchi, S. E. 2016. Empagliflozin, Cardiovascular Outcomes, and Mortality in Type 2 Diabetes. *N Engl J Med,* 374**,** 1094.